Quantification of Interactions among Circadian Clock Proteins via Surface Plasmon Resonance (SPR)

by

Burcu Kepsutlu

A Thesis Submitted to the
Graduate School of Engineering
in Partial Fulfillment of the Requirements for
the Degree of

Master of Science
in
Chemical and Biological Engineering

Koc University

September 2013

Koc University

Graduate School of Sciences and Engineering

This is to certify that I have examined this copy of a master's thesis by

Burcu Kepsutlu

and have found that it is complete and satisfactory in all respects,
and that any and all revisions required by the final
examining committee have been made.

Committee Members:

_____

Seda Kizilel Assist Prof. (Advisor)

_____

Halil Kavakli, Assoc. Prof..

_____

Halil Bayraktar, Assist Prof.

Date: _____

Memento mori & Carpe diem

To my beloved family…

ABSTRACT

Circadian clock is an internal time keeping system recurring 24 hour daily rhythm in physiology and behavior of organisms. Circadian clock contains transcription and translation feedback loop involving CLOCK/NPAS2, BMAL1, *Cry1/2* and *Per1/2*. In common, heterodimer of CLOCK/NPAS2 and BMAL1 binds to E-box element in the promoter of *Per* and *Cry* genes in order to activate their transcription. CRY and PER making heterodimeric complexes enter the nucleus in order to inhibit their own BMAL1:CLOCK activated transcription. The aim of this study was to investigate and quantify real time binding affinities of clock proteins among each other on and off DNA modes using Surface Plasmon Resonance (SPR). The pair wise interaction coefficients among clock proteins, as well as interaction of PER2, CRY2 and PER2:CRY2 proteins with BMAL1:CLOCK complex in the presence and absence of EBOX motif have been investigated via analysis of SPR data with pseudo first order reaction kinetics approximation, and via nonlinear regression curve fitting. The results indicated that CRY2, PER2 and BMAL1, CLOCK proteins form complexes *in vitro*, and that PER2, CRY2 and PER2:CRY2 complex has similar affinities towards BMAL1:CLOCK complex. CRY2 protein had the highest affinity toward EBOX complex while PER2 and CRY2:PER2 complexes displayed low affinity toward EBOX complex. The quantification of the interaction between clock proteins is critical to understand the operation mechanism of the biological clock, to address the behavioral and physiological disorders, and will be useful for the design of new drugs towards clock related diseases.

ÖZET

Memelilerde biyolojik saat 24 saatlik döngü içerisinde organizmanın uyuma-kalkma döngüleri esnasında, birtakım biyokimyasal ve davranışların 24 saatlik ritme göre düzenlenmesini sağlayan hücre içi sinyal mekanizmaları bütünüdür. Moleküler düzeyde saatin 24 saatlik döngüde düzenlenmesi KRİPTOKROM, PERYOD, CLOCK ve BMAL1 proteinleri tarafından gerçekleştirilmektedir. BMAL1:CLOCK ikilisi promotör bölgesindeki E-kutusuna bağlanarak genlerin ifadesini sağlarken, KRİPTOKROM ve PERYOD ikilisi, BMAL1:CLOCK ikilisi ile etkileşerek saate bağlı genlerin anlatımını baskılamaktadır. Bu çalışmada biyolojik saat mekanizmasının temel öğelerinin birbiri ile etkileşim dinamiğini belirlemek için psödo birinci dereceden reaksiyon mekanizması kullanılarak Yüzey Plazma Rezonans (Surface Plasma Resonance (SPR)) tekniği ile dört saat proteinin (KRİPTOKROM2, PERYOD2, CLOCK ve BMAL1) ikili etkileşme dinamiği ve kompleksler halinde etkileşme dinamiği E-kutusu gen motifinin varlığı ve yokluğu esnasında ölçülmüştür. Bu dinamiğe göre incelenen dört saat proteinlerininin ikili etkileşimlerinden en kuvvetli ilişkinin PER2-KRI2 ve BMAL1:CLOCK ikililerinin arasındaki ilişkilerin en kuvvetli oldukları gözlenmiş, bağlanma sabitlerinin 7.54-9.00 (± 0.73) nM ve 3.60-6.90 (±1.86) nM aralıklarında oldukları hesaplanmıştır. KRI2 proteininin BMAL1:CLOCK:EBOX kompleksi ile birleşme eğilimi PER2 ve KRI2:PER2 proteinlerinin EBOX kompleksine olan birleşme eğiliminden daha yüksek olduğu gözlenmiştir. Saat proteinleri arasındaki bağlanma değerlerinin belirlenmesi sadece insan fizyolojik verilerini derinden etkileyen biyolojik saati anlamamıza yardımcı olmakla kalmayıp saate bağlı hastalıkların giderilmesi için ilaç tasarımı yapma olanağı sağlayacaktır.

ACKNOWLEDGEMENTS

There are a number of people without whom this thesis might not have been written, and to whom I am greatly indebted.

Firstly, I whole heartedly thank to Dr. Seda Kizilel (my advisor) and Dr. Riza Kizilel for their hard work, encouragement and guidance throughout this entire thesis process and for believing in my sincerity and abilities. I have gained a great knowledge from them.

I thank Dr. Halil Kavakli for participating in my thesis committee. I acknowledge him for his support and guidance to me throughout the past two years and for his contribution and his laboratory members with preparation of proteins utilized within the thesis project and with their laboratory facilities.

I acknowledge Dr. Halil Bayraktar for participating in my thesis committee. I thank him for his guidance and insight.

I am grateful to Hande Asimgil since she prepared the proteins utilized within the project and Gürkan Mollaoğlu for his support with the experimentation process.

I gratefully thank to my research group friends Caner Nazli for his encouragement, friendship and support, Derya Aydin for her friendship and memorable support, Özlem Çevik for her motivating smiling face, Doğan Gidon and Gözde Sultan Demirer for their previous participation within the project and Tuğba Bal for keeping me motivated all the time.

I acknowledge the Scientific and Technological Research Council of Turkey (TUBITAK), financially assisted us to carry out this research in the form of TUBİTAK Science Fellowship and TUBİTAK 110T423 grant.

I am highly indebted to my father Necat Kepsutlu, my mother Nevin Kepsutlu, my sister Duygu Kepsutlu for their everlasting love, support in all of my efforts, patience, motivation and encouragement. I cannot miss the opportunity to thank my grandmothers Sevim Ayanoğlu and Nusret Kepsutlu, my grandfathers Rafet Ayanoğlu and Necati Kepsutlu and

my aunt Rezzan Kepsutlu, who are like a second family to me, for their love, support, and motivation. I would like to express my gratitude for my entire family members and my relatives for their love and support.

I also thank my flat mates Melek Arı and Çığıl Ece Madan for their support, cooperation and friendship. I additionally thank to my beloved friends Gizem Erdim, Nil Yüksekkaya, Işılay Tügel, Elif Uluünlü, İpek Sarıoğlu, Merve Başöz, Müge Kader, Özkan Batumoğlu, Kaan Koper, Figen Önal, Alp Akıncı, Bahar Ege and Gökçe Gülaçtı for their motivation, friendship and support.

Table of Contents

List of Tables

List of Figures

NOMENCLATURE

SPR	Surface Plasmon Resonance
RU	Response Unit
SCN	Suprachiasmatic Nucleus
EBOX	Enhancer Box
EDC	N-ethyl-N' (dimethylaminopropyl) carbodimide
NHS	N-hydroxysuccinimide
MTL	The mass transfer limitation
k_a	The rate constant for association
k_d	The rate constant for dissociation
k_T	The rate constant of diffusion
K_A	Association constant
K_D	Dissociation constant
A,B,C	Molecular species reacting on sensor surface
AB, CB, AB*	Molecular complexes formed during reaction
[A], C_A	Free analyte concentration
C_S	The injection concentration of analyte
[B], C_B	Free receptor concentration at the surface
[AB]	Concentration of complex formed on the surface
$[A_t]$	Total ligand concentration
$[B_t]$	Total receptor concentration
$[AB]/[B_t]$	Fractional Saturation
$[A_b]$	Concentration of bound analyte
S	The signal of affinity sensor
p	The normalizing factor for molecular mass in competing reaction
θ	The fraction of occupied sites on the surface

α	Amplification factor during signal processing
E	Efficiency of fluorescence resonance energy transfer
R_o	Förster distance
r	The distance between two fluorophores
β	Polarization direction of plasmon wave field
ω	Angular frequency of the plasmon wave field
c	The speed of light in vacuum
ε_M	Permittivity of metal
ε_D	Permittivity of dielectric material
Δn	The refractive index change
$\frac{dn}{dc}$	The refractive index change of analyte molecule
Γ	The surface concentration
h_i	Thickness of the thin layer where binding event occur
R_{max}	Total concentration of immobilized pairs
R, R_1, R_2	SPR signal obtained as species formed during the reaction in RU
R_a	The amplitude of the dissociation phase in a sensogram
R_i	The signal at the point of analyte injection in a sensogram
D	The diffusion coefficient of analyte
v_c	The flow velocity in the center of the flow cell
h	The height of flow cell
h_{diff}	The characteristic height of the diffusion layer
b	The width of the flo cell
l	The length of sensor surface
L_m	The Onsager coefficient for mass transfer
L_r	The Onsager coefficient of reaction flux
F	The bulk flow rate

l_1 , l_2	The start and end point of complex formation within flow cell
η	The viscosity of water
R_H	The hydrodynamic radius
k	Boltzman's constant
MW	Molecular weight

Chapter 1: INTRODUCTION

Living systems, ranging from cyanobacteria to humans, own an internal biological clock. [1-2] The self-sustained and cell autonomous circadian clock keeps the time for approximately 24 hours and create biological rhythms by endocrine and autonomic mechanisms.[3] The external environmental cues, if present, entrain biological clock to synchronize daily biological rhythm of the system to regularly occurring environmental changes. [1-2] In multi-cellular organisms such as mammals, almost every cell in the body contains a tissue specific circadian clock. These circadian clocks are organized in a hierarchical manner. [1, 4-5] In mammals, a master oscillator in hypothalamic suprachiasmatic nucleus (SCN) synchronizes slave oscillators dispersed throughout the body to environmental changes through neural and humoral cues. [1-2, 4] Both central and peripheral clocks receive an input, process this input in a transcriptional-translational feedback loop of genes and proteins, and generate oscillating behavioral outputs. [1-2, 4] A transcriptional-translational feedback loop and posttranslational mechanism form the molecular basis of mammalian circadian clockwork and have gained significant attention recently. [5-6] This feedback cycle approximately lasts 24 hours. [4] Oscillations in the gene expression levels create rhythmic changes in cell, tissue and system physiology. [7] Within circadian clockwork, a core loop and an auxiliary loop take roles besides some secondary loops. At positive limb of the core loop, transcriptional activators, BMAL1 and CLOCK as a heterodimer, bind to E-box promoter elements (CACGTG) of *Period (Per1, Per2)* and *Cryptochrome (Cry1, Cry2)* genes, and positively regulate their expression. PER and CRY accumulate in the cytoplasm and constitute negative limp of the translational-transcriptional loop. These proteins form oligomers in cytoplasm and translocate into the nucleus to repress their own

BMAL1:CLOCK activated transcription. [1, 4-5] In the auxiliary loop, BMAL1:CLOCK complex positively regulate expression of *Rev-erbα* and *Rorα* by binding the E-box region of those genes. [1, 4] Rorα proteins activate while Rev-erb*α* protein inhibit transcription of BMAL1. This loop provides an antiphase oscillation of BMAL1. [5] Besides transcriptional control, clock proteins are also exposed to post translational modifications which affect their nucleocytoplasmic localization, degradation and function. [4]

A well-functioning circadian rhythm is very important since physiological and biological variations in body have certain links with circadian clock mechanism. [8] It controls a variety of biological processes such as daily sleep/wake cycles in animals, and physiological processes such as body temperature, hormone secretion, cell-cycle progression and glucose homeostasis. [8] When circadian rhythms are disrupted, biological and physiological processes lose their habitual order. Many diseases such as obesity, [9-10] cancer, [11-15] cardiovascular problems, [16-17] diabetes, [18-20] hypertension,[21-22] depression and mood disorders occur. [23-24]

In tissues, 6-8% of all genes show circadian expression pattern and these genes have roles in several biochemical reactions in the metabolism.[6] Previous biochemical studies provided evidence for the exact circadian clock mechanism and timing of circadian oscillations,[25-28] however, the kinetics of this physiologically important mechanism, and quantification of binding constants among these important proteins have not been studied.

Since 1990, SPR biosensor has been used to measure binding affinities and kinetic constants of reversible interactions among macromolecules such as nucleic acids, lipids, drugs, carbohydrates and proteins like receptors, antibodies and antigens. [29-34] The basic optical configuration of an SPR biosensor consists of a prism and a thin metal film. SPR biosensors exploit surface plasmon resonance phenomenon. [35] A typical SPR biosensor experiment contains association, dissociation and regeneration phases. Firstly, one reactant is covalently attached to the surface. This macromolecule is called immobilized ligand. In

association phase, second reactant, the analyte, is introduced to the sensor surface at constant concentration. The association of the immobilized and mobile reactant is monitored at the surface. Later, the inflow of mobile reactant is ceased and dissociation phase starts. During this dissociation phase, the time course of dissociation is recorded. [29-30] The purpose of the regeneration part is to remove the mobile reactant from the surface using various buffers. [29]

A SPR biosensor measures adsorption or desorption at the sensor surface via optical phenomenon of surface plasmon resonance. Basically, interaction at SPR chip surface change the local refractive index in the vicinity of the surface, and the resonance angle shifts proportional to the surface concentration of molecules. [29-30] This time dependent change of refractive index is measured in resonance units (RU). Approximately, a change of 1000RU corresponds to 0.1^{o} shift in the surface plasmon angle. For globular proteins, 1000 RU is equivalent to surface concentration of 1 ng/mm^{2}.[236] By detecting resonance unit for different time points, an RU versus time curve is obtained. [29] This sensogram is analyzed to calculate chemical rate constants and thermodynamic equilibrium constants of the interaction for a specific analyte concentration. [29] To analyze a sensogram, various quantitative models are exploited such as rapid mixing model, [30-31, 37] two-compartment model, [30, 38] competitive reaction and conformational change models [39] depending on the experimental conditions and the sensogram data. [31]

In previous studies, interaction of clock proteins have been investigated with various assays such as co-immunoprecipitation [40-43], luciferase reporter gene assay [44], pull-down assays, [45-46] yeast two hybrid, [44] chromatin immunoprecipitation assay[26] and fluorescence anisotropy.[47] Some of these assays such as, co-immunoprecipitation, pull-down, yeast two hybrid, are complicated, and costly, and they do not provide a quantitative information.[45] ELISA-like assays such as protein probing, gel filtration column,[48] protein domain microarrays[49] require high amounts of sample, and hence are not economical.[50]

Fluorescence assays such as fluorescence quenching, fluorescence resonance energy transfer,[51] and fluorescence polarization require tags, which require additional labeling steps.[48, 52] Furthermore, many of these biochemical techniques require a secondary experimental processing which may lead to data misrepresentation.[51] Alternatively, computational docking techniques could be utilized, however these needed to be validated through experimental measurements.[53] In this study, we investigated real time pairwise interactions among clock proteins, as well as PER2, CRY2 and PER2:CRY2 proteins with BMAL1:CLOCK complex in the presence and absence of EBOX motif using SPR. SPR is a central tool for biomolecular interaction studies,[54-55] and has some advantages over existing biochemical assays. Analysis with SPR biosensor is a label-free and real-time, which detects reliable equilibrium and rate constants of biomolecular interactions with optical approach.[30, 55-56] Our results demonstrated that the binding constant for the interaction between BMAL1 and CLOCK was within 3.78- 6.90 nM range, where the binding constant for the interaction of CRY2 and PER2 is within the 12.83-17.13 nM range. These values are consistent, and have similar order of magnitudes with the interaction constants found in previous biochemical assays for BMAL1-CLOCK, and CRY2-PER2. [25, 46, 69-70] The interaction of PER2, CRY2 and PER2:CRY2 proteins with BMAL1:CLOCK complex in the presence and absence of EBOX motif have also been investigated, here. The binding constant values for PER2, CRY2, and PER2:CRY2 with BMAL1:CLOCK complex in the presence and absence of EBOX motif were all within nanomolar range. These findings support previous results, where interaction with few of these proteins and complex were studied in a biochemical assay, and presence of interactions have been only shown qualitatively.[26, 40, 57-59] Previous biochemical studies suggest that CRY2 binds to EBOX, [26] however, biochemical studies conflict about the binding of PER2 and PER2:CRY2 with BMAL1:CLOCK:EBOX complex.[26, 47, 59-60] According to our results, the binding constant of interaction between CRY2 and

BMAL1:CLOCK:EBOX ternary complex is between 0.87-1.22 nM range. The binding constant of interaction of CRY2:PER2 with EBOX complex varies between 31.06-39.05 nM, and the binding constant of the interaction between PER2 and BMAL1:CLOCK:EBOX complex is between 106.33- 171.76 nM. According to our knowledge, this study is the first example for a comprehensive examination of clock protein interactions.

In the second chapter of this thesis, extensive information is given about circadian clock, biological significance and kinetics of protein-protein interactions have been introduced, methods to investigate protein-protein interactions have been explained along with the approach used in SPR Biosensors. The third chapter includes the utilized methods and results for quantification of interactions among circadian proteins via SPR Technique.

Chapter 2: LITERATURE REVIEW

Biological Clock

Human spends approximately one-third of their lives in sleep which is common to all humankind. The sleep was resembled to a short-term death since it is unavoidable and it gained great philosophic attention. Aristotle believed that cooling of heart as body's sensory center causes sleep. Later, early scientific thought by Greek philosophers and physicians such as Plato and Galen perceived sleep as a passive condition in which brain is isolated from the other parts of the body. This belief continues during Middle Ages, the Renaissance and even later. Some of the philosophers associated the sleep not with whole brain but with a unique organ within it. In eighteenth and nineteenth centuries, the reason of sleep was related to a lack or an excess of blood in the brain during the night, a short circuit due to separation of nerve cells and a hypnotoxin accumulation. In the beginning of the twentieth century, newer approaches appeared which claims the presence of a special center for sleep control in the brain. During the second half of the twentieth century, a scientific revolution occurred in the approach to sleep. Nervous system activity variations and variations of hormone secretion was observed to synchronize with the rhythm of the sleep stages plus the daily rhythm of sleep and wakefulness. This rhythmicity is later believed to be derived by an internal biological clock. [61]

Different types of molecules interact for the persistence of the life in the universe. Biological phenomena are basically explained by behavior of the molecules. Cells are composed of some of these molecules and their fate depends on the behavior of molecules. However, biological functions cannot only be explained as molecular interactions since cellular environment is very noisy; however, the functional outcomes of the interactions are very systematic such as signaling pathways. Biological functions are derived by various

adaptations, robustness, insulation, error correction and error coincidence detection through centuries. Cells store the required information in their DNA to stay alive and reproduce. Complex sets of molecules in cells steadily interact to form functional modules which receive inputs and create outputs. These cellular processes can be examined through genome wide analysis of gene expression, synthetic biology and computational modeling. Synthetic biology will evaluate the current understanding level of biological design principles. [62]

Living things have a unique rhythm. An individual time keeping system simulates this rhythm. [63] All living organisms have a biological clock such as hourglasses and oscillators. Hourglasses measure time-spans in species and determine timing of biological events such as embryonic development duration, the time of sexual maturity or menopause. However, biological oscillators ensure that periodic processes such as female oestrus cycle, heartbeat and circannual mating rhythms recur. These oscillators are called ultradian or infradian if they generate a period length shorter than 20hours or longer than 30 hours, respectively. The circadian oscillators generate a period between 20 and 30 hours. All light sensitive organisms have cell-autonomous circadian clocks. These clocks are called cell autonomous since they continue to oscillate *in vitro*. [64] These rhythms generate recurring behavioral, physiological and biochemical patterns. [63]

Rhythmic changes in organisms persist despite the organisms are shielded from periodic environmental variations.[63] The biological rhythms which possess a daily period are coined as circadian rhythms to emphasize that the rhythms are not exactly but around 24 hours by Halberg in 1959. The term “circadian” derives from *circa diem* which means about a day. [63, 65] Under unvarying environmental inputs such as constant illumination and temperature, rhythms deviates from 24 hours significantly. The period of free running rhythms range between 22 to 26 hours and it depends on individual and species. [63, 65] The biological clock can be entrained with different environmental inputs to keep organism synchronized with

day length. The rhythmic variations within a natural environment or in artificial 24 hour light-dark cycles are exactly 24 hours. The rhythms of the clock are synchronized to either solar-day or lunar-tidal patterns.[63] Therefore, the biological processes of the organism matches with the local time.[65] The inputs, which synchronizes phase of organism's circadian clock to environmental variations, are called Zeitgeber (time keepers). Light is a dominant Zeitgeber. [63] Therefore, the daily cycle of sunlight and darkness is a natural light input. Other entraining factors are periodic social factors and temperature. [65]

In 1980s circadian rhythmicity for four distinct biological processes in unicellular alga was identified. These processes are carbon fixation capacity by photosynthesis, timing of cell division, two modes of bioluminescent emission and capacity of flashing to respond stimulation and disturbance. The phases of these cyclic processes were believed to be driven by a single pacemaker in unicellular organisms. However, the circadian clock mechanism in multicellular organisms awakened an intense curiosity. [65-68]

In multicellular organisms, circadian timing system contains a master pacemaker and auxiliary oscillators in peripheral cells.[64] The master pacemaker is called "master" clock while oscillators in peripheral organs are called "slave" oscillators. Mollusks, cockroaches, lizards and mammals have their masterpace maker at their eyes, optic lobes, pineal glands and suprachiasmatic nuclei, respectively. The master pacemaker of birds is also located in their pineal glands. The master clock differs anatomically in each species.[65] The clockwork within these circadian clocks contains interconnected translational and transcriptional feedback loops as a manifestation or as the embodiment of the rhythm-generating mechanism.[64] This mechanism consists of gene-protein-gene feedback pathway where protein is the negative feedback component.[69] The clockwork in master pacemaker and peripheral cells are autonomous; however, especially in opaque organisms timing system is organized in a hierarchial manner since light cannot reach inner cells of the body. [64] Cryptochromes have been shown to have a very essential role in this light-transducing

pathway. [69] The master pacemaker receives input from the environment and produces output signals to peripheral clocks.[6] The master pacemaker is synchronized by photic input from photoreceptors and melanopsin-expressing ganglion cells of retina as electrical signals. Since this electrical signaling involves neurotransmitters, glutamate and pituitary adenylate cyclase-activating peptide, many protein kinases are activated via calcium influx and immediate-early genes such as *Per1* and *Per2* are expressed. Clock genes and clock controlled genes are highly expressed in suprachiasmatic nucleus and pineal gland; however, other brain regions have only low amplitudes of these genes. [64] Suprachiasmatic nucleus entrains the peripheral circadian oscillators via neural or hormonal signals. [64, 69] The peripheral clock can be entrained via food intake, hormones and energy balance.[69] During entrainment process after a resynchronization, each peripheral clock may generate distinct periods, lag times and damping coefficients depending on the strength of coupling with master oscillator. This resynchronization may occur due to time zone differences and shift work.[65]

The rods, cone receptors and intrinsically photosensitive retinal ganglion cells (*ip*RGCs) percept the light in the eye. Rods and cones mediate visual vision and do not have a direct association with suprachiasmatic nucleus. *ip*RGCs mediates circadian vision. Therefore, a visually blind people may conserve their circadian vision. [70] Intrinsically photosensitive retinal ganglion cells respond light due to a specialized photo-pigment. This photopigment, melanopsin, is sensitive to wavelengths between 460nm and 480 nm in the visible electromagnetic spectrum.[71-72] Axons derived from *ip*RGCs projects to SCN heterogeneously and transmit electrical messages from retina via the retinohypothalamic tract within optic nerve. [73]

Suprachiasmatic nucleus is in the anterior hypothalamus above the optic chiasm[73] and contains at least four different and interconnecting neuronal elements with specific functions. [69] The neural projections from SCN are highly complex. These neurons carry

different neuropeptides such as vasopressin, vasoactive intestinal peptide, gastrin-releasing peptide or somatostatin. They also co-localize GABA and glutamate.[69] These neural projections generate at least four different neural signaling pathways to synchronize peripheral cells such as direct communication with neuroendocrine neurons, direct communication with autonomic neurons to reach organs directly, communication with hypothalamic structures between suprachiasmatic nucleus and paraventricular nucleus of hypothalamus and communication to areas outside of hypothalamus. The structures between suprachiasmatic nucleus and paraventricular nucleus of hypothalamus are sub-paraverntricular nucleus of hypothalamus, dorsomedial nucleus of the hypothalamus and medial peroptic area. The communication areas outside of hypothalamus are lateral geniculate nucleus and paraventricular nucleus of the thalamus; therefore, hypothalamic-induced behavior and locomotor activity are synchronized. The projections of paraventricular nucleus of hypothalamus to nucleus tractus solitarius is proposed to coordinate motor behavior.[69]

The biological clock is essential for the daily well-being of organisms [69] since circadian clock influences most physiological activities such as sleep-wake cycles, cardiovascular activity, body temperature, endocrine system secretion, detoxification and hepatic metabolism in mammals.[64] Mutations in clock-relevant genes such as *hClock* polymorphism[74], mutations in *hPer2*[75], *hP*er3 gene polymorphism may increase incidence of circadian rhythm sleep disorders[76]. Circadian biology influences also mental health.[65] Many drug metabolizing enzymes such as cytochrome P450, carboxylesterases and their regulators such as cytochrome P450 oxidoreductase, aminolevulinic acid synthase possesses a circadian rhythmic production.[64] Circadian genes involve in cell proliferation, apoptosis, cell cycle control and DNA damage processes. [77-78]

Pattern of blood corticosterone is regulated by a stimulating and an inhibiting component and the daily vasopressin secretion by suprachiasmatic nucleus. Suprachiasmatic nucleus

reaches paraventricular nucleus of hypothalamus parasympathetic, sympathetic or corticotropic-releasing hormone containing neurons via its direct projections or indirectly. In indirect pathway, vasopressin fibers originating from suprachiasmatic nucleus excite GABA-ergic neurons in dorsomedial nucleus of hypothalamus and sub-paraventricular nucleus region. At day time, GABA-ergic neurons suppresses corticotropic-releasing hormone containing neurons and sympathetic neurons in paraventricular nucleus of hypothalamus. Corticotropic-releasing hormone containing neurons in paraventricular nucleus of hypothalamus regulates adrenocorticotrophin secretion.[69]

The secretion of melatonin is also regulated by circadian timing system. The neurons from suprachiasmatic nucleus project to paraventricular nuclei of anterior hypothalamus. This photic information delivered to preganglionic sympathetic neurons of intermediolateral cell column of the upper segments of the spinal cord via axons projecting down from paraventricular nuclei to brain stem.[79] Intermediolateral cell column is located in thoracic and upper lumbar spinal cord. The axons of preganglionic neurons synapse on postganglionic sympathetic nerve cells in the superior cervical ganglia. These axons, forming a nervi conarii with internal carotid arteries and its branches, penetrate into endocrine units of pineal gland to stimulate melatonin secretion.[80-81] Pineal melatonin is synthesized during night. The melatonin level alternate daily and seasonally. This alteration is interpreted as circadian entrainment[82] and calendar information.[83] Melatonin plays an important role in human metabolism. For instance, it has a modulatory effect on antibody response to antigens,[84] natural killer cell activity and the effects of immunosuppressive drugs.[85] It also has antioxidant, antimitotic and antiangiogenic activity which are related to cancer formation. This pineal hormone even alters fat metabolism through alteration of cAMP production and linoelic acid uptake. [86]

Circadian cycle has a potential role in immune response. The expression of natural killing cells,[87] T-helper cells, T-suppressor cells and splenic B-cells have a 24-hour oscillation.[88] Sleep disorders affect the expression of hypothalamic pituitary adrenal axis which affects the expression of pro-inflammatory cytokine IL-6 and TNF-alpha. These immune factors play an important role in acute response.[89-90]

Circadian clockwork confers timing information to the body by diffusible molecules such as TGFα[91] and prokineticin 2 (PK2).[92] PK2 expression is directly mediated by CLOCK:BMAL1 heterodimer via EBOX motif within promoter region of PK2.[93]

Circadian clock and its regulatory rhythmic outputs can be misaligned by some environmental factors. These factors are called circadian disruptors[94] such as light-at-night, suspected food, physical activities and biological stress.[95-96] These disruptors may lead chronodisruption in the downstream cellular physiology such as jet lag and unusual cellular physiology.[95] Agency for Research of Cancer classified shift-work, which disrupt circadian rhythm, as carcinogenic in human in 2007.[95] This statement is explained by light-at-night (LAN) hypothesis. Light exposure at night may disrupt circadian rhythm because this exposure suppresses melatonin production in humans.[97] Since melatonin inhibits cancer formation, melatonin reduction may lead increased risk of breast cancer,[78, 97-99] prostate cancer,[100] endometrial cancer,[86] skin cancer[101] and colon cancer.[102] Additionally, in humans, circadian timing system controls the rhythmic expression of several cyclins and tumor suppressor p53.[103] The circadian regulator CK1ε (Casein Kinase 1ε) promotes cell proliferation and tumorigenesis.[104] Therefore, a robust circadian clock is important for general well-being of the organism. Circadian disruption may also lead hypertension,[105] heart disease,[106-108] endometriosis,[109] diabetes,[20, 110-112] obesity[20] and mood disorders.[113-115] Chronic night shift workers and regular flight attendants across time zones have the highest reported increase in cancer.[98] The mechanisms that lead these disorders with circadian clock disruption are attributed to various reasons. According to epidemiologic and well-

controlled laboratory studies, sleep deprivation causes increase in sympathetic nervous activity, an increase in cortisol levels in the evening and growth hormone in daytime since it disrupts circadian rhythm.[116] Disruption of circadian rhythm also reduces production of leptin while increasing the production of ghrelin, a hunger promoting hormone. This dysregulation of neuroendocrine control of appetite causes an internal misperception of insufficient energy availability. All of these factors are associated with risk of diabetes and obesity.[20, 110, 116]

Since circadian clock is intertwined with many physiological processes, circadian rhythmicity hinders important pharmacological implications. If circadian physiology is completely revealed, the most suitable drug delivery regimens can be scheduled according to the daytime dependent activity and toxicity of drugs for chronopharmacology and chronotherapy fields. For instance, daily uptake of drugs can be scheduled to maximize effectiveness. Tumor cells lose their circadian rhythm and daytime dependent cell cycle progression in contrast to normal proliferative cells. During cancer therapy, this discrimination may ensure the delivery of antiproliferative drugs at a time when the drugs have minimum detriment to the normal cells.[64-65] A drug which manipulate biological clock will be a useful therapeutic tool to adjust a new schedule or may treat problems such as manic depression and sleep disorders.[65]

Since 1980s, many hypothesis were suggested to describe circadian timing system which involves sequential gene transcription, membrane properties, ion transport, cyclic nucleotide levels, mitochondrial oxidative phosphorylation.[65]

Circadian rhythmicity is an endogenous oscillation with a near 24 hour period. These oscillations are cell autonomous; therefore, suprachiasmatic nucleus may generate a circadian signal without cell-to-cell interactions and synchronization. In early 1970s, *Per* gene was identified as a altering factor for the free running period of daily rhythmicity. At similar times, the mammalian transcriptional activator CLOCK, BMAL1 and

CRYPTOCHROME was also identified. These components form the core loop of the circadian clockwork.[117] The molecular clockwork of circadian oscillators is explained by a complex feedback loop of transcriptions and translation among various clock genes such as *Period1(Per1), Period2(Per2), Period3(Per3), cryptochrome1(Cry1), cryptochrome2(Cry2), Tim, Clock, Bmal1, casein kinase Iε/δ (CKIε/δ)*. [118-119] The output of this circadian oscillation is clock-controlled genes. Clock-control genes regulate cell functions. 2-10% of all mammalian genes are clock-controlled genes.[120-121] Circadian clock is an oscillator which derives rhythmic daily physiology and behavior of organisms.[41]

Clock, Bmal1 genes form the positive limb of the feedback circuit. The expressed CLOCK:BMAL1 heterodimer binds to E-boxes (5'-CACGTG-3') and E'-boxes (5'-CACGTT-3') in the promoters of target genes to activate transcription.[58, 122] These target genes include Period and Cryptochrome genes which negatively regulate their own protein expressions.[40, 58, 123] Expressed three PERIOD and two CRYPTOCHROME proteins forms complexes to associate with transcription factor BMAL1:CLOCK complex to inhibit their own expression. Turnover of PER and CRY depresses CLOCK:BMAL1 activity to initiate a new cycle.[41] Since PER and CRY analogs compensate each other, at least one member of each family is enough for circadian rhythmicity. However, if all analogs of PER or CRY are lost, the circadian rhythmicity is not observed.[124] The individual stabilities of PER or CRY proteins determine pacemaker period. Formation of PER and CRY complexes facilitates nuclear entry and mediates transcriptional negative feedback.[125] The stability of PER and CRY is regulated by posttranslational mechanism such as phosphorylation and ubiquitination events. The enzyme casein kinase 1ε (CK1ε) and casein kinase 1δ (CK1δ) phosphorylate PER for ubiquitination by βTrCP and degradation by the 26S proteasome.[124] Likewise, FBXl3 poly-ubiquitinates CRY proteins for proteosomal degradation after phosphorylation. CRY1 is phosphorylated by AMPK1. CRY2 is phosphorylated by a sequential DYRK1A/GSK-3β cascade.[124] This negative feedback is essential for the clock;

however, its mechanism has been extensively investigated via biochemical studies.[41] The level of PER proteins determine the phase of the clock.[126] During night time, the level of PER is low. In the night acute administration of light induces Per1 and Per2 transcription to increase PER1 and PER2 levels which delays the phase of the circadian rhythm.[127] Per genes are activated by light through CREB/MAPK signaling acting on cAMP-response elements in the *per* promoters.[128]

Other targets of CLOCK:BMAL1 heterodimer are Rev-erbα and Ror α/β genes. These genes are orphan nuclear-receptor genes. Within this auxiliary feedback loop in coordination with the first main loop, ERB and ROR proteins competitively bind to a binding site within the promoter region of *Bmal1*. This binding site is retinoic acid related orphan receptor response element (RORE). The expression of BMAL1 is initiated by ROR while inhibited by REV-ERB proteins.[129-130] A set of PAR bZIP genes participates in another transcriptional loop. They have D-box elements in their promoters.[124] These auxiliary loop and D-box accessory loops are not required for clock function; however, they increase the robustness and precision of the period of the circadian rhythm.[129, 131-132]

Protein Interactions and Kinetics

The human genome contains 20000-30000 genes coding for over 500000 different proteins. A cell can produce over 10000 different protein at a given time.[133] Proteins control the biological activities within dynamic context of cells.[134] Eighty percent of proteins function with partners or as components of large molecular assemblies.[133] Each cell type within a single species contains different populations of proteins. Across species, this composition difference gain more significance. Additionally, function and expression levels of these proteins also differ significantly across species.[134]

A protein is an amphoteric polyelectrolyte biological polymer with various aminoacid residues with various side chains. Amino-acid residues may be nonpolar, polar and charged.[135-136] The marginal structural stability of a protein is due to hydrophobic

interactions between nonpolar side chains, hydrogen bonds, Coulombic interactions between charged residues and van der Waals interactions. [135] The adsorbent surface competes for similar interactions which reduces the total free energy of the protein.[135]

As a result of interfacial activities of proteins, protein interactions including complex formation and dissociation occur. [137] The binding of two proteins are driven by shape and chemistry of the binding surface such as aminoacid sequence and ternary structure of the binding site. Interacting proteins usually have complementary surfaces. The complexes formed by proteins may be transient or permanent depending on the strength of the molecular interaction among macromolecules.[138] Proteins may form monomers, homodimers or larger homomeric complexes and hetero-oligomers.[138] Binding process has a kinetic nature which includes transition states and intermediates.[137] During protein interactions, energy exchanges and conformational statistics result in reversible and irreversible processes.[139] Any mutation, pH and salt concentration affects kinetics of complex formation and dissocation.[137] The unique native conformation, large size, an internal cohesion and heterogeneous surface electrostatic forces of proteins result conformational changes and surface aggregation during protein adsorption[136, 139] as well as denaturation to lose its activity, exchange with other proteins in solution, dissociation from the surface and orientation change.[140] For two proteins to associate, they must collide with each other within a rigid geometrical schema after a diffusion step. This collision may be followed by a precise docking step which includes desolvation and structural rearrangement. [137] Proteins associate from their binding sites and rate of association depends on the geometric constraints of this sites. Also diffusion is another factor which affects the rate of association between proteins. [137] The protein adsorption is defined with time required for the protein to reach to the surface and the strength of the interaction.[139]

For *in vitro* protein studies, the rate of diffusion step can be altered via adjustments on solution viscosity, salt concentration to affect electrostatic interactions and use of crowding

agents such as Polyethylene Glycol (PEG) and Bovine Serum Albumin (BSA). Therefore, the association rate constant can be altered using different conditions of reaction where diffusion is the rate determining factor for the reaction. [137]

Association of a protein means formation of a protein complex (AB) from unbound individual components (A+B).[141] According to four states model, during association, firstly an initial unstable form of complex, which can redissociate with a reverse reaction, is formed as a result of diffusion. This initial complex evolves to an intermediate complex and the final complex. This four state model can be reduced up to two state model depending on the specific reaction mechanism.[137] To characterize protein adsorption, quantitative description of adsorption must be done. This is possible via measuring adsorption isotherms, describing association and dissociation kinetics, adsorption layer thickness and adsorption layer refractive index.[135] An adsorption isotherm relates the measured adsorbed amount of protein per unit area to the solution concentration of protein. An adsorption plateau in these isotherms represents saturation of the surface with the ligate. This plateau; however, does not always mean that true equilibrium is attained. The basic parameters of adsorption kinetics are the number of protein molecules adsorbed per unit area per time. [135]

The strength of the interaction in the cell is critical to evaluate the protein interactions. To evaluate strength, binding constant between proteins, which is the ratio of rate constants of reverse and forward reaction of interaction, must be calculated. Cofactors requirements, cellular compartmentalization, competing proteins, reaction solution conditions such as pH, salt concentration must be considered during binding constant calculation since these parameters affect the strength of the reactions.[48] Affinity is kinetic and thermo-dynamic explanation of tendency of molecules to associate with each other such as ligands and receptors via association constant, free energy of binding, entropy, activation energy of association and dissociation plus kinetic association and dissociation constant. Adsorption

isotherm obtained by an affinity sensor is a calibration curve usually at a constant temperature which correlates the dependence between the volume of the analyte concentration and surface concentration of immobilized protein. Analysis of this curve with a mathematical description provides information about binding process.[142] Since to define binding between proteins is very important to ultimately interpret the consequences of protein-protein interactions within the cell, many studies investigated the strength of protein-protein interactions. Dissociation constant between p85 (PI3K) and tyrosine-phosphorylated peptide from PDGF was calculated as 5.2×10^{-8} via Surface Plasmon Resonance Biosensor.[143] The binding constant was 3×10^{-8} M between CheY and CheA via SPR studies.[144] This constant was calculated as 1.1×10^{-6} M between T7 gene 2.5 protein and T7 DNA polymerase protein via fluorescence anisotropy.[145] The binding constant between trypsin and pancreatic trypsin inhibitor was calculated as 6×10^{-14} M via competition kinetics.[146] Via sucrose gradient sedimentation method, the dissociation constant between NusB and S10 was calculated as 1×10^{-7} M. [147] 3×10^{-9} M is binding constant of TαGDP and PDEγ via intrinsic fluorescence.[148] Via GST precipitation, the binding constant between ras and raf was 5×10^{-8} M.[149] Binding of biotin to streptavidin was calculated to be 1×10^{-14} M via Si-NW FETs.[150]

Besides binding affinity of protein interactions, binding kinetics such as rate of association and rate of dissociation are significant for biological systems. For instance, biological activity of interleukin-4 and human growth hormone, while they react with their receptors, was found to be linearly proportional to the association rate constant of the reaction while dissociation rate does not affect bioactivity.[151-152] A hyperbolic dependence of association rate constant on protein concentration means that the reaction is not diffusion controlled while a linear dependence shows a diffusion limited association reaction. For most low concentration protein-protein interactions, diffusion limitation was not detected.[137]

In the simple ligand-receptor interaction, when ligand (A) binds to receptor (B), a complex (AB) is formed.[141, 153] In the simple ligand-receptor interaction, the rate of association depends on ligand concentration and the fraction of uncoated binding sites. The rate of association is depicted as $k_a*C_A*(1-\theta)$ while the dissociation is depicted as $k_d*C_A*\theta$ where θ is the fraction of occupied sites on surface, C_A symbolizes concentration of ligand and k_a and k_d are rate constants for association and dissociation phases respectively. At the equilibrium conditions, the rate of association equals to the rate of dissociation. This fact yields Langmuir adsorption isotherm model as following equation[142, 154]

$$\theta_{eq} = \frac{C_A * K_A}{1 + C_A * K_A} \quad (2.1)$$

where K_A is association constant.

The assumptions behind analysis of simple protein interactions are reversible interaction, equivalent and independent receptors and response proportional to the number of occupied receptor sites. Also, the reactions are assumed to be observed at equilibrium conditions. The components are at their free and unbound states [153] as well as Langmuir isotherm model At low analyte and ligand concentrations, the Langmuir adsorption isotherm model is reduced to Henry adsorption isotherm[142, 154]

$$\theta_{eq} = C_A * K_A \quad (2.2)$$

The signal of an affinity sensor depends on the surface coverage and depicted as follows

$$S = \alpha * \frac{C_A*K_A}{1+C_A*K_A} \quad (2.3)$$

where α is a coefficient proportional to type of transducer and an amplification factor during signal processing.

During analysis, the critical concern is to extract binding constant K_A obtained under quasi-equilibrium conditions. Calculation of binding affinity constant is performed by direct

nonlinear fitting using Eq.2.3. This method is basically fitting equilibrium data to Langmuir isotherms.[142, 154-155] However, this is a linear transform and they transform the errors in the primary equilibrium data and provide little information about the reproducibility and certainty of the calculated parameters.[36]

K_A is association constant with unit of M^{-1} and K_D is dissociation constant in M. They are calculated as follows[153]

$$K_A = \frac{k_a}{k_d} = \frac{[AB]}{[A] * [B]} \quad (2.4)$$

$$K_D = \frac{k_d}{k_a} = \frac{[A] * [B]}{[AB]} \quad (2.5)$$

While predicting protein-protein interaction kinetics, detecting the errors is very critical. During interpreting protein kinetics via various models within the domain of statistical analysis, the main assumptions underlying the model and the awareness of possible errors deviations from the model is important.[156] The residual plots are one method to estimate deviation of the calculated values via selected model from the observed data. In a residual plot, the ordinate is usually the weighted difference between observed value (y) and model estimated value ($\hat{y}$) which is $w^{0.5}(y-\hat{y})$ while abscissa variable is $\hat{y}$. The points must be scattered in a band parallel to the horizontal axis and they must be evenly distributed.[156]

To visualize whether the simple model conforms with the protein-protein binding interpretations, a plot of fractional saturation $[AB]/[B_t]$ against free ligand concentration [A] must be ensured to give a rectangular hyperbola. This correlation is obtained by rewriting Eq.5 in terms of total ligand concentration $[A_t]$ and total receptor concentration $[B_t]$ where $[A]= [A_t]-[AB]$ and $[B]=[B_t]-[AB]$.

$$\frac{([A_t] - [AB]) * ([B_t] - [AB])}{[AB]} = K_d \quad (2.6)$$

$$\frac{[AB]}{[B_t]} = \frac{[A_t] - [AB]}{K_D + [A_t] - [AB]} = \frac{[A]}{K_D + [A]} \quad (2.7)$$

A Scatchard plot of the same data is also useful to visualize the extent of the data conform to the Langmuir model.[154] A Scatchard plot is plotted the fraction of concentration of bound analyte concentration to free analyte concentration $[A_b]/[A]$ against concentration of bound protein [A].[153-154] The Scatchard plot is described by

$$\frac{[A_b]}{[A]} = \frac{-[A_b]}{K_D} + \frac{n * [B_t]}{K_D} \quad (2.8)$$

A linear Scatchard plot indicates direct interaction between analyte and ligand[157] and conformation of the data with Langmuir model.[154] A concave up Scatchard plot indicates ligand heterogenecity, multivalent analyte and negative cooperativity between binding sites. A concave down Scatchard plot indicates positive cooperativity between binding sites and self-association of the analyte.[153-154]

Methods to Detect Protein-Protein Interactions

Transient protein-protein interactions are fundamental for cellular function such as growth, cell cycle, metabolic pathways and signal transduction.[48, 138] Proteins interact as multi-subunit enzymic nanomachines, cohort and client protein binding via chaperons, protein binding via protein kinases and multiple protein interactions in metabolic events.[158] All modifications of proteins contain protein interactions with protein modifying enzymes such as protein kinases, protein phosphatases, glycosyltransfreases, acyl transferases, proteases.[48] Additionally, protein-protein interactions participates in interaction of transcription complex with gene promoters, transport of proteins across membranes, protein folding, assembly of cellular components such as actin fibers cell regulation, immune response and enzymatic regulation. [48, 137] Protein-protein interactions are significant for cellular processes. Protein interactions, molecular mechanism of interactions and consequences of interactions must be well characterized.[48, 138] Additionally, biotechnological techniques such as bioseperations, biocatalysis and biosensing involve

protein adsorption.[136] These biotechnological technologies include surface bound proteins; therefore, it is critical to learn factors affecting protein adsorption, kinetics and equilibrium behavior of proteins during adsorption is important for improving biotechnological techniques. [139]

Many methods have been invented to detect protein-protein interactions. Some of methods defines the existence of an interaction between proteins; some of them evaluate binding interactions quantitatively.[48] Some of methods defines the existence of an interaction between proteins; some of them evaluate binding interactions quantitatively.[48] These methods are solution depletion techniques which are batch methods, optical techniques such as Ellipsometry, Angle Reflectometry and Surface Plasmon Resonance, autoradiography and microscopic techniques and spectroscopic techniques are methods to study protein adsorption. [135] Solution depletion technique is performed via concentration measurement in bulk solution before and after adsorption via UV absorption, fluorescence, colorimetric methods and other techniques which requires tagging. This method usually requires a chromatographic adsorption media. In such methods, the beaded surface is washed with buffers which free equilibrium bulk concentration is not clearly defined.[135] Library based techniques such as protein probing, phage display, two-hybrid systems[48] are characterized in the solution depletion technique. Optical techniques rely on interaction of light between adsorbed protein layer such as, fluorescence-based techniques, analysis with mass spectroscopy, surface plasmon resonance spectroscopy.[138] Spectroscopic techniques investigate the interaction of photons with adsorbed protein molecule. Some of the spectroscopic techniques are fluorescence spectroscopy, infrared absorption, Raman scattering and circular dichroism.[135, 138] The association can be investigated in the bulk phase via NMR titration.[142]

There are many *in vitro* biochemical strategies for identifying interacting proteins such as coimmunoprecipitation, gel electrophoresis, in vitro binding assays, protein crosslinking

and rate-zonal centrifugation.[158] *In vivo* protein interaction assays includes in vivo affinity fusion-based protein purification techniques[133], crosslinking of proteins with cell penetrating reagents and resonance energy transfer techniques between dye-coupled proteins.[159]

Biochemical mechanism of circadian systems, which includes various protein associations and dissociations, have been investigated intensely.[65] So far, researchers have perturbed clockwork via drug treatment or mutation and have examined biochemical site of the action. They have sought a photoreceptor and have explored its entrainment pathway. They also studied an rhythmic output and its coupling with the clockwork mechanism.[65]

Biochemical Methods

Coimmunoprecipitation

The co-immunoprecipitation (co-IP) is a very common method to identify associated proteins in vivo and in vitro. [48, 133, 158, 160-161] In a typical experiment, cell lysates are generated. Supernatants are incubated with an antibody and the balt complexes are captured. Later, the antibody is immobilized using protein A and protein G which are covalently attached to sepharose beads. The ligand co-precipitated since it is stably associated to the protein which is immunoprecipitated with the antibody.[134, 158] Proteins, which bind to the antigen, are analysed after multiple washing steps. To detect a synthetic peptide coupled or a specific epitope tagged protein can be done through a polyclonal or monoclonal antibody.[48, 158] Any contaminating antibodies must be eliminated.[48] Also, to choose a proper control is very critical to ensure that co-immunoprecipitated protein is a protein of interest.[134] This method assays a specific protein pair interaction in the presence of a pool of competing proteins; therefore, the method provides a specificity control. [48] Method is relatively easy, and convenient for downstream analysis with different methods such as immunoblotting and SDS-PAGE.[158] Additionally, since proteins are at their natural state of posttranslational modifications, the method is quite accurate.[48]

High-Throughput Screening Assays

High throughput screening methods include yeast two hybrid assays[138, 162-164], the mating-based split-ubiquitin system (mbSUS)[138] and affinity purification-mass spectroscopy.[13884-85] High throughput assay provides the ability to analyze interaction of proteins which cannot withstand *in vitro* conditions.[159] In high throughput assays, limited number of replica tests is performed and interactions are scored in an all-or-nothing scheme. Also, due to overexpression of proteins and elimination of competing interaction partners, the reaction conditions deviates from *in vivo* state. Therefore, the interaction screens obtained with this method are designated as 'potential interactions'. [138]

The yeast two-hybrid system is a simple and robust genetic method in which direct binary interactions between proteins are measured according to transcriptional activity. [48, 138, 165] Yeast two hybrid system is a mating assay.[165] The method uses split transcription factors. The transcription factor is splitted into two DNA-binding domain and transcription activation domain. One of the transcription factor pieces is fused with interested protein while the other piece is fused to the ligand of the interested protein.[138] These fusion proteins are expressed in different yeasts and yeasts are allowed to mate.[165] When proteins are co-expressed and localized to nucleus, if the fused protein and its fused ligand interacts, the transcription factor is reconstituted from its split pieces to activate the transcription of the marker gene in the nucleus.[138] The assay is generally performed in yeast cells which is an eukaryotic cell like mammalian cells.[48] The method may be enhanced via low copy plasmids, implementation of different markers such as URA3, HIS3, ADE2, lacZ, GFP and use of de novo autoactuators.[138]

The yeast two hybrid interaction datasets can be validated using orthogonal assays such as co-affinity purification, mass spectroscopy and computational methods. [166] In AP-MS method, a co-affinity purification technique combined with mass spectroscopy, large-scale

PPI datasets which were obtained by yeast two hybrid assay are complemented.[138, 167-168] Computational methods of bioinformatics field predict protein-protein interactions using information from databases such as BIND, MIPS, HPRD and annotations by Pfam and GO.[166, 169-170]

The yeast two hybrid is a powerful method; however, it is limited to soluble proteins or their soluble domains.[171] The mbSUS system is another high throughput assay to detect protein-protein interactions.[159] It is similar to Y2H system; however, it additionally provides analysis of interactions of membrane proteins such as nuclear envelope, endoplasmic reticulum, golgi, vacuole, mitochondria and plasma membrane.[138] In this system, a split ubiquitin, which contains a mutated N-terminal (1-34 aminoacids) and a wild-type C-terminal (35-76 aminoacids) domain of ubiquitin, is utilized. C-terminal fragment is fused to a transcription factor and an interested membrane protein while the other ubiquitin split is fused to a ligand of the interested protein.[138, 159] The system depends on release of a transcriptional factor when fused membrane proteins interact. An intact ubiquitin is reconstituted only if two fused proteins interact since N-terminus of the ubiquitin is mutated to eliminate a natural reconstruction.[138] Ubiquitin is a conserved protein which attach to N terminus of the proteins as a signal for degradation.[171] The reconstructed ubiquitin moiety is recognized by endogenous ubiquitin-specific proteases and ubiquitin is cleaved from fused proteins and to release of transcription factor into the cytoplasm which activates reporter genes in the nucleus.[138, 159, 171] Interaction between proteins can be detected by analyzing liberated reporter proteins.[171] This method enables kinetic and equilibrium calculations of protein-protein interactions in a natural living cell.[159] High throughput assays are improved with many novel techniques; however, they still contain false negatives which reduce the reliability of the assay.[138, 165] 40-80% false negatives and 30-60% false positives are estimated for high throughput studies which are combined with affinity based techniques, two-hybrid techniques and computational

methods.[133] It is estimated that only 50% and 10% of yeast and human interaction map has been completed so far, respectively due to high rate of false positives using high throughput screens.[133]

Protein probing

Protein probing is another method in which a labeled protein screens an expression library to identify different protein interactions with the probe.[48, 172] The labeled protein is produced using a transformed bacteria with a translational construct which includes coding sequence of tag and probe as a fusion. When bacteria is induced for expression, the labeled protein is purified via different methods such as affinity chromatography.[158] Later, this purified recombinant fusion protein is incubated *in vitro* with interested cellular fractions.[158] Any protein can be used as a probe such as GST fusion vectors, [48] His tags, the maltose-binding domain (MBP), the CaM-binding peptide (CBP), and epitope tags such as myc.[158] This protein probe can be manipulated in vitro to provide a specific posttranslational modification or a metal cofactor if this modification is essential for the binding.[48] After incubation of tagged probe with the expression library, the mixture washed and eluted. Binding partner is analyzed via mass spectroscopy following gel electrophoresis.[158] This method is a relatively easy and straightforward method.[158] However, the method has some disadvantages. The proteins encoded by the library must fold properly and protect their three dimensional structure during processes even they experience many processes which may denature the proteins. Also binding conditions does not reflect native cellular environment. Since the posttranslational modifications required for an interaction may differ across species, the use of different species for expression of proteins may reduce accuracy.[48] In this method, overexpression of the interested protein *in vivo* may occur. Overexpression may sometimes yield cytotoxicity.[133] Also, the tag may be hindered within protein which obstruct purification, may alter the interaction affinity

between interested protein pairs and alter the localization of protein within the cell.[133] Also some of the binding may be lost due to harsh conditions of washing steps such as detergents and high salt concentrations. Additionally, some proteins in the cell may act as contaminants.[133]

Affinity Blotting

In affinity blotting is another application to detect protein-protein interactions. The proteins are fractionated by PAGE. PAGE is transferred to a nitrocellulose membrane and the binding ability of the proteins to each other is detected. This method eliminates the purification requirement; however, to pre-fractionate cell lysate before gel chromatography may increase the sensitivity of the method. Since denaturing gels may inactivate the proteins and may separate subunits of the complexes, the denaturants are removed during blotting or nondenaturing gel systems are preferred. The protein probe should be carefully selected. Fusing tags may facilitate the procedure such as glutathione S-transferase (GST) fusion, epitope tags or other tagging pairs.[48]

Protein Affinity Chromatography

Protein Affinity Chromatography is one of these methods.[48, 173] A protein, covalently immobilized to a matrix, is used to select ligand proteins. In the method, a pool of proteins is passed through a column which is covered by a matrix containing immobilized proteins. The proteins which have an affinity to the immobilized protein are retained while the rest flows through the column. Strong retainment reveals strong interaction between the extract protein and the immobilized protein. After the extract protein binds to matrix, it is eluted by high salt solutions, cofactors, chaotropic solvents and sodium dodecyl sulfate. If interested extract protein is labeled in vivo before experiment, the sensitivity of the identification increases.[48, 173] By protein affinity chromatography, binding constant of the interaction of

proteins can be calculated. The detection depends on the concentration of analyte in the solution instead of the amount of bound protein. In the method, the bound ligand is assumed to be always in equilibrium with the solution ligand during experiment. Also, solid phase bound protein is used instead of a free protein in liquid state.[48]

Tandem affinity purification (TAP)

Tandem affinity purification method is another protein-protein interaction detection method.[133, 174-175] In this method, a TAP-tag which contains two sequential affinity tags spaced with a cleavage site . This site with a sequence of Glu-X-X-Tyr-X-Gln/Ser can be cleaved with tobacco etch virus protease. This specific sequence is rare in mammal cells; therefore, this site is not cleaved spontaneously within mammalian cells without addition of the specific protease.[133] In the method, after expression of the protein with TAP-tag within cellular environment, the cells are lysed and passed through an elution column to isolate the specific tag-protein-ligand complex as the tag bind to the column. Later, TEV protease is sent to cleave the tag leaving remaining part of the tag on the protein-ligand complex. Protein fused to the remaining part of the tag is passed through a second column to isolate the protein once more.[133, 175-176] This method provides complex formation *in vivo* and reduced nonspecific binding due to double purification step. However, a high amount of starting material is required due to this double purification step. [133]

Far Western Assay

Far western (overlay assay) assays is based on western blotting. In both procedures, samples are run on SDS-PAGE gels and transferred to nitrocellulose or PVDF. Then, blot is overlaid with a soluble protein. [134] In Far western, the overlaid probe is a probe of interest which is usually a fusion protein such as a recombinant Glutathione-S-Transferase fusion protein[177], a polyhistidine tag[178], maltose binding protein fusions[179], since it is easy

to detect.[177] Overlaid protein can be detected with tags for defined antigenic regions[180], incubation with streptavidin after biotinylation[180-182] and autoradiography if the probe is radiolabeled with ^{32}P.[180, 183-184] This method can also define affinity of protein pairs when the concentration of overlaid probe is increased until a maximal amount of specific binding is attained. After forming a ligand binding curve, the slope of the binding curve can be used to determine affinity constant (K_D) of the interaction.[177] Since the method involves multiple washing steps, a very high affinity is required for interaction to be detected. Radiolabeled samples requires a special handling and the radiolabeling may alter the properties of the protein.[177]

***In vivo* and *in vitro* crosslinking**

Crosslinking is another method to detect protein-protein interactions *in vivo* or *in vitro*. [48, 133, 158, 185] This method is used to determine the architecture of the complexes and to detect interacting proteins.[48] The crosslinker must contain at least two reactive groups such as primary amines and sulfhydryls. The water solubility, membrane permeability, buffer interference possibility, cleavability, arm length between two reactive groups are important considerations for choosing the appropriate crosslinker among diverse crosslinking reagent options including polyethylene glycol.[158] In this method, most strategies involve SDS-PAGE technique. The complex is firstly reacted with a cleavable bifunctional crosslinker. Later, the proteins are fractionated on an SDS-gel in the absence of reducing agents to separate proteins based on their molecular weight. Later, another dimension of SDS-gel is used to run proteins in the presence of an agent which cleaves the crosslinker. Since molecular weight of non-crosslinked proteins does not change, they have a similar mobility in both dimensions of SDS gel and form a diagonal. The crosslinked proteins diverge from the diagonal since the crosslinked protein is divided into two smaller molecular weights when agent is broken down.[48] This crosslinker can be broken using reducing agents if the

crosslinker contains disulfide bonds. [48] The crosslinker can also be boiled in SDS-PAGE sample buffer instead of using reducing agents, if it is volatile.[158] *In vivo* detection enables detection of transient protein interactions via stabilizing these interactions.[48, 158] This technique requires membrane permeable crosslinking agents such as formaldehyde.[48, 158]

Phage Display

Another approach is phage display. Filamentous phages can express a fusion protein with a foreign peptide on its surface. Since these foreign aminoacids are accessible by antibody, "fusion phage" can be designated among other phages. Fusion phage libraries can be screened to determine proteins which bind to a specific antibody.[48]

Sedimentation through gradients

Sedimentation through gradients is another method to detect protein-protein interactions. This method measures populations of protein complexes according to their sedimentation rate through gradients of glycerol or sucrose. At protein concentrations above binding constant, the proteins will sediment as a complex. If the concentration is below the binding constant, they will sediment in their native forms. This is judged by appropriate assays for activity or immunoblotting on the fractions. By varying the concentrations of the proteins, which form the interested complex, the binding constant can be identified.[48]

Fluorescence Based Techniques

Fluorescence based techniques to detect protein-protein interactions range from fluorescent tagging to fluorescence resonance energy transfer based methods. Fluorescence resonance energy transfer based methods may inform about the dynamics and localization of the interactions *in vivo* [138] while *in vitro* tests cannot examine protein interactions in the native cellular environment.[138]

Fluorescence facilitates detecting proteins through their tryptophan residues. Using fluorescence, the binding constants of the proteins can be determined. Fluorescence spectrum is a fluorescence method to determine binding coefficients of proteins. In the method, the changes in fluorescence emission spectrum are traced as a protein and its ligand forms complexes. Fluorescence intensity at a particular wavelength is utilized to evaluate the dissociation constant. The method is effective and simple. However, the probability of detecting a change in the fluorescence spectrum declines as the tryptophan number within proteins reduces. The fluorescence emission change is not easily predictable. Additionally, fluorescent tags may be used as long as tagging does not affect the function of the protein.[48]

Fluorescence resonance energy transfer (FRET) is another fluorescence based method to analyze protein interactions.[176] measures energy transfer between fluorophore pairs attached to proteins.[186] Due to this energy transfer between donor and acceptor, some of the energy absorbed by the donor is emitted. The efficiency of this energy transfer is the fraction of the photons absorbed by the donor to the photons transferred to the acceptor. This efficiency (E) is formulated as follows

$$E = \frac{{R_0}^6}{{R_0}^6 + r^6} \quad (2.9)$$

where r is the distance between two fluorophores and R_0 is Förster distance which is unique to the donor-acceptor pair. Förster distance depends on spectral overlap between fluorophore pairs, quantum yield of the donor, refractive index of the reaction medium and orientation of the dipole moment of the molecules. Since this efficiency depends on molecular distance, FRET can measure a complex formation and conformational changes in the 1-10 nm range. This spatial resolution value exceeds diffraction limits of an optical microscope. The energy transfer efficiency is evaluated by estimating the relative fluorescence of the donor fluorophore in the presence or absence of acceptor fluorophore.

However, in vivo imaging, the determination of donor levels in the presence and absence of acceptor is difficult. [138, 187] Filter-based FRET, spectral imaging, acceptor photobleaching, lifetime measurements are some of the methods that employs FRET. The choice of optimal fluorophore pair is a critical consideration for FRET methods. CFP/YFP, BFP/GFP,and BFP/EGFP are common FRET pairs.[176]

Fluorescence polarization (anisotropy) is another way to detect binding constant which monitors the rotational motion of proteins bearing a covalently attached fluorescent group. Rotational correlation time of the molecules depends on their sizes. An idealized 2400 Da molecule has a 1 ns rotational motion time. An rotational motion time increases as the size of the molecule increases. The rotational motion time is calculated using fluorescence emission at parallel and perpendicular planes following excitation with a plane-polarized light.[48]

Bioluminescence resonance energy transfer (BRET) is another alternative method which utilizes a fluorophore acceptor and RET donor. In the method, luciferase catalyzes the oxidation of luciferin to emit light. The energy of the reaction is transferred to the fluorophore if the donor and acceptor are at close proximity up to 50Å. The method eliminates light excitation, photodamaging, photobleach and autofluorescence problems.[188-189]

Other Methods

If proteins form a complex, they are expected to colocalize within the same physical conditions. Confocal microscopy is used to measure the colocalization of the proteins. In the method, the interested protein and ligand are expressed with tagged using plasmid transfection into cells. The cells are fixed and screened with different primary antibodies directed against the tags, individually. Later, the fixed molecules are treated with secondary antibodies specific to different primary antibodies. Each secondary antibody is fused with a different fluorophore tag. If the proteins are colocalized on the immobilized surface, the

fluorophores, which display different emission maxima, are expected to colocalize. However, if tagging may alter binding and localization properties, the accuracy of the method may decline.[133]

Fluorescence Correlation Spectroscopy (FCS) measures the fluorescence intensity fluctuations due to diffusion and conformational changes of fluorescent tagged molecule via confocal microscope. With the methods, diffusion rate, aggregate formation, rotational dynamics of the labeled molecule can be estimated via polarized light. This method does not provide spatial information of labeled proteins in vivo but it studies in vivo and in vitro molecular interactions. When a fluorophore diffuses into the interrogated volume created by confocal microscope, multiple cycles of excitation and emission start a burst of electrons until fluorophore leaves the interrogated volume. The burst is correlated with the diffusion rate which depends on size of molecule which changes with binding events. Dimerization is difficult to detect since it triggers insignificant amount of the diffusion rate change.[190-191]

Isothermal titration calorimetry is an equilibrium method to investigate protein interactions via heat changes caused by the interaction of molecules in solution without need of labeling and immobilization.[192] For each successive complex formation event for different analyte concentrations, a heat output is recorded until a binding isotherm is formed. The analysis yields Gibbs free energy, entropy and heat capacity. The method is advantageous since it provides real equilibrium values; however, it requires high amount of sample.[155]

Surface Plasmon Resonance

Affinity biosensors are developed to analyze ligand-protein, protein-protein interactions and to calculate their kinetic data.[31, 150] In the last decades, the affinity biosensors developed rapidly. An affinity biosensor consists of an electrochemical, piezoelectric or optical transducer and a biological recognition element to interact with the analyte.

Fluorescence spectroscopy, interferometry, grating couplers, resonant mirror and surface plasmon resonance are examples of biosensors. Fluorescence based biosensors are highly sensitive; however, label requirement, multi-step detection protocols reduced its effectivity.[193]

Rich and Myszka argue that surface plasmon resonance may arouse three emotion which are bewilderment since you cannot believe such kind of a technology exists or love since you are very fascinated by the technology. Or you hate since you think that this technology does not work.[194] This chapter introduces surface plasmon resonance technology for you to decide how you feel about surface plasmon resonance.

Surface plasmon idea was launched at 1902 when a polychromatic white light was irradiated on a ruled metallic gratings which yielded an illumination with narrow dark bands, anamolies, in the spectrum of the diffracted light.[195] The surface plasmon phenomena was further improved by Rayleigh[196] and Fano.[197] In 1968, the drop in reflectivity in different attenuated total reflection method after illumination thin metal films on a substrate was explained by excitation of surface plasmons by Otto, Kretschmann and Raether.[198-199] In 1970s, surface plasmon phenomena was firstly employed for thin film characterization.[200] In 1983, surface plasmon resonance application was firstly demonstrated in the pursuit of label-free, real-time detection of biomolecular interactions by Liedberg.[35] In mid-1980s, optical transducer principles such as ellipsometry, surface plasmon resonance and interferometric principles gained popularity to investigate biomolecular binding events.[201]

Surface plasmon sensing is a research tool for environmental monitoring, pharmaceutical development and clinical analysis. SPR is a refractrometric device and it investigates surface events using evanescent waves. [55] SPR provides thermodynamic and kinetic parameters of biochemical binding events which increase the understanding of protein interactions and provides a detection range of affinities to utilize at different protein

interaction methods for interested protein pairs.[138] SPR platforms can be classified through three modulation approaches such as angular, wavelength and intensity. [55]

The performance of an SPR is characterized with sensitivity and resolution. Sensor sensitivity is the ratio sensor output change to the change in measured quantity. Resolution is the smallest change in the bulk refractive index that generates a detectable change in sensor output.[202]

A typical SPR experimentation and sensogram

A typical optical biosensor contains a flow cell, injection loop sensor chip, liquid handling system, optical detector system, electronics, software and its user interface. [203] Inside the flow cell, liquid sample and buffer flows over the sensor chip which is coupled with receptors. The samples such as analyte or ligand are injected into an injection loop from the injection port. [203] The ligand is covalently immobilized to the sensor chip to form a biospecific surface using various immobilization techniques. Later, analyte with various concentrations at a constant flow rate is passed over this biospecific surface for complex formation.[204] Sample injections are performed by the help of an injection valve. It switches access of injected sample and the buffer flow from the buffer reservoir to the flowcell. Using the injection valve, sample is flowed over the immobilized surface for a defined time to obtain a sensogram. The excess sample flows into the waste reservoir since sample flows with a constant flow rate. The sample flow is ceased by switching injection valve to a load position and buffer starts to flow into flow cell with a definite constant flow rate from the buffer reservoir.[203] A typical SPR biosensor experiment contains association, dissociation and regeneration phases after covalent attachment of one reactant to the surface. [29-30, 205-206]

In the association phase, the analyte is injected over the immobilized surface for complex formation. As analyte forms complex with the immobilized ligand on the sensor surface, the refractive index of the liquid over surface increases.[204] After analyte injection for association, analyte flow is ceased and buffer is flowed over the surface for dissociation of

analyte from the immobilized surface. Complex dissociates and the refractive index of the liquid over surface decreases.[204] In SPR, the refractive index change is measured in close proximity to the sensor surface, nearly 300 nm. A flow cell is around 20-60 nL volume from which an aqueous solution passes with a defined flow rate between 1-150 μL/min.[154] The optical detector monitors the changes in SPR signal during binding events; the exchangeable sensor chip provides the surface that the biomolecular interaction occurs while liquid handling system controls the buffer and sample flow. The usual geometric configuration of a biosensor contains 50 nm layer of gold thin layer between a glass layer and the buffer or sample in liquid phase.[203] The monochromatic light with 830 nm wavelength travels through the prism and strikes back at the gold coated surface at the angels greater than critical angle. In SPR system, the reflected light is emitted by the sensor's light emitting diodes. Later, this light strikes to metal coated SPR surface and reflects from the mirror on top of the sensor. The light strikes a linear diode array. The each specific incident angle have a specific position along the diode array; therefore, reading array gives a reflectivity measurement depending on the angle. The reflectivity measurement is used to analyze binding events.[203] The changes at SPR angle is monitored in real time for a defined time course for association and dissociation phases. For a definite analyte concentration, the changes in SPR angle are plotted as a sensogram. A sensogram is a curve which plots the reaction data as response unit versus time. Many cycles of experimentation for various analyte concentrations are performed and each cycle yields a sensogram. Several sensograms for different analyte concentrations are superimposed to yield SPR Data. [204] In association phase of a sensogram, the response unit increases for a while until it reaches to a plateau region which is the point where steady-state gain is attained. In this dynamic equilibrium state, association rate of analyte is equal to dissociation rate of the analyte. However, due to limited time of association phase. Some curves may not react that planar region since they require more time to reach steady-state

condition. These curves usually for lower analyte concentrations compared to analytes which attained steady-state condition during pseudo first order reaction within the definite time gap. In dissociation phase where the sample flow replaced with buffer flow, the analyte dissociates from the surface and sensogram experiences an exponential decline for one-to-one mechanisms. For complexes which have a very slow dissociation rates, the surface may need to be regenerated. Degradation must not completely degrade the surface while dissociating the analyte from the surface rapidly. [204] In regeneration phase, a regeneration reagent brings signal back to the initial baseline by dissociating remnants of analyte on the surface.[205-206] When sensograms are fit to the mathematical reaction models using global fitting or local fitting, the kinetic constants and the binding constant can be calculated.[204]

To obtain high quality data via SPR, sample preparation is a critical consideration. The analyte and the ligand should be in monomeric forms to conform one-to-one reaction kinetics. The solution of the analyte buffer should be same with the running buffer which is used to establish the baseline. If the solubility of the analyte in the buffer is low, a concentration stock solution in another buffer can be diluted with the running buffer or small amount of an organic solvent can be added to the solution. The same amount of this organic buffer must also be added to the running buffer to eliminate unwanted refractive index changes.[204] The injected sample concentrations must vary over a wide range at least 100 fold. For a more accurate data, the injection order of the analyte must be arranged from lowest concentration to highest. This arrangement eliminates unwanted adsorptions and carry-overs. Also to check the reproducibility, the same analyte concentration must be injected twice. [204]

Instrument cleanness is another critical factor for data quality. [204] The sensor priming must be performed regularly. Before experimentation, baseline drift must be minimized up to one RU per minute. To perform control experiments via injection buffer is important to

ensure stability of the system.[207] During experimentation, small air bubbles and contaminant particles must be avoided from flow system to increase the quality of the data.[154]

Another important criteria to obtain reliable reaction data is to configure the appropriate concentration of immobilized compound to eliminate nonspecific binding, steric hindrance, crowding and aggregation.[29, 202, 204, 207] The smallest amount of the material is aimed to immobilize for kinetic studies to minimize mass transfer limitation effect while maintaining the necessary signal to noise ratio. Mass transfer limitation will cause the rate of mass transfer to be slower than the reaction rate; therefore, the mass transfer will be a rate limiting factor and reduce the data quality and accuracy of the analysis with one-to-one reaction assumption.[204] Additionally, coupling of ligand to the surface must be stable.[207] The stability of the immobilization can be enhanced by multiple adsorption technique. This technique increases the irreversible protein clusters on the surface which increases reacting surface area. However, this technique may increase the binding proteins at a given time compared to one step immobilization procedure which may trigger mass transfer limitation.[136] To use a reference surface may eliminate the adverse effects of bulk refractive index changes, matrix effects, nonspecific binding, injection noise and baseline drift on SPR data.[207]

Flow rate adjustment, washing steps to regenerate of remnants of analyte on the surface, blank injections, replicating experiments are also important to increase the data quality.[207] If any remnants of analyte stay on the bioactive sensor, for more accurate results, the surface must be regenerated via regeneration solutions. Acetonitrile is highly hydrophobic regeneration solution as well as ethylene glycol. 10-100% Ethanol is also utilized as regeneration solution; however, it may denature the proteins like 10-100 mM NaOH. 10 mM Glycine NaOH provides regeneration for intermediate interactions. 10- 1000 mM HCl and 1-20% Formic acid, 0.01-2M Glycine-HCl at pH 2-3 are mild degeneration solutions

and they are highly recommended. 0.01-20% SDS is good in combination with HCL or NaOH. 10 mM HEPES-NaOH at pH values lower than 9, 1M NaCl are good regeneration solutions for weak interactions. 6M Guanidine chloride, 2-4M $MgCl_2$ are ionic regeneration solutions. Phosphoric acid as a strong acid and 8M urea can be utilized for high affinity protein-protein interactions.[208]

The degree of nonspecific binding and unadjusted surface parameters may affect the data. To interpret the sensogram data correctly, constant concentration of analyte over surface must be maintained and sample switching must be purified from carry-over effects. Also mere refractive index effects close to the surface should be discriminated from refractive index changes related to binding events. To use a reference surface is useful to discriminate the signals results from refractive index changes between sample and running buffer. Reference signal compensate for refractive index effects of long term baseline drift and unwanted cyclic events such as filling pumps. Therefore, the quality of the data is increased. The existence of nonspecific binding can be analyzed by injecting buffer among sample injections and comparing sensograms of buffer injections with sensograms of analyte.[31]

Electromagnetic Theory behind SPR Biosensors

Surface plasmons are quanta of plasma oscillations at the interface of a metal and a dielectric. If the thickness of the metal film exceeds the plasmon skin depth, independent surface plasmon modes are sustained.[209] A surface plasmon polarization is an electromagnetic wave. This wave is a transverse-magnetic wave which is a magnetic vector perpendicular to the direction of propagation and parallel to the interface plane. [193] It is characterized with a propagation constant and electromagnetic field distribution.[193] To understand electromagnetic theory of optical waveguides, Maxwell's electric field and magnetic field equations is solved via the modal method through appropriate boundary

conditions at isotropic conditions at zero medium charge density and zero current density to obtain the electric and magnetic field vectors. They are expressed as modal field which is a finite sum of bound portion of power along the waveguide and the power that is radiated from the waveguide. The equations can be bounded by specific number of homogeneous media with defined electrical permittivity and refractive indices. Solutions of these equations are plane waves which describes polarization, propagation direction (β) and angular frequency of the field (ω). [209] The wave equation reveals a dispersion relation between the magnitudes of polarization vector and angular frequency. In an interface of two media with opposite signs of dielectric constants such as metal and dielectric material, the light enters one of the materials refracts depending on a dispersion relation. The propagation constant of a surface plasmon wave is defined by

$$\beta = \frac{\omega}{c} * \sqrt{\frac{\varepsilon_M * \varepsilon_D}{\varepsilon_M + \varepsilon_D}} \quad (2.10)$$

where c is the speed of light in vacuum, ε_M and ε_D are permittivities of metal and dielectric material, respectively. [209 54, 193] This equation explains a surface plasmon wave only if ε_M is negative and its absolute value is smaller than ε_D. [193] At optical wavelengths, this condition holds for many metals including gold. [193] The electromagnetic field of surface plasmon wave is confined at metal-dielectric interface and it is distributed into metal and dielectric media in an exponentially decreasing manner. This surface plasmon resonance distribution is sensitive to the refractive index of the dielectric media which underlies the affinity biosensor working principle. As refractive index of the dielectric medium increases, propagation constant of the wave along metal surface increases. The propagation constant change in metal medium is measured by optical means.[193]

The propagation length, penetration depth of surface plasmon wave into metal surface and dielectric is metal and wavelength specific in the visible and near-infrared spectral regions. For a gold surface, at 630 nm wavelength, propagation length is 3μm, penetration depth

into metal is 29 nm, penetration rate into dielectric is 162 nm and concentration of field in dielectric is 85%. At 850 nm wavelength, propagation length is 24μm, penetration depth into metal is 25 nm, penetration rate into dielectric is 400 nm and concentration of field in dielectric is 94%.[210]

According to the Perturbation theory, if the complex formation occurs within whole depth of surface plasmon wave, binding induced refractive index change, Δn, changes propagation constant.

$$Re\{\Delta\beta\} = k * \Delta n \quad (2.11)$$

where k is free-space wavenumber.

However, if the binding event occurs at a distance from the surface much smaller than the penetration depth of surface plasmon wave, the correlation differs

$$Re\{\Delta\beta\} = F * k * \Delta n \quad (2.12)$$

Where F represents the fraction of surface plasmon resonance probed the interaction.[193, 211]

An SPR optical biosensor typically contains an optical system, a transducing medium which combines optical domain and biochemical domain and an electronic system. Transducing medium and optical system determined the stability, sensitivity and resolution of the sensor.[193]

In a typical surface plasmon resonance, surface plasmon wave is excited by an optical wave by resonant transfer. The momentum of the incident optical wave should match the momentum of surface plasmon wave. [193] Therefore, many methods were developed to optically excite the plasmons. The fundamental methods to optically excite surface plasmons are the attenuated total reflection (prism coupling), diffraction on a metallic grating (grating coupling) and evanescent wave coupling between dielectric and plasmonic waveguides(waveguide coupling). [54, 193]

In attenuated total reflection method, Kretschmann geometry is widely used in SPR. At this configuration, a light wave is reflected at the interface between a prism coupler and a thin metal layer.[193] Total internal reflection occurs where light is reflected at the interface of an optically dense medium such as glass and a less dense medium such as buffer while traveling through the optically dense medium. This reflection occurs when the incidence angle of light is greater than the critical reflection angle specific for the medium pair. If the incident light is monochromatic and plane polarized and a thin metal is present at the interface between two medium, the evanescent wave, a component of incident light momentum, interacts with the oscillating electrons in the metal film surface. The oscillating electrons are also called plasmons. The term plasmon refers to a classical optics or electromagnetic theory including light reflection, transmission and absorption. It is quasi-particle representation of plasma frequency. In plasma oscillation, the free electrons of metal surface oscillate in cooperation when the positive charge of metal bind of the free electrons. The surface plasmon resonance occurs only at a specific incident angle.[36, 202] In this incident angle, the reflectivity of light is zero and the surface plasma wave of metal surface couples to part of the incident light. This angle is called SPR angle and it is sensitive to the refractivity of the sample at the close proximity to the surface. As a result of surface plasmon excitation, the reflection spectrum of light exhibits a dip at a specific wavelength.[212] As reaction occurs in the reaction chamber, the refractive index of the buffer changes at the close proximity to the SPR chip surface[36]; therefore, the dip in light reflectivity shifts in wavelength[212] combined following resonance angle change. Since some of the reflected light lost by coupling to the evanescence wave, the reduced reflected light intensity is detected and quantified by the instrument.[36] By continuously monitoring the refractive index change by means of changes in resonance angle, refractive index change is recorded as resonance units and plotted against time to obtain a sensogram.[36] The

angle change is converted to resonance units (RU) where 1000 RU response corresponds to 1ng/mm^2 surface concentration change of bound molecule in the surface.[29, 204]

The refractive index change due to complex formation via following correlation[202]

$$\Delta n = \left(\frac{dn}{dc}\right) * \frac{\Gamma}{h} \quad (2.13)$$

where Δn is refractive index change, $\frac{dn}{dc}$ is refractive index change of analyte molecule (ranging from 0.1-0.3mL/g usually), Γ represents surface concentration in mass/area and h is the thickness of thin layer where binding events occur.

Applications, Pros and Cons of SPR Technique

Surface plasmon resonance sensors have wide range of applications. Surface plasmon resonance sensors have been used for physical quantities such as displacement measurement[213], angular position[214], humidity[215] and temperature[216]. It has also been used for chemical sensing and biosensing applications.[54, 217-219] SPR biosensors are utilized in food safety to detect foodborne pathogens such as Salmonella enteric[220] and toxins such as staphylococcal enterotoxins.[203] The SPR also utilized in medical diagnostics such as cancer markers[221] and heart attack markers and antibodies against specific viruses.[222-224] Environmental monitoring is another application area that SPR is engaged such as detection of pesticides.[225]

By using SPR sensor, absolute quantitative analysis of binding amounts can be calculated, kinetic and equilibrium studies to detect affinity and enthalpy can be performed. The affinity range of SPR varies from high affinity interactions with equilibrium constants lower than 10nM to weak affinity interactions with equilibrium constants higher than 100μM.[154]

Swedish BIACORE of GE Healthcare launched first commercial SPR biosensor in 1990.[194] Later, the BIAcore sensor technology improved with several models. Analytical μ-

systems, Biosensing Instruments, DKK-TOA, Autolab of EcoChemie, IBIS, K-MAC, Neosensors, Optrel, Resonant Probes, Thermo Scientific, Alphasniffer, Bio-Rad, Genoptics of horiba, Farfield Sensors, ForteBio, maven Biotechnologies, Silicon Kinetics,[226] Bio TuL Bio Instruments GmbH in Germany, Xantec Analysensysteme GbR in Germany and EBI Sensors in USA are some of the manufacturers of various SPR biosensors.[193] Additionally, Texas instruments in USA launched SensiQ Technologies.[34, 193, 226] The commercially available biosensor technologies are usually complementary but not competing each other since they reply different requirements in biochemical studies.[194]

The binding affinity including the equilibrium constant and Gibbs free energy of binding, stoichiometry of the reaction, binding kinetics defines characteristics of biomolecular interactions.[204] Surface plasmon resonance is a powerful method to investigate protein interactions since the system measures the refractive index or mass changes at the sensor surface as complex formation happens in real time.[204] Binding constant and rate constants can be calculated from one data set easily.[31, 150] Since these biosensors offer a detailed information of binding affinities, technique is valuable for disease diagnosis, genetic screening and drug discovery.[150]

The experimentation is very simple and inexpensive.[50, 141] SPR provides a high speed for data analysis compared to other protein-protein methods. If the SPR instrumentation is coupled with auto-samplers, the instrument can run unattended and data quality and sample throughput increases. [194] No fluorescent and radioactive labels are required for kinetic analysis.[194, 227] Protein labels affect the structure and amphiphilicity of a protein which may greatly alter the binding abilities.[228] The regeneration of surfaces for reuse is another attractive property of SPR. Compared to other protein-protein interaction methods, SPR experiments requires low amount of material and works with a wide range of affinities. [133] [194] SPR provides kinetic measurements at wide range of chemical and physical conditions such as pH, temperature, ionic strength and chemical additives. Although SPR is an optical

detection technique, the measurements can be done using colored, opaque and turbid solutions.[176] In temperature controlled SPR models, the binding kinetics and affinities can be calculated at different temperatures easily.[194]

Surface plasmon resonance techniques are sometimes disadvantageous. To produce high quality data via SPR biosensors, the instrument requires robust detectors, robotics and fluidics plus efficient and reliable surface chemistries, software and customer support.[194]

Since the biosensor requires integration with optical components which increases the cost of operation. Molecules with molecular weights smaller than 2000 g/mol cannot be detected by SPR, since they yield only small changes of mass in sensor surface.[150] The method is good only for soluble proteins.[138] Additionally, fixed cost of purchasing a SPR instrument is high.[194] Also the shelf life of the sensor chip is limited depending on its functional chemical stability. The major drawback of SPR is the surface. The binding of receptor to a surface may affect the binding interaction of the receptor with the analyte if the experiment is poorly designed.[29] Since the measurements are done close to the surface, the values may not reflect bulk values.[133]

Kinetic considerations for Data Analysis

The rate equation of association phase for a one-to-one reaction is as follows and it is derived as explained in the following section. [29, 36, 141]

$$A+B \rightarrow AB \quad (2.14)$$

$$\frac{dR}{dt} = k_a * C_A * (R_{max} - R) - k_d * R \quad (2.15)$$

R_{max} is the total concentration of immobilized pairs. k_a ($M^{-1}s^{-1}$) and k_d (s^{-1}) are rate constants for association (forward) and dissociation (reverse) reaction phases, respectively. C_A is the concentration of analyte A.

Association part of the binding reaction equation is

$$\frac{d[AB]}{dt} = k_a * [A] * [B] \quad (2.16)$$

Dissociation part of the binding reaction equation is

$$\frac{d[AB]}{dt} = -k_d * [AB] \quad (2.17)$$

The observed rate of formation is as the sum of reaction rate equations

$$\frac{d[AB]}{dt} = k_a * [A] * [B] - k_d * [AB] \quad (2.18)$$

The concentration of immobilized ligand B is described according to time

$$[B]_t = [B]_{t=0} - [AB]_t \quad (2.19)$$

Substitution in above equation yields

$$\frac{d[AB]}{dt} = k_a * [A] * ([B]_{t=0} - [AB]_t) - k_d * [AB] \quad (2.20)$$

Complex formation of AB in real-time is proportional to SPR signal obtained. Therefore, AB can be replaced by R. Also, the concentration of analyte (A) is assumed to be constant within the flow chamber and depicted as C. The above equation is rewritten as follows

$$\frac{d[R]}{dt} = k_a * C * (R_{max} - R_t) - k_d * R_t \quad (2.21)$$

$$\frac{d[R]}{dt} = k_a * C * R_{max} - (k_a * C + k_d) * R_t \quad (2.22)$$

Following the same approach, the rate of dissociation is described by

$$\frac{d[R]}{dt} = -k_d * [R] \quad (2.23)$$

The sensogram is analyzed by fitting the curve to the directly integrated forms of the differential rate equations.

For association phase,

$$R_t = \frac{C*k_a*R_{max}*(1-e^{-(C*k_a+k_d)*t}}{C*k_a+k_d} + R_i \quad (2.24)$$

where R_i is the signal at the point of analyte injection (t=0)

For dissociation phase,

$$R_t = R_a * e^{-k_d*t} + R_{i(t\to\infty)} \quad (2.25)$$

where R_a is the amplitude of the dissociation process and $R_{i(t\to\infty)}$ is the baseline when dissociation is complete.

The sensograms can be analyzed through global analysis[141 31] or local analysis using a selected reaction model via commercially available kinetic analysis softwares.[205]

The SPR signal in a typical experiment contains effects of chemical association and dissociation processes and transport processes of diffusion and flow. One –to-one simple interaction model assumes analyte to be uniform and constant at bulk region and at the close proximity to the surface. Therefore, the analyte is assumed to constantly flow over the immobilized surface. This model also called as rapid mixing model.[30] However, the mass transfer rate may be slower than the reaction rate which yields mass transfer limitation which result in an unstirred layer above the surface.[29, 141]

The steps of the transport of analyte is macroscopic transport through the microfluidic system and across the surface, diffusion through nonstirred layer over the surface and diffusion the array of binding sites at the sensor surface.[29] Mass transfer limitation is failure to maintain a uniform analyte concentration over the surface.[29] Mass transfer limited model is simplified by dividing the reaction mechanism into complex formation following analyte transport to the surface. This model is called two-compartment model.[30] In two compartment model, the flow chamber is divided into two compartments: outer and inner compartment. In the outer compartment, the analyte concentration is constant and equal to the injection concentration. However, in the inner compartment where the binding event occurs, analyte concentration varies since analyte is transported between two compartments and it dynamically reacts with the surface.[160] Mass transfer limitation affects both association and dissociation phases of the binding event. For association phase, transport limitation causes local depletion of the analyte. The replenishment is also limited by mass transport limitation and since rate of dissociation is higher than transport rate, analyte rebinds to the available binding sites on the surface to yield an increased retention.[29]

Mathematical explanation of mass transfer limitation can be done as in the following correlations[31, 229]

$$A_0 \rightarrow A \quad (2.26)$$

$$A+B \rightarrow AB \quad (2.27)$$

$$\frac{dC_s}{dt} = k_T * (C_A - C_s) - k_a * C_s * (R_{max} - R) + k_d * R \quad (2.28)$$

$$\frac{dR}{dt} = k_a * C_s * (R_{max} - R) - k_d * R \quad (2.29)$$

where A and B are molecular species, AB molecular complex formed during the reaction. The differential equations represents binding curves within a sensogram. R represents molecular species formed while C_A is constant concentration of analyte A in M. C_s is the injection concentration of analyte A at the surface in mass transfer limited reaction model in M. R_{max} is the total concentration of immobilized pairs in RU. k_a and k_d are rate constants for association in $M^{-1}s^{-1}$ and dissociation in s^{-1}, respectively. k_T denotes transport coefficient which describes transport movement of analyte to the surface in cm/s.

The initial conditions for the binding phase of experiment are Cs=0, R=0 at t=0. If the association phase is sufficiently long, the steady state condition is reached in which $C_S=C_A$ and $R = \frac{K*C_A*R_{max}}{1+K*C_A}$. [30]

k_T is diffusion rate constant and it is averaged over the sensor surface. It depends on diffucion coefficient of the analyte, the dimensions of the flow cell and the flow rate.[141] Therefore, reaction kinetics should be slower than the rate of transport to eliminate transfer limitations.[30, 230] k_T can be calculated from following correlation in cm/s[230]

$$\langle k_T \rangle = 1.282 * \left(\frac{v_c * D^2}{h * l} \right)^{1/3} \quad (2.30)$$

where l is length of sensor surface and h is the height of the flow cell, D denotes the diffusion coefficient of the analyte and v_c represents the flow velocity in the center of flow cell.

For unit consistency k_T in cm/s is converted to s^{-1} as in the following correlation where 1RU=10^{-10} g/cm^2 [30, 230]

$$k_T\ (s^{-1}) = (1\ RU/M)\ k_T\ (cm/s) = (10^{-7}\ cm * g/mol)\ k_T\ (cm/s) \quad (2.31)$$

Later, for data analysis, as taking k_a, k_d, k_T and R_{max} as free parameters, the sensograms can be analyzed via nonlinear least-squares fitting to calculate the best fit values of these free parameters.[30]

For accurate estimation of reaction kinetics, the detection of the existence of mass transfer limitation is critical since in case of mass transfer limitation the obtained sensogram does not correspond to the simple reaction model. To determine the existence of mass transfer limitation the rate of transportation should be compared to rate of reaction. When k_a*R_{max} value is equal or bigger than k_T where k_a is in $M^{-1}s^{-1}$, R_{max} in M and k_T in cm/s, transport limitation occurs. [30] To check the existence of mass transfer limitation, flow rate experiments may also be conducted. The binding curves should be independent of flow rate if mass transfer is not a limiting factor.[31, 141]

Another method to understand the existence of mass transfer limitation is to calculate MTL (mass transfer limitation).[231] In this method, the binding rate is expressed as in the following correlation[231]

$$\frac{dC_s}{dt} = \frac{L_m * (C_A - C_s) - k_a * C_s * C_B + k_d * R}{h_{diff}} \quad (2.32)$$

$$\frac{dR}{dt} = k_a * C_s * C_B - k_d * R \quad (2.33)$$

where

$$h_{diff} = \sqrt[3]{\frac{D * h^2 * b * l}{F}} \quad (2.34)$$

where C_s is injection concentration of analyte in nM, C_B is ligand concentration at the surface, L_m are coefficients of Onsager for mass transfer in m/s, h_{diff} denotes characteristic height of the diffusion layer, D is the diffusion coefficient of analyte in the buffer in m^2/s, F is bulk flow rate in µl/min, h is height, b is width and l is length of the flow cell in m.

L_m depends on flow rate, flow cell dimensions and diffusion coefficient of the analyte. It can be calculated either by analysis of sensor data via given differential equations or via following equation after a correct estimation of flow cell lenght.[231]

$$L_m = C_{Lm} * \sqrt[3]{\frac{D^2 * F}{h^2 * b * l_2}} \quad (2.35)$$

where

$$C_{Lm} = 1.47 * \frac{1 - (\frac{l_1}{l_2})^{2/3}}{1 - \frac{l_1}{l_2}} \quad (2.36)$$

where l_1 and l_2 are the start and end point of complex formation within the total length of flow cell.

Mass transport limitation (MTL) is expressed as[231]

$$MTL = \frac{L_r}{L_r + L_m} \quad (2.37)$$

where L_r is Onsager coefficient of reaction flux (m/s). MTL varies between zero and one. When MTL is zero, no mass transport limitation exists. When it is one, the binding is completely dominated by mass transport.[231]

To eliminate mass transfer limitation, low surface capacity which is lower than 100 RU and high flow rates which is higher than 30μL/min can be preferred. High flow rate reduces the unstirred surface layer which obstructs mass transfer for association and dissociation phases.[141] An elegant way to eliminate mass transport limitation at dissociation phase is to add binding competitor to the dissociation buffer since competitor may block empty sites and may reduce retention time of interested analyte at the unstirred buffer layer over sensor surface.[29]

The reaction mechanism between molecules may deviate from one-to-one reaction mechanism not only due to mass transfer effects which yield rebinding of the analyte onto a surface but also immobilization heterogeneity, crosslinking effects.[227, 232-233] Parallel and competitive reactions can happen when the surface or the analyte is heterogeneous. Additionally, the conformation may change during reaction. All of these models are explained by different reaction rate equations.[31] The other reasons for deviation from one-to-one reaction kinetics are chemical and conformational impurity of samples, sample self-association and aggregation, crowding, steric hindrance, sample carry-over, injection noise, baseline drift noise, nonspecific binding of analyte and pH and temperature effects.[141]

The rate equations of association phase for models different than one-to-one simple reaction mechanism and one to one including mass transfer limitation are as follows[31]

Competing reactions

$$A+B \rightarrow AB \quad (2.38)$$

$$C+B \rightarrow CB \quad (2.39)$$

$$\frac{dR_1}{dt} = k_{a_1} * C_A * (R_{max} - R_1 - R_2 * p) - k_{d_1} * R_1 \quad (2.40)$$

$$\frac{dR_2}{dt} = k_{a_2} * C_c * \left(R_{max} * \frac{1}{p} - R_1 * \frac{1}{p} - R_2\right) - k_{d_2} * R_2 \quad (2.41)$$

Two state reaction

$$A+B \rightarrow AB \quad (2.42)$$

$$AB \rightarrow AB^* \quad (2.43)$$

$$\frac{dR_1}{dt} = k_{a_1} * C_A * (R_{max} - R_1 - R_2) - k_{d_1} * R_1 - k_{a_2} * R_1 + k_{d_2} * R_2 \quad (2.44)$$

$$\frac{dR_2}{dt} = k_{a_2} * R_1 - k_{d_2} * R_2 \quad (2.45)$$

where A, B and C are molecular species, AB, CB and AB* are molecular complexes formed during the reaction. The differential equations represents binding curves within a sensogram. R, R_1 and R_2 represent molecular species formed while A_o, C_A and C_C are initial or constant concentrations of analytes A and C. C_s is the concentration of analyte A at the surface in mass transfer limited reaction model. R_{max} is the total concentration of immobilized pairs. p is the normalizing factor for analyte molecular weight in the competing reaction. k_a and k_d are rate constants for association and dissociation, respectively. k_T denotes rate constant of mass transfer.

Surface Immobilization Methods

The sensor surface and the immobilization technique is important to obtain accurate results.[29] The goal is to couple the ligand to the sensor surface stably and in an active form.[205] A binding capacity up to 50 to 200 fold of instrument noise can be appropriate for kinetic experiments via SPR sensor which corresponds to 50 to 200 RU.[205] Immobilization orientation of the protein may not allow any binding since active site is hindered. Immobilized proteins may undergo denaturation upon adsorption. Also the surface may eliminate a conformational change which is essential for the biochemical activity.[234]

A protein can be immobilized on sensor chip directly or in a three dimensional matrix.[202] Proteins, small molecules or oligonucleotides may be attached to the surface via physical

adsorption[235], covalent attachment via hydrophobic and electrostatic groups via nucleophilic groups and electrophilic groups on the surface[235] and covalent attachment with pre-functionalized capture molecules on sensor surface via biochemical affinity reactions. [236] The most frequent functional groups on SPR sensor to provide immobilization are nucleophilic groups such as amines, thiol groups and electrophilic groups such as aldehyde and carboxylic groups. These functional groups on surface can be covalently coupled with molecules from their corresponding groups without a need of functional group derivatization. [236-237]

Direct immobilization on surface is more straightforward; however, the binding capacity is limited to the surface capacity due to steric hindrance caused by the molecule to be immobilized. Immobilization into matrix provides more binding sites and preserves the immobilized molecules during a prolonged storage.[202] In 1980s until the beginning of 1990s, physical immobilization of receptors on the surface was common via Langmuir Blodgett technique and electrostatic adsorption.[142] For physical adsorption hydrophobic or positively and negatively charged surfaces were used. The yield immobilized layer is usually heterogeneous in structure and orientation of proteins. Additionally, the Vroman effect, which is the exchange of soluble proteins during assay, makes noncovalent and nonspecific binding impractical.[234] Direct immobilization on the surface is performed via self-assembled monolayers of alkanethiolates and disulfides.[140, 238-239] To attain desired surface concentration and to create a non-fouling background, self-assembled monolayers of oligo(ethylene glycol) or functional group terminated alkathiolates were used. Oligo(ethylene glycol) termination reduces nonspecific binding.[239-240]

Many sensor chips are available nowadays from bare gold to lipid bilayers.[208] In most of the biochemical applications, a hydrophilic three dimensional non cross-linked carboxymetylated hydrogel is preferred. Any ligand can be coupled to the carboxy group on this type of sensor chip. [208] The carboxymetylated dextran surface, which is a flexible

matrix with a thickness around 100nm-400nm[29], and polycarboxylate layer covered sensor chips are widely preferred. [208] Density and thickness of this polymer on the surface are a critical factor which may block partitioning of large molecules and influence diffusion rate into the matrix, respectively. This matrix can be functionalized with different functional groups to allow different coupling chemistries. Dextran matrix provides a good access of immobilized protein to its ligate and a more efficient use of evanescent field. [29]

The commercially available hydrophobic and lipophilic sensors can be used to fuse liposomes or other vehicles to the surface to form a hybrid lipid monolayer. These surfaces provide opportunity to monitor protein-lipid interactions. This surfaces are stable and provides to opportunity to immobilize transmembrane receptors.[241]

Amine Coupling: A widely utilized immobilization method is activation of carboxy groups of dextran with N-hydroxysuccinimide (NHS) and N-ethyl-N' (dimethylaminopropyl) carbodimide (EDC) to form reactive NHS esters on the surface. NHS esters couples proteins to the surface from their amino groups.[29, 32] Amine coupling is easy to perform.[208] However, the immobilization must be carefully designed since the technique may result in protein denaturation and random coupling of proteins from their various lysine residues. Random coupling may affect the accessibility and reactivity of the binding site of immobilized protein.[29] This method employed at pH values 1 to 2 pH units below pI of the protein to avoid charge screening and to eliminate primary amines.[205] Also to immobilize acidic ligand via this surface chemistry is difficult since the carboxymethylated dextran is negatively charged.[236]

Coupling by thiol/disulfide exchange: This immobilization technique is frequently used for acidic proteins, for small peptides. The method is successful to maintain a specific orientation during immobilization. The immobilization is conducted via introduction of an active disulfide group on the sensor surface to react with thiol groups of ligand. Or, sensor surface can be derivatized by a thiol groups to react with disulfide groups of the ligand. The

protocol is selected depending on the situation of thiol groups and disulfide groups within the ligand. The presence of reducing agents fails the experiment since it breaks disulfide bonds.[205]

Aldehyde coupling: Aldehyde coupling is an alternative procedure for ligand immobilization to the sensor surfaces. Sialic groups or cis-diol groups of ligands are oxidized to aldehyde groups via sodium metaperiodate.[208]

Covalent immobilization is stable; however, it results in random orientation of immobilized proteins since a protein contains high number of functional groups to couple with the functionalized surface. Covalent immobilization may also impair the conformational structure of protein and its function. [202]

One of the chemical coupling methods is via streptavidin-biotin chemistry. This chemistry is called sandwich coupling and it is a type of indirect immobilization via capture molecules on the surface. This system is useful for nucleic acid immobilization and for molecules is difficult to immobilize due to its charge and activity.[208] The method follows biochemical affinity chemistry. The sensor chip surface can be modified with streptavidin or pre-made streptavidin sensor chips can be purchased. Later, a biotin conjugated molecule is flowed over the streptavidin modified surface. [31, 34, 204] Since biotin has a high affinity towards streptavidin, the biotin labeled molecule is strictly immobilized.[205] This method does not require preconcentration of protein in the matrix[29] and avoids exposure of proteins to pH values lower than their pI values.[29] However, since streptavidin coated surfaces are sticky, nonspecific binding must be carefully handled.[205] A streptavidin functionalization method of a sensor chip may be streptavidin coupling to EDC/NHS activated carboxymethylated dextran surface via amine coupling. For immobilization step, a biotinylated ligand is injected to couple with the streptavidin.[31, 205]

Additionally, antibodies can be immobilized via interaction between their Fc region and protein A or protein G. This method provides a successful access to the binding site of the antibody; however, orientation problems still prevail. [202]

Introduction of specific tags into ligands to couple with specific surface chemistries is another elegant of immobilization.[205] For instance, hexahistidine tagged proteins are coupled to surfaces with chelated Ni(II) ion.[242] The binding of GST fusions to glutathione-modified substrates is another tagging approach for surface coupling chemistries. However, GST and glutathione has a weak affinity towards each other, so, the immobilized protein may dissociate from the surface.[243]

Other methods for immobilization are DNA-directed immobilization[244] and interaction between histidine tagged protein and chelated metal ions,[202] hydrazide group coupling and sulfhydryl group coupling. [236] In the DNA-directed immobilization method, proteins are coupled with the chip contains stable patterns of single-stranded DNA.[202]

Chapter 3: QUANTIFICATION OF INTERACTIONS AMONG CIRCADIAN CLOCK PROTEINS VIA SURFACE PLASMON RESONANCE (SPR)

Materials and Methods

Apparatus and Reagents

For all experiments, two-channel SPR device SensiQ Discovery and COOH1 surfaces, which is a two dimensional carboxylated surface doped with polyethylene glycol to resist non-specific binding, were used. (ICx Nomadics, Oklohoma City, USA). All experiments were conducted at a flow rate of 50µl/min at room temperature. The circadian clock core loop proteins (BMAL1, CLOCK, PER2, CRY2) were generated using Baculovirus expression system. Single stranded oligonucleotides (template and complementary sequences) with EBOX sequence (CACGTG) were purchased. The sequence of the amine modified single stranded template oligonucleotide is 5'-(NH_2)-CGTCTAGATGCTTATGCTTATGGCACGTGGTACGTGGCCTAGGGGCG-3'while the sequence of complementary single stranded oligonucleotide is 3'-GCAGATCTACGAATACGAATACCGTGCACCATGCACCGGATCCCCGC-5'. The SPR buffer reagent was 1x Phosphate Buffered Saline (PBS) at pH 7.4. 1xPBS was prepared via 1:10 dilution of 10x PBS (80.0 g NaCl, 2.0g KCl, 14.4g Na_2HPO_4, 2.4g KH_2PO_4 in 1L H_2O) The hybridization buffer to anneal single stranded oligonucleotides into double stranded oligonucleotides contains 50 mM Tris and 20 mM NaCl. Surface activation reagents are NHS (N-hydroxysuccinimide) and EDC (N-(3-dimethylaminopropyl)-N'-ethylcarbodiimide hydrochloride). EDC and NHS was rapidly weighted and dissolved in water at 0.4 M and 0.1 M, respectively. They were divided into 50 µl aliquots and stored at -20^{o}C.

The proteins were stored at -20^{o}C within 50% (v) glycerol solution for long term storage. For short term (less than one day) use of proteins, the storage condition was

changed as 4^{o}C without glycerol. In order to remove glycerol, 6 hour dialysis with 3.5 kDa molecular weight cut off dialysis cassettes (ThermoScientific Slide-A-Lyzer, 3-12 ml capacity) was performed. Dialysis solution was filtered and degassed 1x PBS. The final concentration of proteins was measured at 280 nm using NanoDrop spectrophotometer (ThermoScientific NanoDrop Spectrophotometers).

The single stranded template and complementary oligonucleotide pellets were dissolved within filtered and degassed 1xPBS with 1μg/μl concentration and directly stored at -20^{o}C for long term storage. Prior to use, the oligonucleotide solutions were stored at 4^{o}C.

Storage Conditions

The proteins are stored at -20^{o}C within 50%(v) glycerol solution for long term storage. If the proteins will be used in the short term (less than one day), the storage conditions changed as 4^{o}C after 6 hour dialysis of proteins with 3.5 kDa molecular weight cut off dialysis cassettes (ThermoScientific Slide-A-Lyzer, 3-12 ml capacity). Dialysis solution is 1x PBS which is filtered and degassed. The final concentration of proteins was measured via A280 method. (ThermoScientific NanoDrop Spectrophotometers)

The single stranded template and complementary oligonucleotide pellets are dissolved within filtered and degassed 1xPBS with 1μg/μl concentration and directly strored at -20^{o}C for long term storage. Prior to use, the oligonucleotide solutions are stored at 4^{o}C.

Preparation of BMAL1:CLOCK, PER2:CRY2 and Ebox Complex

In order to prepare BMAL1:CLOCK and PER:CRY complexes, dialyzed proteins were mixed with equimolar amounts in filtered and degassed 1xPBS solution. The protein mixture was left for complex formation under constant stirring condition overnight at 4^{o}C.To prepare EBOX complex, firstly, equimolar amounts of single stranded template and complementary oligonucleotides with EBOX region were annealed within hybridization buffer. For annealing, 20 μl of 1 μg/μl DNA strands (40mer) were mixed with 160μl of

hybridization buffer. The mixture was heated up to 90^{o}C and slowly cooled to 25^{o}C with 1^{o}C per minute cooling rate using a Thermal Cycler. Later, heat shock was applied via reducing the temperature to 4^{o}C. The efficiency of annealing procedure was tested via running the annealed product with single stranded oligonucleotides at 2% agarose gel with EtBr dye. In order to produce BMAL1:CLOCK:EBOX ternary complex, BMAL1:CLOCK complex and double stranded oligonucleotide containing EBOX region was mixed at equimolar amounts for ten minutes at room temperature under constant stirring.[47]

Immobilization of Reagents

1x PBS is freshly prepared via dilution of 10xPBS with distilled water at room temperature just before the experimentation started. The buffer is filtered through 0.2µm surfactant-free cellulose acetate (SFCA) filters to eliminate blockages in the instrument via reducing particle load. The solution degassed just before the experiment starts via fifteen minutes of incubation within a vacuum pump, fifteen minutes of sonication and ten minutes of centrifugation at 900rpm to eliminate small bubbles which may block buffer flow during experimentation. The pH of the buffer confirmed as 7.4 via MeserLab PHM210 standard pH meter. The reagent to be immobilized (BMAL1, PER2, CLOCK, BMAL1:CLOCK, EBOX Complex) is diluted to the desired concentration in filtered and degassed 1xPBS solution. After equilibration of the instrument with 1x PBS, for immobilization, the carboxylated surface was cleaned with 100µl 0.1M HCl at 50µl/min flow rate. After several washing steps, 5µl EDC and 5µl NHS were mixed in 900µl distillated water and 100µl of this solution immediately injected at 50µl/min flow rate to activate carboxyl groups at the surface. The 150µl of ligand is injected through surface with 5µl/min flow rate. The system is allowed to equilibrate at 50µl/min.

Assay Design

The interaction between circadian clock proteins was analyzed in three separate sets. In the first set of experiments, pairwise interactions of circadian clock proteins (BMAL1, CLOCK and PER2, CRY2) were analyzed through immobilization of CLOCK and PER2 as ligand and injection of analyte (BMAL1, CRY2) through the immobilized surface. In the second set of experiments, BMAL1:CLOCK complex is immobilized as the ligand and PER2, CRY2 and PER2:CRY2 proteins were injected as analyte through the surface to analyze complex interactions of clock proteins. On the third set of experiments, EBOX complex is immobilized onto the surface and PER2, CRY2 and PER2:CRY2 proteins were injected as analyte through the surface. The injection was performed at 50 µl/min. During one cycle of association and dissociation, the system was waited to equilibrate for 60 seconds. For another 60 seconds, the analyte was injected through the surface. At the end of 60 seconds, the analyte injection was ceased and the buffer flow was initiated to dissociate the complex. These cycles were performed for various concentrations of analyte which were prepared via serial dilution with filtered and degassed 1x PBS. Injection was repeated with the same analyte, in order to ensure reproducibility. The assay design includes a reference channel and buffer injection through immobilized surface between each analyte injection as a blank measurement.

Kinetic Measurements

SPR data can be fitted to a preferred model of reaction mechanism. The simplest model assumes that one ligand reacts directly with one analyte molecule which is called pseudo-first order kinetics. In the model, binding sites are assumed to be equivalent and independent. The rate equation of complex formation for a simple one-to-one reaction is as follows:[29, 34, 208, 245]

$$A+B \leftrightarrow AB \tag{3.1}$$

$$\frac{d[AB]}{dt} = k_a * [A] * ([B]_{t=0} - [AB]_t) - k_d * [AB] \tag{3.2}$$

Complex formation of AB in real-time is proportional to SPR signal obtained. Therefore, AB can be replaced by R. Also, the concentration of analyte (A) is assumed to be constant within the flow chamber and depicted as C. Where $0<t<t_0$, the above equation is depicted as follows

$$\frac{dR}{dt} = k_a * [A] * (R_{max} - R) - k_d * R \tag{3.3}$$

For $t>t_0$The rate of dissociation is described by

$$\frac{d[R]}{dt} = -k_d * [R] \tag{3.4}$$

t_0 is the time when the association phase ends and dissociation phase starts since analyte injection was ceased. R_{max} is the response at complete saturation of the immobilized binding sites. Rate constants for association (forward) and dissociation (reverse) reaction phases are denoted as k_a ($M^{-1}s^{-1}$) and k_d (s^{-1}) , respectively.

Local analysis was performed on each sensogram within a SPR data to calculate R_{max}, k_d and k_a. The sensograms were analyzed by fitting a curve to SPR data through the directly integrated forms of the differential rate equations via SensiQ Discovery Data Analysis Tool and MATLAB CurveFittingTool.

For association phase,[34]

$$R_t = \frac{C*k_a*R_{max}*(1-e^{-(C*k_a+k_d)*t}}{C*k_a+k_d} + R_i \tag{3.5}$$

where R_i is the signal at the point of analyte injection (t=0)

For dissociation phase,

$$R_t = R_a * e^{-k_d*(t)} + R_{i(t\to\infty)} \tag{3.6}$$

where R_a is the amplitude of the dissociation process and $R_{i(t\to\infty)}$ is the baseline when dissociation is complete.

Mass Transfer Limitation Calculations

The SPR signal in a typical experiment contains effects of chemical association and dissociation processes and transport processes of diffusion and flow. One–to-one simple interaction model assumes that the analyte is assumed to be uniform and constant at bulk region and at the close proximity to the surface.[30] However, the mass transfer rate may be slower than the reaction rate which results in mass transfer limitation with an unstirred layer above the surface.[29, 141] For accurate estimation of reaction kinetics, the detection of the existence of mass transfer limitation is critical since in case of mass transfer limitation the obtained sensogram does not correspond to the simple reaction model.[30]

Mass transport limitation (MTL) is expressed as : [231]

$$MTL = \frac{L_r}{L_r + L_m} \tag{3.7}$$

where L_r is Onsager coefficient of reaction flux (m/s). MTL varies between zero and one. When MTL is zero, no mass transport limitation exists. When it is one, the binding is completely dominated by mass transport.[231]

L_r is Onsager coefficient of reaction flux (m/s) and is equal to k_a*[B].[231] L_m depends on flow rate, flow cell dimensions and diffusion coefficient of the analyte. It can be calculated with the following equation after a correct estimation of flow cell length.[231]

$$L_m = C_{Lm} * \sqrt[3]{\frac{D^2 * F}{h^2 * b * l_2}} \tag{3.8}$$

$$C_{Lm} = 1.47 * \frac{1 - (\frac{l_1}{l_2})^{2/3}}{1 - \frac{l_1}{l_2}} \tag{3.9}$$

where l_1 and l_2 are the start and end point of complex formation within the total length of flow cell, D represents the diffusion coefficient of analyte, F is the flow rate, h and b are dimensions of the flow cell.

The diffusivity of the proteins was calculated with Stokes-Einstein correlation:[246]

$$Do = \frac{k*T}{6*\pi*\eta*R_H} \quad (3.10)$$

where D_o represents diffusivity in water at a given temperature, η is viscosity of water ($6.915x10^{-4}$ nm/s^2), R_H is hydrodynamic radius, k is Boltzman's constant ($1.38x10^{-23}$ J/K), T is temperature (298K).

To calculate hydrodynamic radius of the proteins a power law which correlates molecular mass of the protein to its hydrodynamic radius for globular proteins was utilized,[247]

$$MW = 3.4{R_H}^{2.34} \quad (3.11)$$

where MW is molecular weight of the protein in kDa and R_H in nanometers.

Equilibrium Measurements

Equilibrium analysis was performed to determine the strength of the interaction of biomolecules. The analysis was performed via interaction of various amounts of analyte with immobilized surface sequentially and a sensogram was obtained for each injection. As analyte concentration increases, the plateaus of association step increase. These plateaus depict the dynamic equilibrium condition for the specific analyte concentration. The binding constant, time required to reach the equilibrium condition, can be calculated from the ratio of dissociation rate constant to association rate constant. [34, 153]

$$K_D = \frac{k_d}{k_a} \quad (3.12)$$

Results and Discussion

SPR technique was used to investigate interactions and quantify binding constant between circadian clock components. The sensograms obtained from clock component interactions are analyzed to calculate chemical rate constants and thermodynamic

equilibrium constants of the interaction for a specific analyte concentration. In order to analyze a sensogram, rapid mixing model via pseudo first order reaction mechanism approximation was selected. The experiments were conducted in three sets. The first set of the experiments included pairwise interactions between BMAL1 and CLOCK as well as between PER2 and CRY2 proteins. The second set considers the interaction of BMAL1:CLOCK complex with PER2, CRY2 and PER2:CRY2 complex, where in the third set the interaction kinetics and binding affinity between BMAL1:CLOCK:EBOX ternary complex and PER2, CRY2 and PER2:CRY2 were monitored. The gold coated surface was functionalized with carboxylic groups (COOH), which allowed immobilization of the ligand to the surface via amine coupling through activation of carboxylic groups with EDC/NHS chemistry.[29, 208] The surface also included triethoxy groups in order to minimize non-specific protein binding on the surface.[245] During SPR experiments, the baseline drift was carefully monitored in order not to exceed 1 RU per minute, so that higher accuracies would be obtained. The flow rate of 50 μl/min was selected for the experiments to minimize mass transport limitation.[29, 34, 56] SPR data is analyzed with QDAT Data analysis tool and the best fit curves were established using one-to-one simple reaction model.

The expression level and purities of circadian clock proteins were assayed via Western Blot technique and SDS-PAGE Silver Staining method, respectively by Kavakli Laboratory. The activities of circadian clock proteins were assayed via co-immunoprecipitation method prior to SPR experimentation kindly by Kavakli Laboratory.

Before starting SPR experiments, to establish SPR dip is critical to ensure that the normalization after chip replacement is done effectively and SPR geometry configuration is appropriate. In Figure 1, percent reflection against pixel number graph depicts the dip at Channel 1 with red color while depicting Channel 2 with blue color. The dips for two channels must be as convergent as possible. Since the refractive index of air is lower than the refractive index of 1x PBS, any bubbles may lead loss of SPR dip, inconvergent dip

and optical defects. After ensuring a convergent SPR dip, the experimentation was started. For further analyzing the stability of the system, a buffer injection assay was conducted at least three times until a reproducible sensogram is obtained for three subsequent buffer injections.

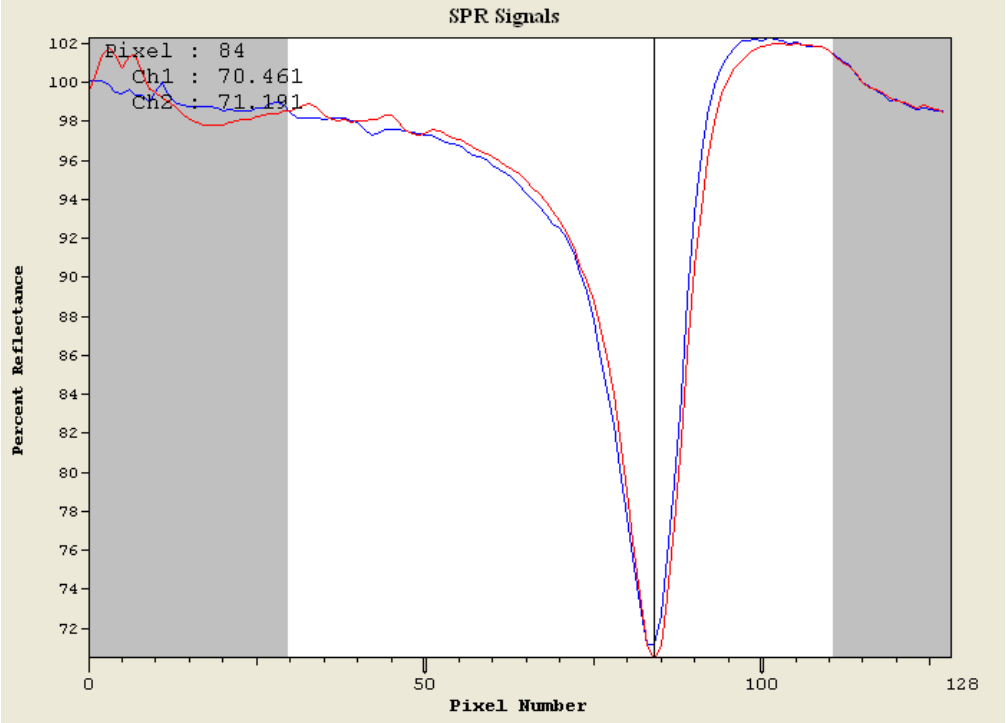

Figure 1. An Established SPR Dip

The absence of mass transfer limitation was confirmed with calculation of % MTL value for each binding pair. The required values for the calculation were given in Table 1 and the parameters calculated to obtain % MTL were tabulated with the section specific tables. The value of %MTL close to 0 indicates the complete absence of mass transfer limitation effect on reaction kinetics, where % MTL close to is 100 represents complete limitation of reaction kinetics with mass transfer. Since % MTL values calculated are all

Molecules	MW (kDa)	R_H (nm)	D (m^2/s)
PER2	136	4.83	0.445×10^{-10}
CRY2	67	3.57	0.601×10^{-10}
BMAL1	69	3.61	0.595×10^{-10}
CLOCK	95	4.15	0.517×10^{-10}
PER2:CRY2	203	5.74	0.373×10^{-10}
BMAL1:CLOCK	166	5.26	0.408×10^{-10}

Table 1. Molecular weight, hydrodynamic radius and diffusion coefficient of Core Circadian Clock Components

lower than 5%, the mass transfer limitation was neglected in data analysis [231] During %MTL calculation, diffusion coefficient of analyte was calculated via Stokes Einstein Equation. It was observed that the limitation for mass transfer increased as the size of the protein decreased. Since the globular form of a molecule represents the most compact structure, the analyte molecules were assumed to have globular structure. [205] Even if the molecule has a higher hydrodynamic radius than a globular protein, the mass transfer limitation effect is lower than the predicted amount with globular molecule assumption. This size effect on mass transfer limitation was also observed in our results. For both BMAL1:CLOCK and EBOX complex interactions with CRY2, CRY2:PER2 and PER2, the highest percent mass transfer limitation belongs to CRY2, which is the lightest analyte protein.

Characterization of annealing

The double stranded DNA and single stranded template and complementary oligonucleotides are runned at 2% agarose gel with EtBr to characterize the annealing procedure. In Figure 2, the second well contained hybridization solution, where the third

and fourth wells contained single stranded oligonucleotides as control. The single stranded oligonucleotides were visible in third and fourth wells at a specific band for their sizes. The second well did not contain any molecule at this specific band value. This result confirmed that annealing process was successful and that double stranded DNA could be used for EBOX experiments.

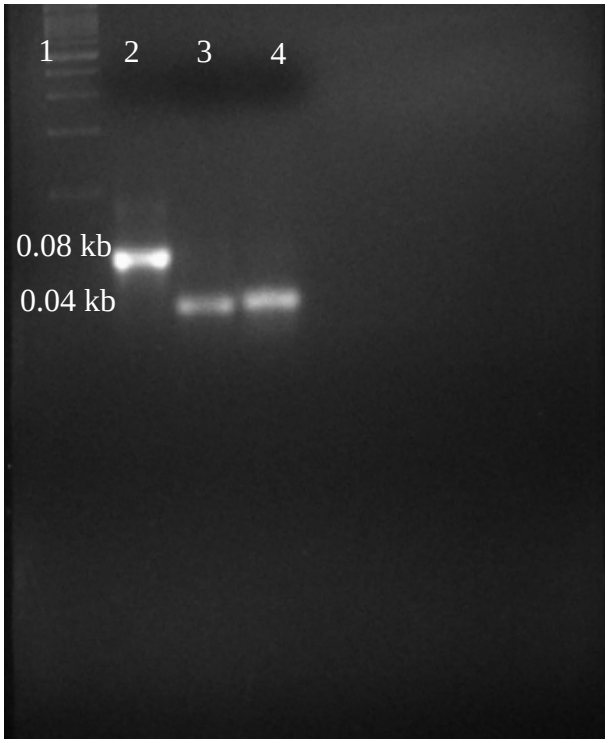

Figure 2. Characterization of DNA annealing via Agarose Gel Electrophoresis

Interaction of BMAL1 and CRY2

Pairwise interactions among clock proteins were analyzed as a control for the EBOX complex interactions in the pursuit of investigation of circadian clockwork kinetics and binding affinities.

In order to analyze interaction between BMAL1 and CRY2, BMAL1 was successfully immobilized onto the surface, and CRY2 protein as analyte was injected through the

surface. Figure 3 shows the binding interaction curves between immobilized BMAL1 and CRY2 within concentration range of 3.73- 37.3 nM. The injection concentration range for the analyte was kept wide enough so that a realistic estimation for interaction kinetics and binding affinity between BMAL1 and CRY2 proteins could be obtained. In the SPR data, as concentration of analyte increases, the plateau response unit also increases. The response

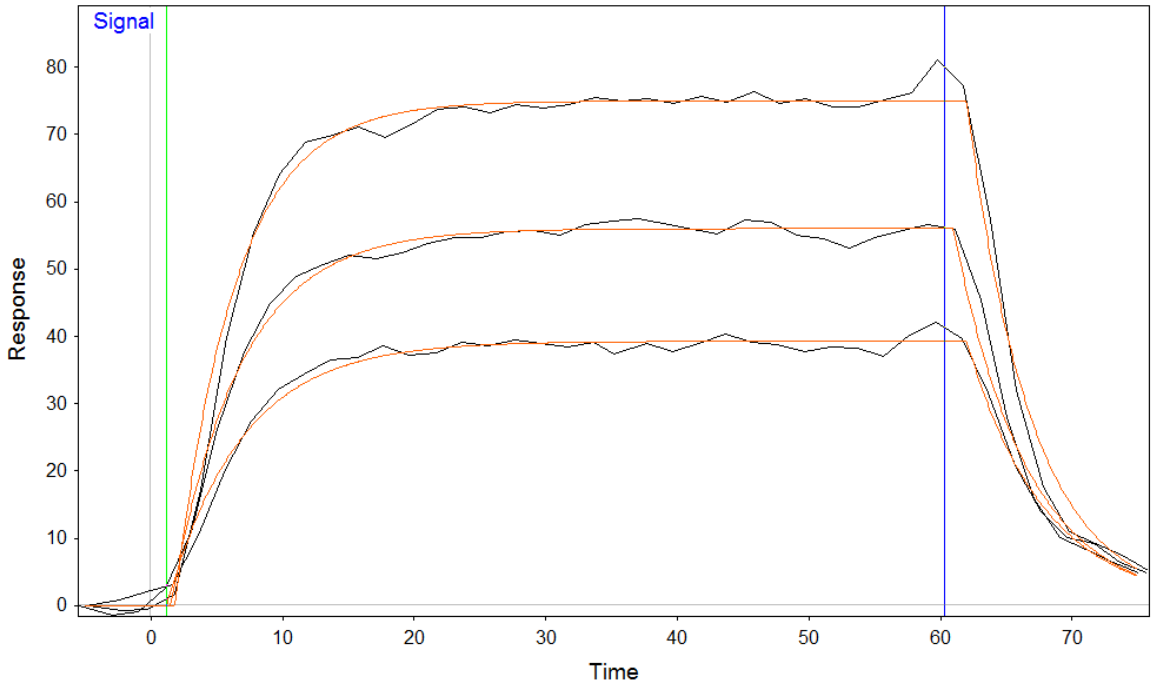

Figure 3. Response Unit vs. Time Graph for Interaction between BMAL1 and CRY2

versus concentration data ensures that the SPR signal in response units is directly proportional to analyte concentration.(Figure 4) A simple pseudo-first order binding interaction model (A+B=AB), which requires only three parameters, i.e. an association rate constant (k_a), a dissociation rate constant (k_d) and a maximum surface capacity (R_{max}), was fitted using Qdat analysis software. Reference surface data were subtracted from the reaction surface data in order to eliminate the refractive index change.

During nonlinear regression curve fitting, all fitted parameters were fitted as a local parameter. The analysis yielded an association rate constant ranging between $4.40x10^5$ $M^{-1}s^{-1}$ and $5.72\ x10^6$ $M^{-1}s^{-1}$. The dissociation rate constant of interaction of BMAL1 and CRY2 ranges between $0.17s^{-1}$ and $0.21s^{-1}$. The maximum surface capacity was calculated

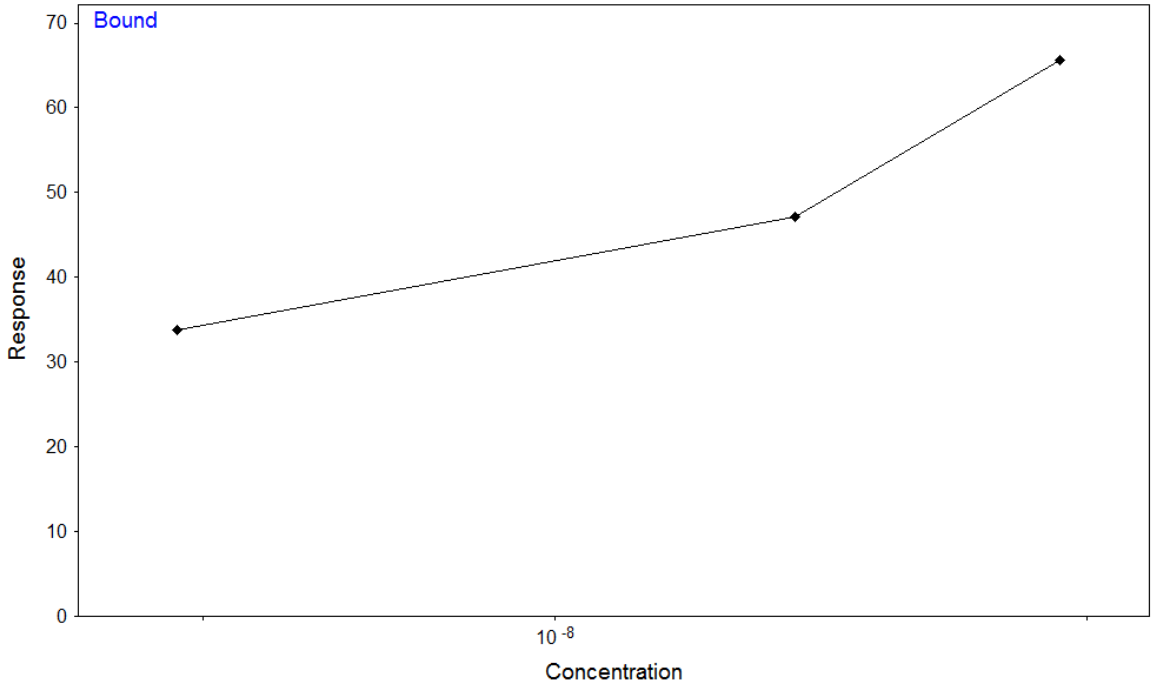

Figure 4. Response vs. Concentration Graph for BMAL1 and CRY2 Interaction

as 1000 RU. The binding constant K_D (k_d/k_a) of the interaction between BMAL1 and CRY2 was found within the range of 91.23 nM and 460.17 nM which indicate a small binding affinity. These data are tabulated at Table 2. The percentage of mass transfer limitation calculated was within 0.08-0.33 range (Table 3), which suggested that the effect of mass transfer on reaction kinetics can be neglected since below 5% %MTL, one-to-one simple model can be utilized instead of two compartment model.[248] Therefore, one-to-one simple kinetics assumption was found to be a valid assumption. Many studies suggest an

interaction between BMAL1 and CRY proteins via coimmunoprecipitation assay.[25-26, 42, 249-250]

Griffin et al. also finds a weak but reproducible interaction between BMAL1 and CRY2 via yeast to hybrid assay.[44] However, kinetics of binding or estimation of the binding constant has not been investigated before.

C (nM)	k_a ($M^{-1}s^{-1}$)	k_d (s^{-1})	K_D (nM)	Res SD
37.3	$4.40x10^5$	0.2025	460.17	2.724
18.7	$5.72x10^5$	0.1802	315.12	1.905
3.73	$1.85x10^6$	0.1691	91.23	1.287

Table 2. Binding Affinities and Kinetic Constants for BMAL1 and CRY2 Interaction

C (nM)	k_a ($M^{-1}s^{-1}$)	R_{max} (RU)	L_r (m/s)	F (μl/min)	L_m (m/s)	Calc %MTL
37.3	$4.40x10^5$	1000	$4.565x10^{-6}$	50	$5.841x10^{-3}$	0.08
18.7	$5.72x10^5$	1000	$5.934x10^{-6}$	50	$5.841x10^{-3}$	0.10
3.73	$1.85x10^6$	1000	$1.923x10^{-5}$	50	$5.841x10^{-3}$	0.33

Table 3. %MTL calculation for BMAL1 and CRY2 Interaction

To analyze the success of the nonlinear regression curve fitting with pseudo-first order approximation, residual standard deviation of the fitted curves from the actual data was calculated . The residual standard deviation ranges between 1.287 and 2.724 where the maximum attained SPR signal is 70 RU in the experiment. The residual standard deviation is found to be within 10% confidence gap. Therefore, fitted kinetic constants are good estimates of the true kinetic constants.

Interaction of BMAL1 and PER2

Next, BMAL1 was immobilized onto SPR sensor surface, and PER2 was injected at 3.73, 18.7 and 37.3 nM concentrations (Figure 5). The association and dissociation constants were calculated from the response unit versus time curves with one-to-one simple reaction mechanism approximation. Since calculated %MTL is lower than %5, mass transfer limitation was neglected (Table 5). [248] The percent mass transfer limitation was calculated between 0.26 and 1.70 and values were tabulated in Table 5. During analysis all fitted parameters were fitted as a local parameter. In the SPR data, as concentration of analyte increases, the plateau response unit also increases. The response versus concentration data ensures that the SPR signal in response units is directly proportional to analyte

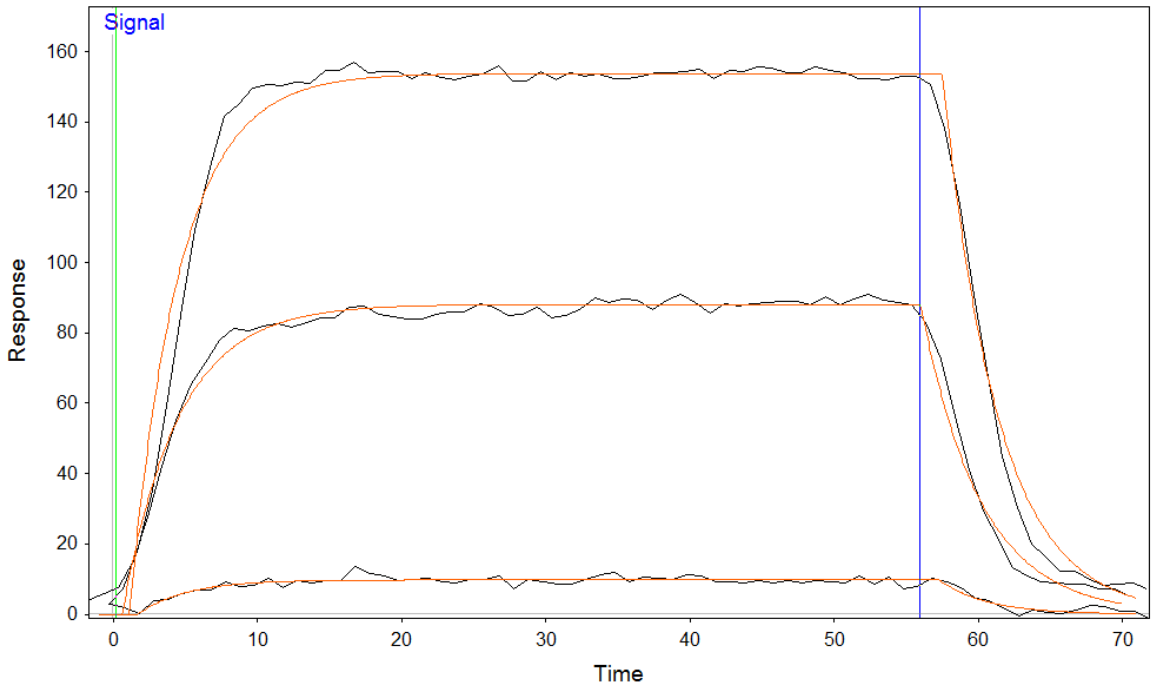

Figure 5. Response Unit vs. Time Graph for Interaction between BMAL1 and PER2

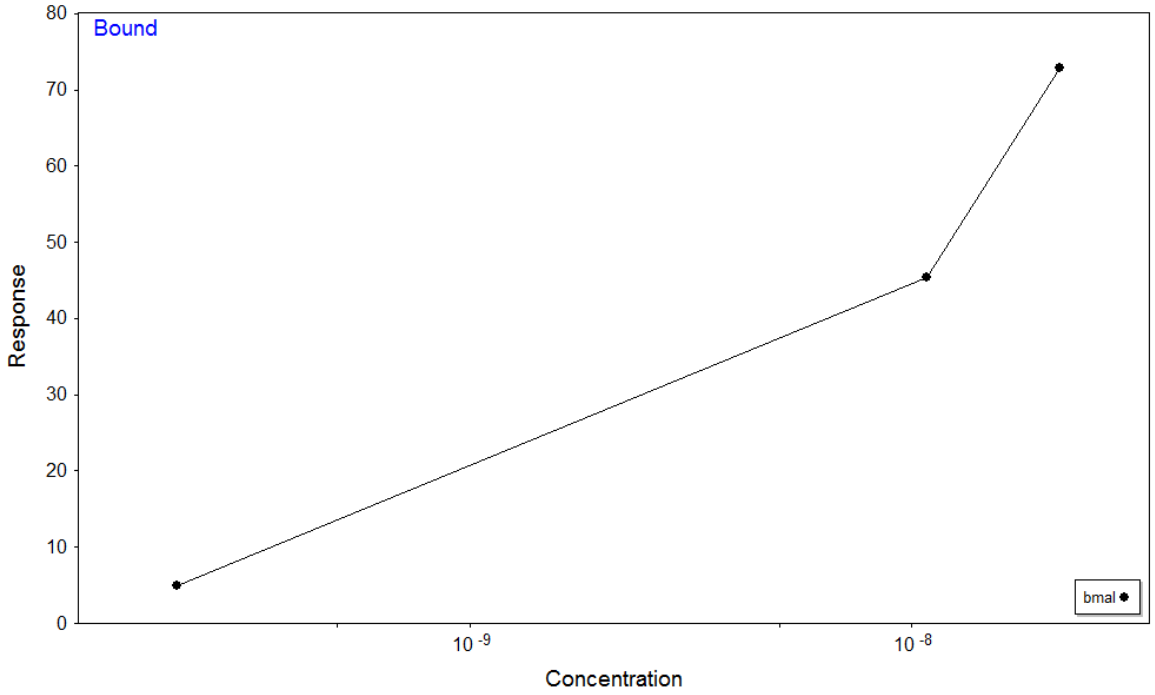

Figure 6. Response vs. Concentration Graph for BMAL1 and PER2 Interaction

concentration (Figure 6). The association rate constants has been found within the range of $1.31x10^6$ - $8.70\ x10^6\ M^{-1}s^{-1}$, where the dissociation rate constant of the interaction ranges between $0.24\text{-}0.29s^{-1}$. The maximum response unit is 1565 RU. The binding constant of the interaction between BMAL1 and PER2 has been found within the range of 34.38-198.19 nM which indicates a small binding affinity. This data is tabulated at Table 4.BMAL1 and PER2 have been found to interact via coimmuno-precipitation technique before.[25-26, 42, 249] However, a quantitative kinetic and affinity data have not been provided before for this interaction pair.

C (nM)	k_a ($M^{-1}s^{-1}$)	k_d (s^{-1})	K_D (nM)	Res SD
21.6	$1.31x10^6$	0.2605	198.19	5.504
10.8	$1.34x10^6$	0.2424	180.98	2.710
0.22	$8.70x10^6$	0.2993	34.38	1.160

Table 4. Binding affinities and kinetic constants for BMAL1 and PER2 Interaction

C (nM)	k_a ($M^{-1}s^{-1}$)	R_{max} (RU)	L_r (m/s)	F (µl/min)	L_m (m/s)	Calc %MTL
21.6	$1.31x10^6$	1565	$1.521x10^{-5}$	50	$5.798x10^{-3}$	0.26
10.8	$1.34x10^6$	1565	$1.542x10^{-5}$	50	$5.798x10^{-3}$	0.27
0.22	$8.70x10^6$	1565	$1.002x10^{-4}$	50	$5.798x10^{-3}$	1.70

Table 5. %MTL calculation for BMAL1 and PER2 Interaction

The efficiency of the nonlinear regression curve fitting with pseudo-first order approximation was analyzed via calculation of residual standard deviation. The residual standard deviation of fitted curves from the actual data ranges between 1.160 and 5.504 where the maximum attained SPR signal is 150 RU in the experiment (Table 4). Therefore, the residual standard deviation stays within 10% confidence gap. Fitted kinetic constants are good estimates of the true kinetic constants.

Interaction of PER2 and CRY2

In order to analyze interaction between PER2 and CRY2, PER2 protein was successfully immobilized onto the surface, and CRY2 protein as analyte was injected through the immobilized surface. Figure 7 shows the binding interaction curves between immobilized PER2 and CRY2 within a concentration range of 1.44-14.4 nM. In the SPR data, as concentration of analyte increases, the plateau response unit also increases. The response versus concentration data ensures that the SPR signal in response units is directly proportional to analyte concentration (Figure 8). The injection concentration range for the analyte was kept wide enough so that a realistic estimation for interaction kinetics and binding affinity between CRY2 and PER2 proteins could be obtained. A simple pseudo-first order binding interaction model was fitted to the response unit versus time data using

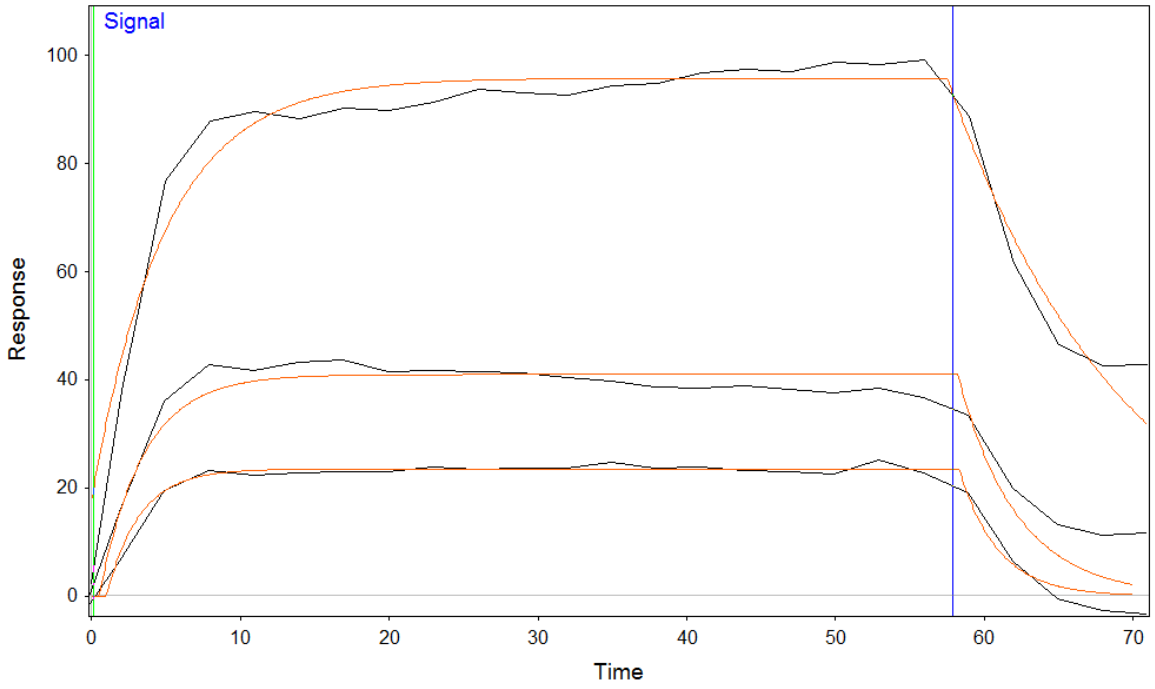

Figure 7. Response Unit vs. Time Graph for Interaction between PER2 and CRY2

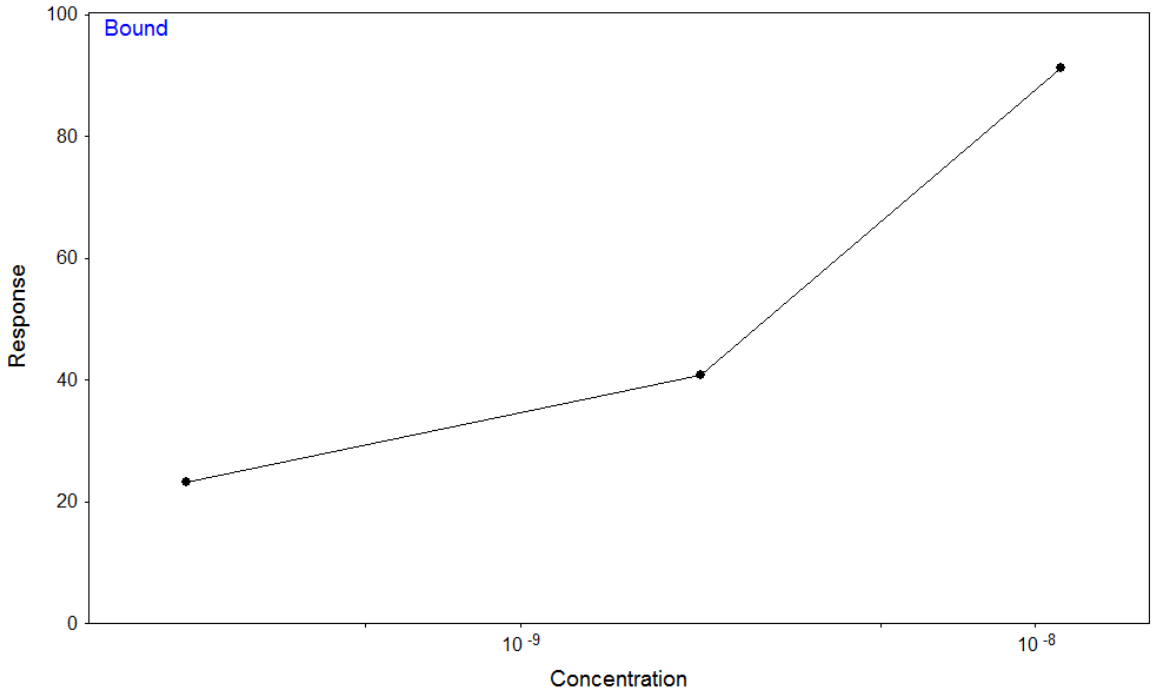

Figure 8. Response vs. Concentration Graph for PER2 and CRY2 Interaction

Qdat analysis software via local parameters. The absence of mass transfer limitation was confirmed via calculating the percentage of mass transfer limitation. (Table 7) The percent mass transfer limitation was calculated between 0.22 and 5.61 which indicates that mass transfer limitation effect on reaction kinetics is negligible since the values are around 5%.[248] Therefore, one-to-one simple kinetics assumption can be a legitimate assumption. During analysis with one-to-one reaction kinetics, reference surface data were subtracted from the reaction surface data in order to eliminate the refractive index change. The analysis yielded a dissociation rate constant ranging between $0.08s^{-1}$ and $0.38s^{-1}$. The association rate constant of PER2 and CRY2 interaction ranges between $1.094x10^{7}$ $M^{-1}s^{-1}$ and $2.951x10^{7}$ $M^{-1}s^{-1}$. The maximum response unit was 160 RU. The binding constant was found within the range of 1.29–7.50 nM which is quite low, and indicates that CRY2 and PER2 proteins interact strong enough, and possibly form complexes under *in vitro*

C (nM)	k_a ($M^{-1}s^{-1}$)	k_d (s^{-1})	K_D (nM)	Res SD
11.2	$1.094x10^7$	0.0821	7.50	5.598
2.24	$3.861x10^7$	0.2512	6.50	3.869
0.22	$2.951x10^8$	0.3836	1.29	1.360

Table 6. Binding Affinities and Kinetic Constants for PER2 and CRY2 Interaction

C (nM)	k_a ($M^{-1}s^{-1}$)	R_{max} (RU)	L_r (m/s)	F (µl/min)	L_m (m/s)	Calc %MTL
11.2	$1.094x10^7$	160	$1.287x10^{-5}$	50	$5.841x10^{-3}$	0.22
2.24	$3.861x10^7$	160	$4.542x10^{-5}$	50	$5.841x10^{-3}$	0.77
0.22	$2.951x10^8$	160	$3.472x10^{-5}$	50	$5.841x10^{-3}$	5.61

Table 7. %MTL Calculation for PER2 and CRY2 Interaction

conditions. The values of k_a, k_d, and K_D are given in Table 6. PER2 and CRY2 proteins are important for negative limb of the circadian clockwork. Some studies suggest that the nuclear entry is regulated by cytoplasmic accumulation of PER2/CRY complex,[251] since PER2, as a limiting factor have interaction with nuclear receptors,[117] and acts as translocator of CRY proteins.[27] Controversially, some studies suggest that CRY proteins take the critical role in translocation of PER proteins to the nucleus.[40] However, all studies agrees that for translocalization of PER and CRY proteins back to nucleus, complex formation is required. [40, 117, 251] After translocalization into nucleus, CRY proteins interact with BMAL1: CLOCK complex on the EBOX region of *per, cry* genes, and clock controlled genes to suppress their expression. In previous studies, CRY and PER proteins were found to form complexes via co-immunoprecipitation assay[40-43] and yeast two hybrid assay; [44] however, the magnitude of this binding has not been provided.

The quality of the best curve fitting to the sensograms was analyzed via calculation of residual standard deviation of the fitted curves from the actual data curve. The residual standard deviation was calculated between 1.360 and 5.598 (Table 6) here the maximum

response unit attained is 100 RU in the experiments. Therefore, deviation is within 10% confidence gap.

Interaction of CLOCK and CRY2

In order to investigate the interactions between CLOCK and CRY2, CLOCK was immobilized onto the SPR sensor surface via amine coupling, and CRY2 injections with successive concentrations in the range of 0.02 - 9.32 nM were carried out. The sensograms (Figure 9) of the interaction were analyzed via nonlinear regression curve fitting using mass transfer limited one-to-one simple reaction model with local data analysis tool of QDAT. The existence of mass transfer limitation was assayed via calculation of %MTL. The percent mass transfer limitation ranges between 3.96 and 55.08 which are higher than %5 %MTL (Table 9). Within this %MTL range, two-compartment model was suggested

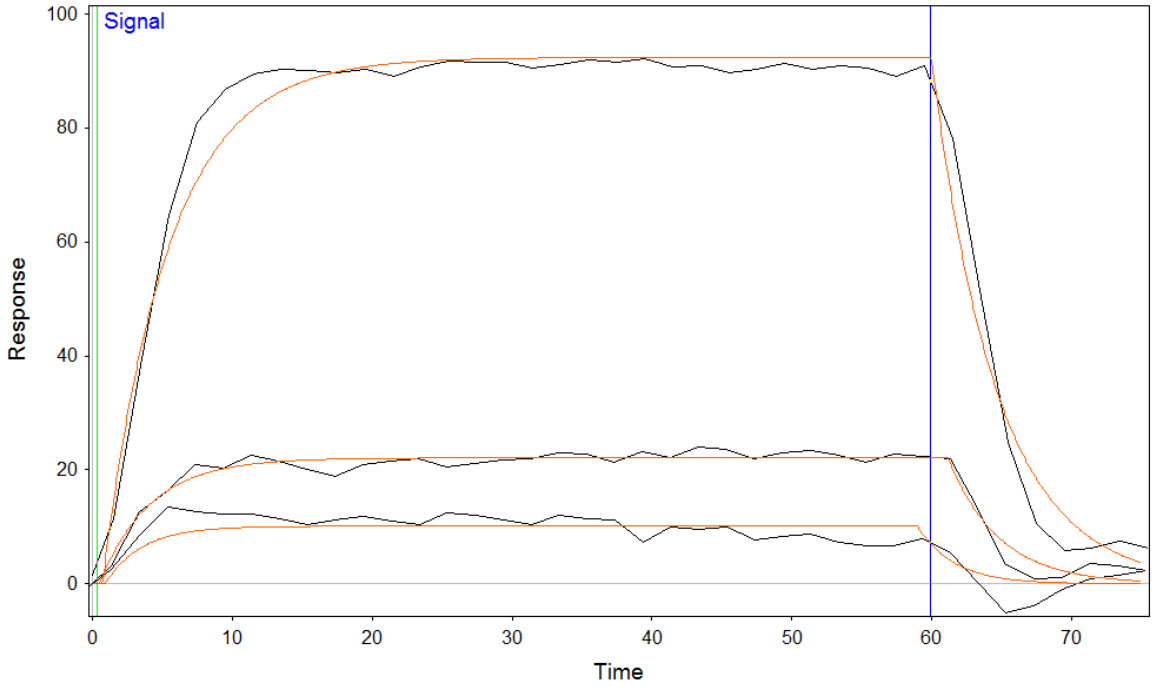

Figure 9. Response Unit vs. Time Graph for Interaction between CLOCK and CRY2

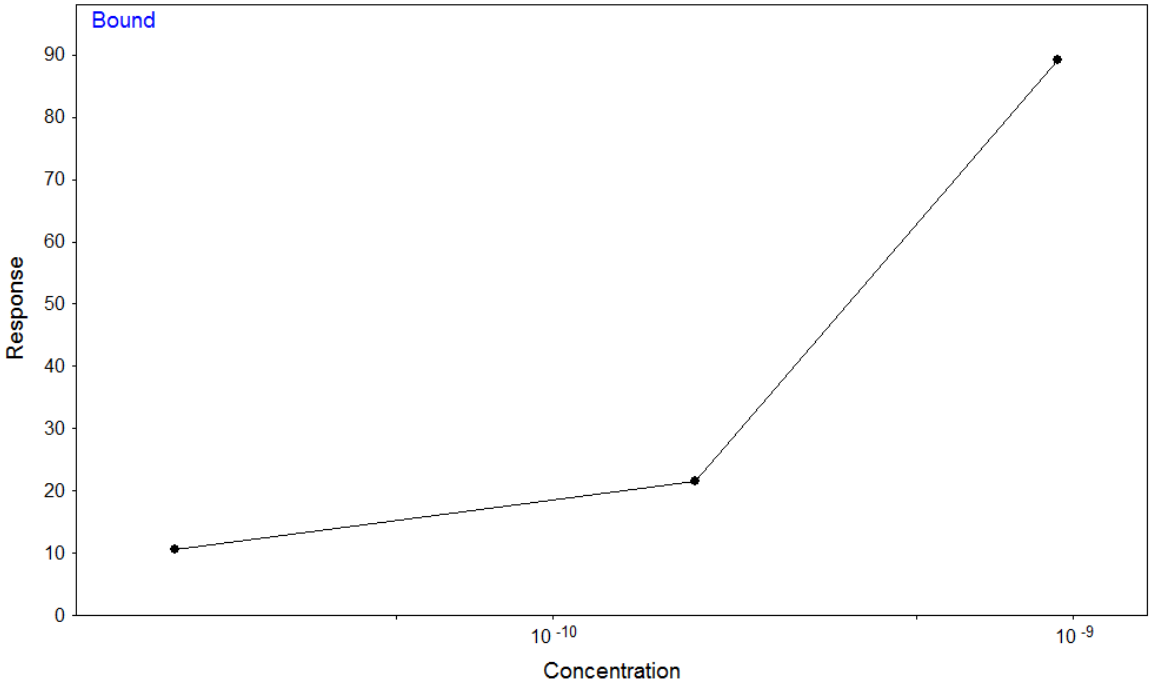

Figure 10. Response vs. Concentration Graph for CLOCK and CRY2 Interaction

instead of one-to-one simple reaction model.[248] In the SPR data, as concentration of analyte increases, the plateau response unit also increases. The response versus concentration data ensures that the SPR signal in response units is directly proportional to analyte concentration (Figure 10). The analysis yielded a mass transfer coefficient of $3.00x10^{11}$ s^{-1}. The dissociation rate constant of the interaction ranges between 0.23- $1.26s^{-1}$ where the association rate constant was found to be within the range of $2.413x10^{5}$ -$7.171 x10^{6}$ $M^{-1}s^{-1}$. The maximum response unit was 94870 RU (Table 8). The maximum response unit value is very high and may indicate some unspecific binding which may deviate the reaction kinetics from selected analysis model.

The success of the nonlinear regression curve fitting was analyzed by quantifying the residual standard deviation of the fitted curves from the actual data curve. The standard deviation is within the convenience range since the residual standard deviation calculated

varies within the range of 1.511 and 4.285 where the maximum response unit is 90 RU (Table 8). Therefore, the high maximum response unit does not indicate unspecific binding and fitted kinetic constants are good estimates of the true kinetic constants. The binding constant of the interaction between CRY2 and CLOCK was calculated in the range of 175.45 nM and 956.19 nM. This high binding constant indicates low affinity of CRY2 and CLOCK to each other. A clear interaction between CRY proteins and CLOCK has not been detected before via co-immunoprecipitation assays.[25-26]

C (nM)	k_T (s^{-1})	k_a ($M^{-1}s^{-1}$)	k_d (s^{-1})	K_D (nM)	Res SD
0.93	$3.00x10^{11}$	$2.413x10^{5}$	0.2307	956.19	4.285
0.18	$3.00x10^{11}$	$3.878x10^{5}$	0.3113	802.84	1.511
0.02	$3.00x10^{11}$	$7.171x10^{6}$	1.258	175.45	2.399

Table 8. Binding Affinities and Kinetic Constants for CLOCK and CRY2 Interaction

C (nM)	k_a ($M^{-1}s^{-1}$)	R_{max} (RU)	L_r (m/s)	F (µl/min)	L_m (m/s)	Calc %MTL
0.93	$2.413x10^{5}$	94870	$2.41x10^{-4}$	50	$5.841x10^{-3}$	3.96
0.18	$3.878x10^{5}$	94870	$3.873x10^{-4}$	50	$5.841x10^{-3}$	6.22
0.02	$7.171x10^{6}$	94870	$7.161x10^{-3}$	50	$5.841x10^{-3}$	55.08

Table 9. %MTL Calculation for CLOCK and CRY2 Interaction

Interaction of CLOCK and PER2

To investigate the interaction between PER2 and CLOCK proteins, after successful immobilization of CLOCK via amine coupling, PER2 was injected over immobilized surface with successive concentrations of 0.18 nM, 0.92 nM and 1.83 nM. The obtained SPR data (Figure 11) was analyzed with one-to-one simple reaction mechanism with mass transfer limitation via QDAT Data Analysis Tool by nonlinear regression curve fitting. In the SPR data, as concentration of analyte increases, the plateau response unit also increases. The response versus concentration data ensures that the SPR signal in response units is directly proportional to analyte concentration (Figure 12).

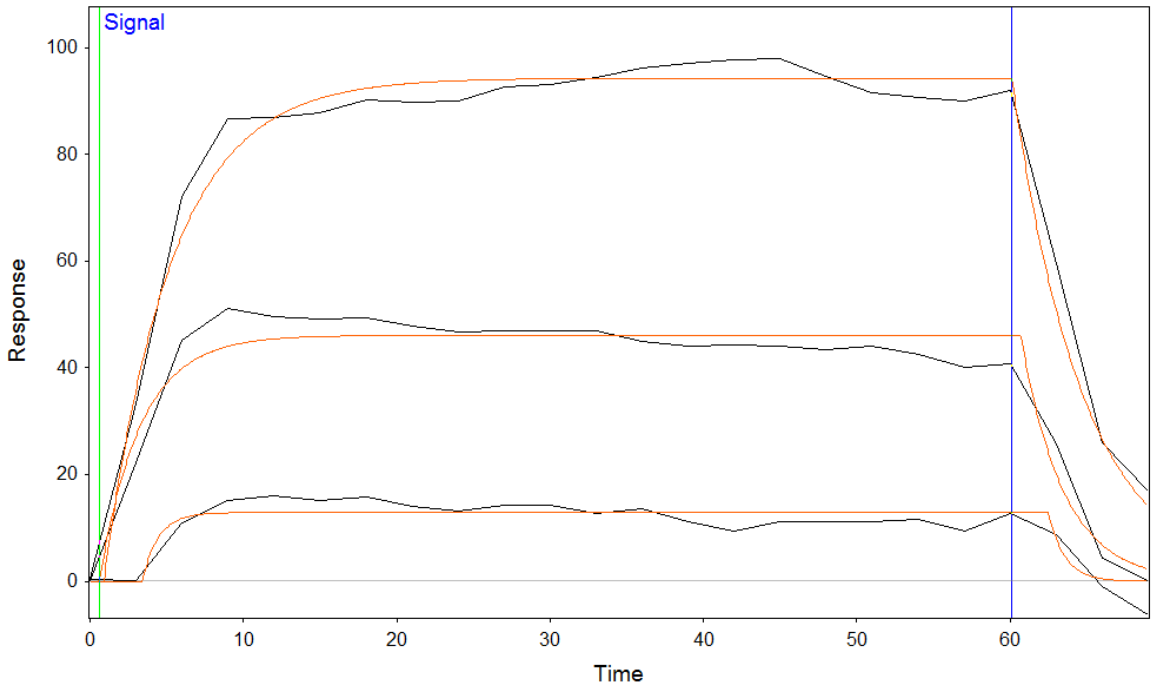

Figure 11. Response Unit vs. Time Graph for Interaction between CLOCK and PER2 via one-to-one reaction model

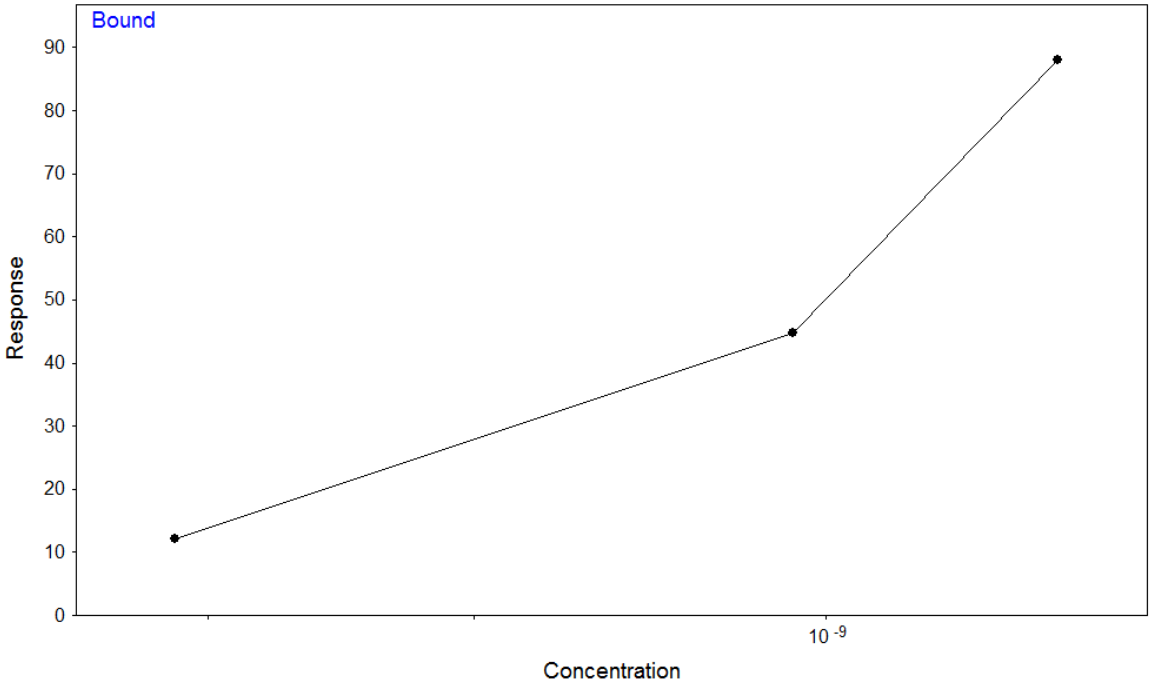

Figure 12. Response vs. Concentration Graph for CLOCK and PER2 via one-to-one reaction model

While analyzing SPR Data, all fitted parameters were fitted as a local parameter. According to initial analysis with pseudo first order reaction assumption, the association rate constants were calculated to be between 7.62 $x10^6$ $M^{-1}s^{-1}$ and 4.334 $x10^7$ $M^{-1}s^{-1}$. The dissociation rate constant ranges between $0.21s^{-1}$ and $0.93s^{-1}$. The dissociation constant of the interaction between PER2 and CLOCK is between 21.68 nM and 29.79 nM where maximum attainable response is 470 RU. This data are tabulated at Table 10. Residual standard deviation is in the convenience range since deviation ranges between 2.388 and 3.683 where the maximum attained signal is 90 RU (Table 10). However, the reaction kinetics is limited by the mass transfer limited effect since %MTL for one of the analyte concentration value is 10.74 (Table 11) while the manufacturer allows maximum 5% mass

transfer limitation for one-to-one assumption to hold. Therefore, analysis further performed with two compartments method. The association rate constant ranges between $1.569x10^{9}$ $M^{-1}s^{-1}$ and $4.731x10^{9}$ $M^{-1}s^{-1}$ while dissociation rate constant ranges between 35.71 s^{-1} and 133.6 s^{-1}. The mass transfer increased the association and dissociation rate greatly. However, the equilibrium condition did not change since the calculated dissociation constant is quite similar to the values of one-to-one model approximation. The equilibrium constant ranges between 22.75 nM and 30.09 nM. The kinetic data and binding affinities of the interaction for mass transfer limited model was listed within Table 12. Figure 13 shows the nonlinear regression curve fitting on the sensograms obtained from CLOCK and PER2 interaction. CLOCK and PER2 proteins have been found to interact according to co-immunoprecipitation assays in the literature.[25-26, 42]

C (nM)	k_a ($M^{-1}s^{-1}$)	k_d (s^{-1})	K_D (nM)	Res SD
1.83	$7.62x10^{6}$	0.2138	28.06	3.918
0.92	$1.209x10^{7}$	0.3603	29.79	3.683
0.18	$4.334x10^{7}$	0.9398	21.68	2.388

Table 10. Binding Affinities and Kinetic Constants for CLOCK and PER2 Interaction via one-to-one reaction model

C (nM)	k_a ($M^{-1}s^{-1}$)	R_{max} (RU)	L_r (m/s)	F (µl/min)	L_m (m/s)	Calc %MTL
1.83	7.62x106	1540	$1.235x10^{-4}$	50	$4.775x10^{-3}$	2.07
0.92	1.209x107	1540	$1.96x10^{-4}$	50	$4.775x10^{-3}$	3.25
0.18	4.334x107	1540	$7.026x10^{-4}$	50	$4.775x10^{-3}$	10.74

Table 11. %MTL calculation for CLOCK and PER2

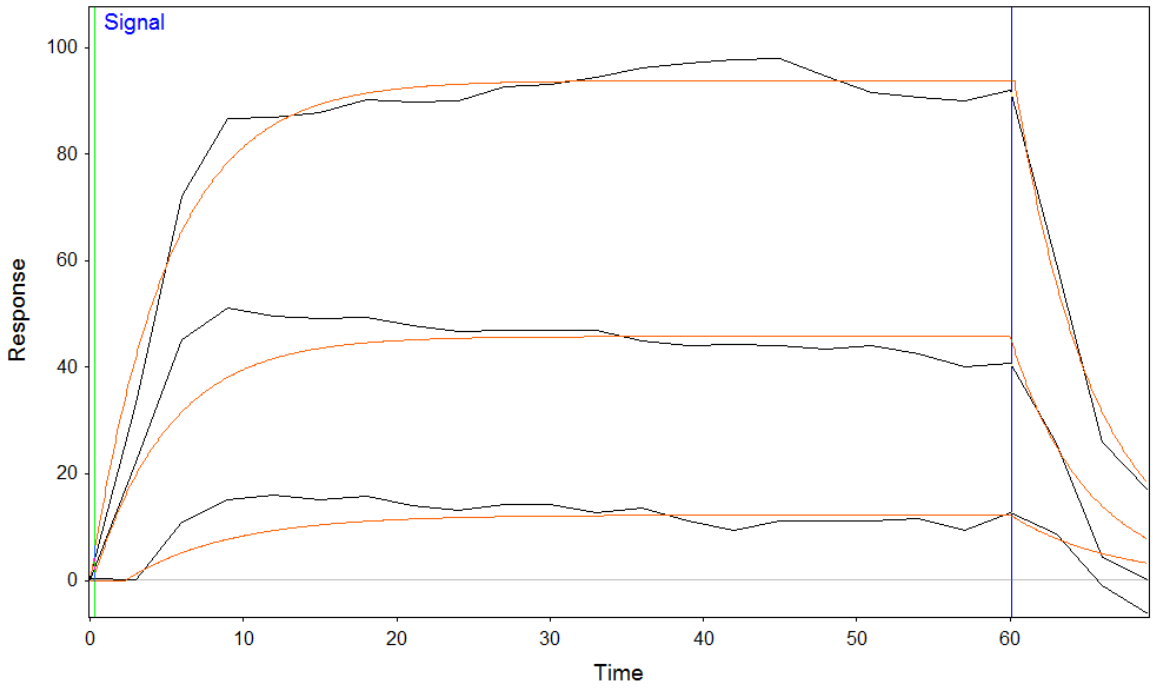

Figure 13. The Responce Unit vs. Time Graph for The Interaction between CLOCK and PER2 with mass transfer limitation

C (nM)	k_T (s^{-1})	k_a ($M^{-1}s^{-1}$)	k_d (s^{-1})	K_D (nM)	Res SD
1.83	9.646×10^{9}	4.731×10^{9}	133.6	28.23	4.723
0.92	1.00×10^{10}	4.366×10^{9}	131.4	30.09	5.603
0.18	1.00×10^{10}	1.569×10^{9}	35.71	22.75	4.121

Table 12. Binding Affinities and Kinetic Constants for CLOCK and PER2 Interaction via one-to-one reaction model with mass transfer limitation

The decline in success of curve fitting is interesting although the correct model was chosen. The residual standard deviation increased to the range between 4.121 and 5.603. Despite

the slight loss of best fitting efficiency, to choose two compartment method is wiser since the mass transfer limitation has a high impact on association and dissociation kinetics.

Interaction of CLOCK and BMAL1

In order to investigate interaction between BMAL1 and CLOCK proteins, CLOCK was immobilized onto the surface via amine coupling, and BMAL1 injections with successive concentrations were carried out. CLOCK and BMAL1 have two basic helix-loop-helix PER-ARBT-SIM (bHLH-PAS) domain protein structures. The structure of the mouse CLOCK:BMAL1 bHLHL-PAS domains at 2.3Å resolution has been recently revealed by Huang et al by tracking mutations and their effects via co-immunoprecipitation and biomolecular fluorescence complementation assay.[47] Three domains within two subunits

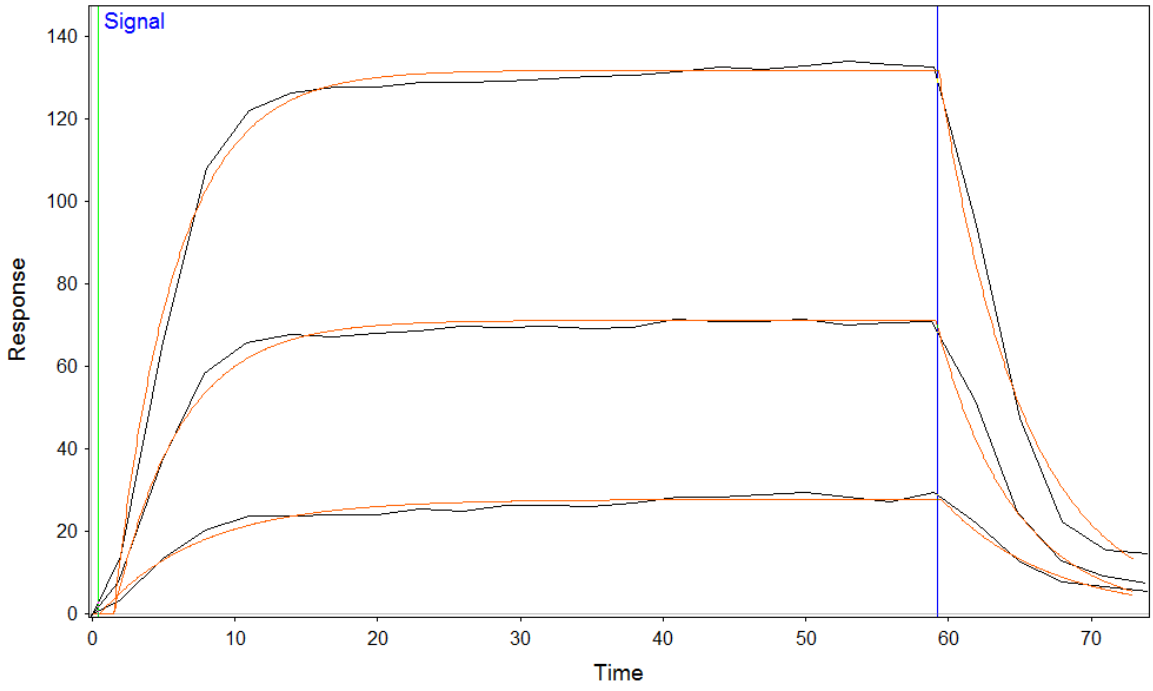

Figure 14. Response Unit vs. Time Graph for Interaction between CLOCK and BMAL1

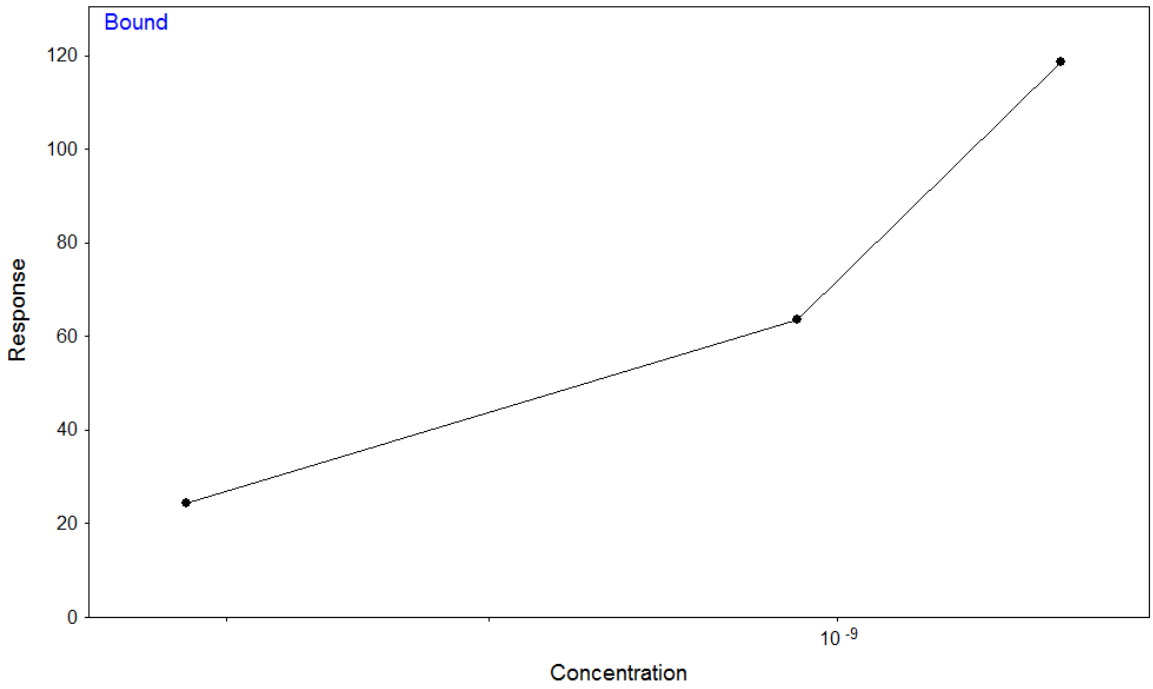

Figure 15. Response vs. Concentration Graph for CLOCK and BMAL1 Interaction

of CLOCK and BMAL1have been found to interact to form a highly intertwined structure which exposes CLOCK PAS domain surfaces with negative electrostatic potential and positively charged or neutral BMAL1 PAS domains.CLOCK:BMAL1 PAS-A dimer interface is mostly mediated by hydrophobic interactions between Phe^{104}, Leu^{105} and Leu^{113} residues of CLOCK and Leu^{159}, Thr^{285}, Tyr^{287}, Val^{315}, Ile^{317} of BMAL1. During PAS-B domain dimerization between BMAL1 and CLOCK proteins, hydrophobic residues are buried. The interaction between Trp^{427} of BMAL1 with Trp^{284} of CLOCK is the most prominent interaction. Dimerization of bHLH domain stabilizes the complex.[47] Since none of these residues contains side chains with amino groups, the binding of CLOCK protein on the surface may not affect the binding between BMAL1 and CLOCK proteins. Figure 14shows the binding interaction curves between immobilized CLOCK and BMAL1 within

C (nM)	k_a ($M^{-1}s^{-1}$)	k_d (s^{-1})	K_D (nM)	Res SD
1.8	$3.645x10^7$	0.1683	4.61	3.917
0.90	$3.676x10^7$	0.1852	5.04	2.665
0.18	$4.681x10^7$	0.1339	2.86	1.441

Table 13. Binding Affinities and Kinetic Constants for CLOCK and BMAL1 Interaction

C (nM)	k_a ($M^{-1}s^{-1}$)	R_{max} (RU)	L_r (m/s)	F (µl/min)	L_m (m/s)	Calc %MTL
1.8	$3.645x10^7$	470	$1.803x10^4$	50	$5.798x10^{-3}$	3.02
0.90	$3.676x10^7$	470	$1.819x10^4$	50	$5.798x10^{-3}$	3.04
0.18	$4.681x10^7$	470	$2.316x10^4$	50	$5.798x10^{-3}$	3.84

Table 14. %MTL calculation for CLOCK and BMAL1 Interaction

a concentration range of 0.18-1.8 nM. Since the percent mass transfer limitation was calculated between 3.02 and 3.84 (Table 14) which indicates that mass transfer limitation effect on reaction kinetics is negligible. Therefore, one-to-one simple kinetics assumption as selected as an appropriate model for SPR data analysis. In the SPR data, as concentration of analyte increases, the plateau response unit also increases. The response versus concentration data ensures that the SPR signal in response units is directly proportional to analyte concentration (Figure 15).The obtained SPR data was analyzed via nonlinear regression curve fitting with pseudo first order reaction model approximation, where the association constant ranges between $3.645x10^7$ – $4.681\ x10^7\ M^{-1}s^{-1}$, and dissociation constant ranges between 0.14-0.19 s^{-1}. Maximum response unit was 470 RU. The binding constant K_D (k_d/k_a) of the interaction was calculated within the range of 2.86-5.04 nM (Table 13). This low binding constant suggests that similar to PER2 and CRY2 proteins BMAL1 and CLOCK proteins also possibly form complexes *in vitro,* where the

interaction is stronger for BMAL1:CLOCK complex than PER2:CRY2 complex. BMAL1 and CLOCK are key integrators at the core circadian clock. The complex binds to EBOX regions of *per*2, *cry*2, and clock controlled genes in order to initiate their expression.[252-254] BMAL1 and CLOCK also play an important role in regulation in the body like glucose homeostasis,[253] rhythmic gene expression in liver[254-255] and skeletal muscle,[255-256] and many other clock controlled gene regulatory motifs.[254] Therefore, the strength of the interaction between BMAL1 and CLOCK is essential for regulation of circadian clock and clock controlled genes. In previous studies, the interaction of these proteins were reported based on bulk biochemical assays such as to yeast two hybrid screen,[58, 257] coimmunoprecipitation,[258] and pulldown assays;[26, 249, 259-260] however, the strength of this binding also has not been quantified, and real-time binding studies have not been investigated before.

To analyze the efficiency of the nonlinear regression curve fitting with pseudo-first order approximation, residual standard deviation of the fitted curves from the actual data curve was calculated. The residual standard deviation ranges between 1.441 and 3.917 where the maximum attained SPR signal is 130 RU in the experiment (Table 13). Since the residual standard deviation is within the convenience range, the calculated kinetic values via pseudo-first order reaction kinetics mechanism are good estimate of true kinetic constants.

Interaction of CRY2 with BMAL1:CLOCK complex

BMAL1:CLOCK complex interactions with PER2, CRY2 and PER2:CRY2 were performed as control before studying the interactions with EBOX complex and PER2, CRY2, PER2:CRY2 complex. In order to investigate interaction of BMAL1:CLOCK complex with CRY2, 0.75, 1.87, and 3.73 nM concentrations of CRY2 was injected over immobilized BMAL1:CLOCK surface subsequently. Response curves obtained from the SPR data was analyzed with one-to-one simple reaction mechanism (Figure 16). In the SPR data, as concentration of analyte increases, the plateau response unit also increases. The response versus concentration data ensures that the SPR signal in response units is directly

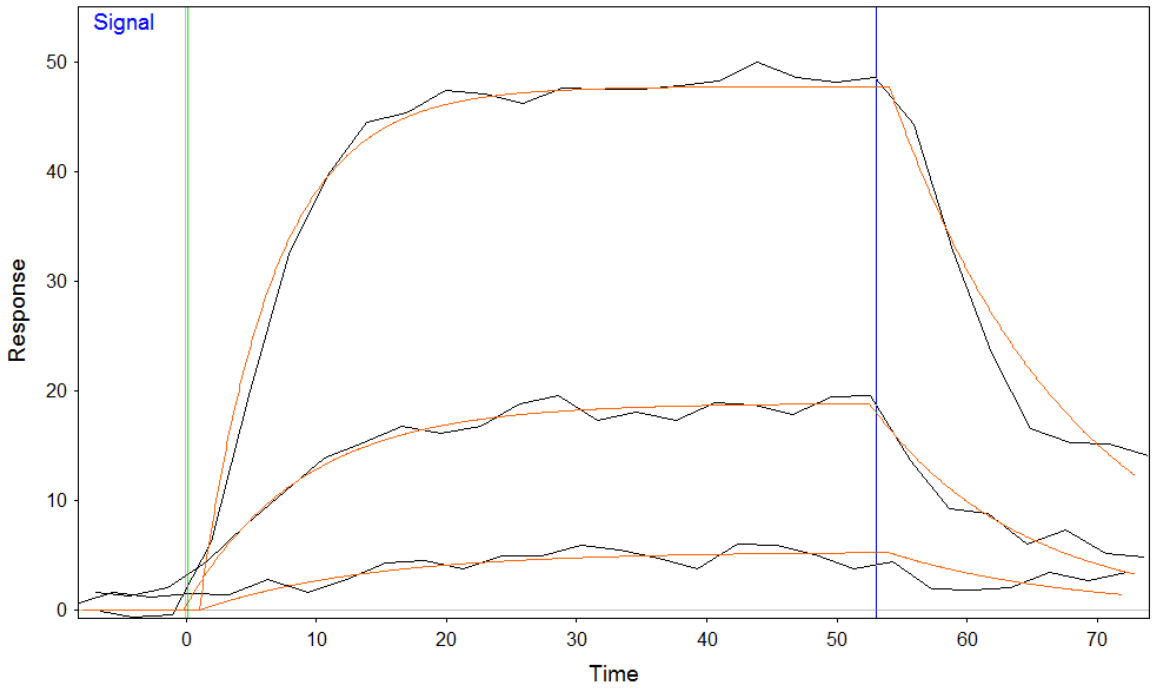

Figure 16. Response Unit vs. Time Graph for Interaction between CRY2 and BMAL1:CLOCK

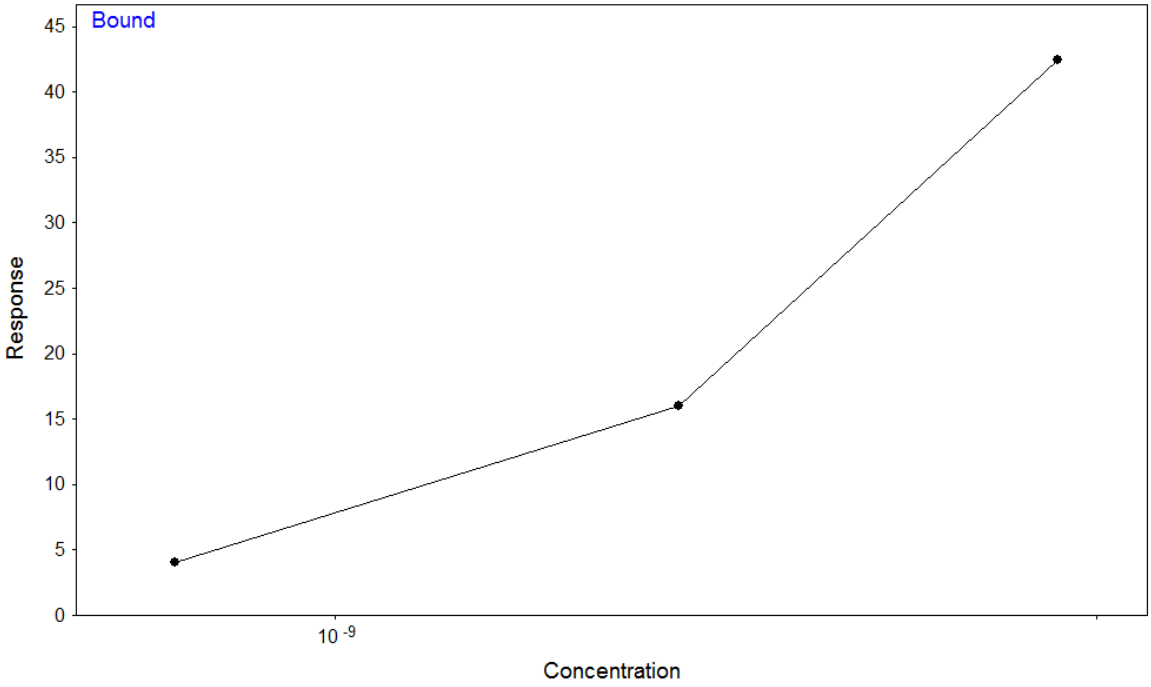

Figure 17. Response vs. Concentration for CRY2 and BMAL1:CLOCK Interaction

proportional to analyte concentration (Figure 17). While analyzing SPR Data, all fitted parameters were fitted as a local parameter. The maximum response for the complex formation was calculated as 80 response units. The association constant, k_a, and dissociation constant of the interaction was within the range of $6.96x10^6$ -$2.85x10^7$ $M^{-1}s^{-1}$, and $0.07s^{-1}$-$0.09s^{-1}$, respectively. Based on these analyses, the binding constant K_D (k_d/k_a) of the interaction between CRY2 protein with BMAL1:CLOCK complex was calculated within the range of 2.51-10.4 nM (Table 17).

Due to the complexity of binding between protein complex as reacting species and complexes, mass transfer limitation was also considered and included in the analyses, as was detailed in the previous section. The percent of mass transfer limitation calculated was

C (nM)	k_a ($M^{-1}s^{-1}$)	k_d (s^{-1})	K_D (nM)	Res SD
3.73	$2.86x10^7$	0.0718	2.51	1.999
1.87	$1.42x10^7$	0.0856	6.04	1.039
0.75	$6.96x10^6$	0.0725	10.42	1.069

Table 15. Binding Affinities and Kinetic Constants for CRY2 and BMAL1:CLOCK Interaction

C (nM)	k_a ($M^{-1}s^{-1}$)	R_{max} (RU)	L_r (m/s)	F (µl/min)	L_m (m/s)	Calc %MTL
3.73	$2.86x10^7$	80	$1.37x10^{-5}$	50	$5.84x10^{-3}$	0.24
1.87	$1.42x10^7$	80	$6.83x10^{-6}$	50	$5.84x10^{-3}$	0.12
0.75	$6.96x10^6$	80	$3.35x10^{-6}$	50	$5.84x10^{-3}$	0.06

Table 16. %MTL calculation for CRY2 and BMAL1:CLOCK Interaction

within 0.06- 0.24 range, which suggested that this effect could be neglected (Table 2). Therefore, one-to-one simple kinetics assumption was found to be a valid assumption. Since it is postulated that CRY binds to BMAL1:CLOCK:EBOX complex directly from BMAL1:CLOCK region,[26] it is important to investigate this binding. According to Griffin et al., CRY1 and CRY2 inhibit CLOCK-BMAL1 by forming direct contacts with it via luciferase reporter gene assay.[44] CRY also has been reported to bind CLOCK:BMAL1 heterodimer via yeast two hybrid, protein-protein pull-down and co-immunoprecipitation assays.[40, 57-58] However, kinetics of binding or estimation of the binding constant has not been investigated before.

To analyze the success of the nonlinear regression curve fitting with pseudo-first order approximation, residual standard deviation of the fitted curves from the actual data curve was calculated. According to the manufacturer, residuals that represent less than 5% of the

maximum experimental response indicate a satisfactory fit while residuals up to 10% are also accepted. For this reaction pair, the residual standard deviation is within 10% convenience gap (Table 17).

Interaction of CRY2: PER2 with BMAL1:CLOCK complex

Next, BMAL1:CLOCK complex was immobilized onto SPR sensor surface, and CRY2:PER2 complex was injected at 5, 10, 25 nM concentrations (Figure 18). In the SPR data, as concentration of analyte increases, the plateau response unit also increases. The response versus concentration data ensures that the SPR signal in response units is directly

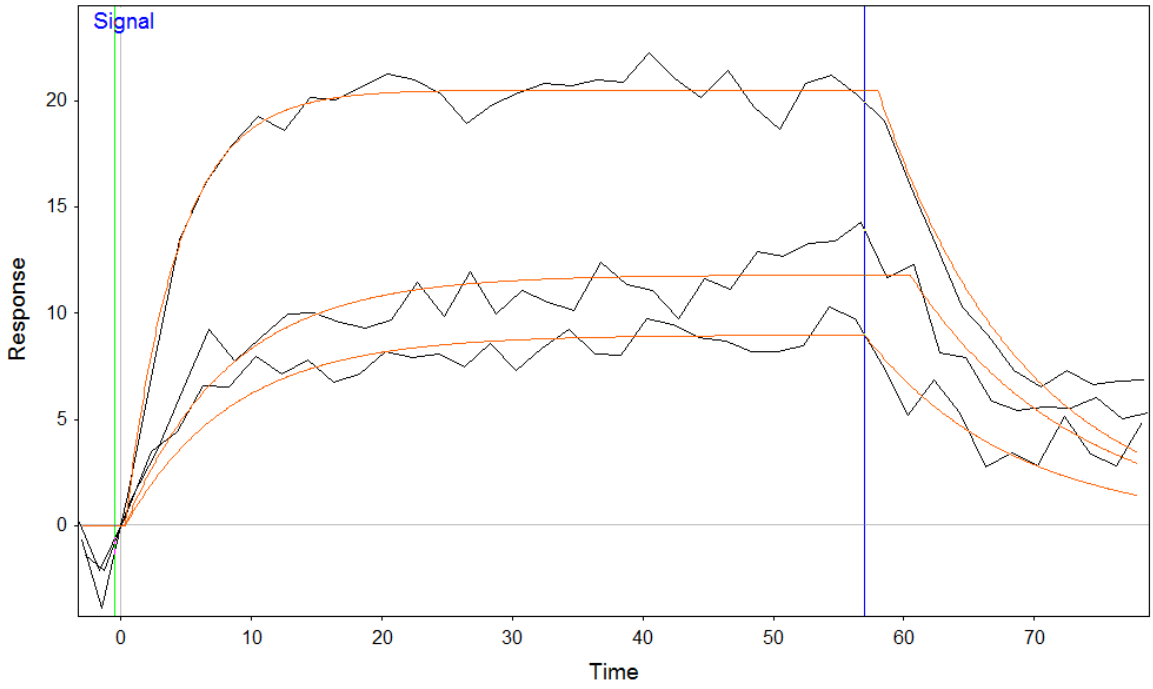

Figure 18. Response Unit vs. Time Graph for Interaction between CRY2:PER2 and BMAL1:CLOCK

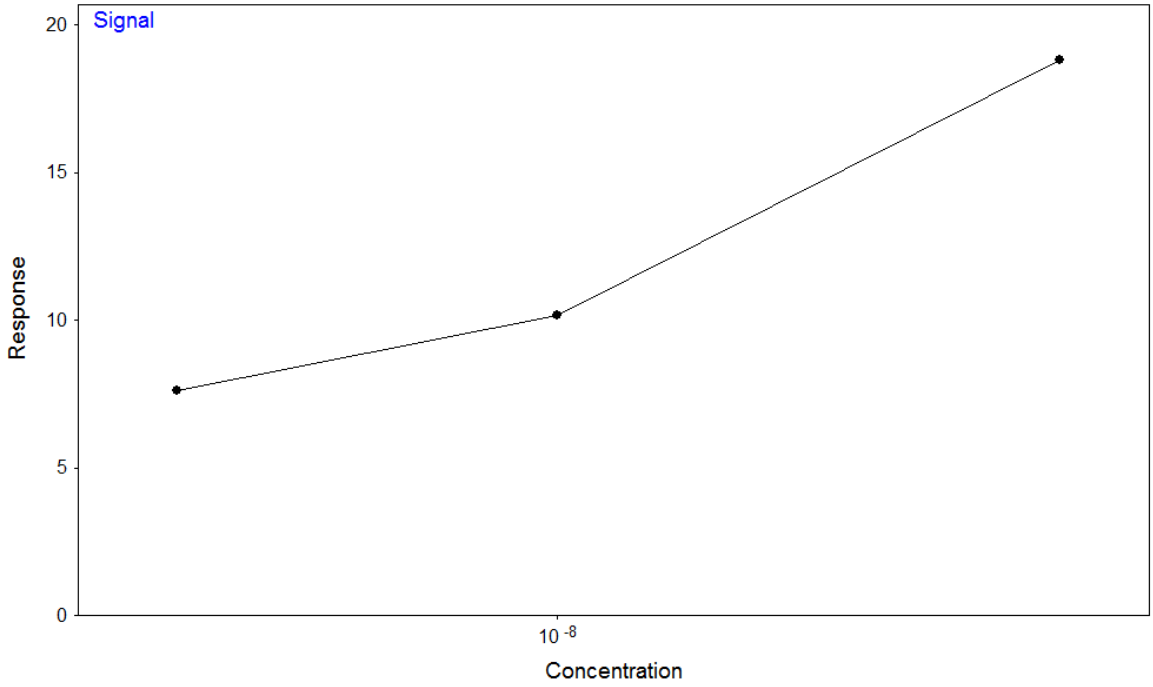

Figure 19. Response vs. Concentration Graph for CRY2:PER2 and BMAL1:CLOCK Interaction

proportional to analyte concentration (Figure 19). While analyzing SPR Data, all fitted parameters were fitted as a local parameter. The association and dissociation constants calculated from the response unit versus time curves are listed in Table 17. From the calculated k_a and k_d values, the binding constant K_D (k_d/k_a) of this interaction has been found within the range of 12.83-17.13 nM, which suggested high affinity of BMAL1:CLOCK and CRY2:PER2 complexes for each other. Mass transfer limitation has been found not very significant for this interaction (Table 18). The maximum attainable response is 32 response units The association rate constant of the interaction varies between $4.66x10^{-6}$ -$6.83x10^{-6}$ $M^{-1}s^{-1}$ range, where dissociation rate constant of the interaction is between 0.08-0.09 s^{-1}(Table 17). In transcriptional and translational feedback loop (TTFL)

model, PER and CRY were proposed to bind to CLOCK:BMAL1:EBOX complex from its CLOCK:BMAL1 as heterodimers.[26] Also, in a previous biochemical study via gene reporter assay, PER2:CRY2 was reported to react with BMAL1:CLOCK from its CLOCK to block activity of the transcription factor in the liver of mice in the presence of Casein Kinase I Delta/Epsilon.[258] However, a quantitative binding data have not been provided for the interaction of PER2:CRY2 complex with BMAL1:CLOCK complex.

C (nM)	k_a ($M^{-1}s^{-1}$)	k_d (s^{-1})	K_D (nM)	Res SD
25.0	$6.37x10^6$	0.0895	14.03	1.112
10.0	$4.66x10^6$	0.0798	17.13	1.285
5.0	$6.83x10^6$	0.0877	12.83	1.182

Table 17. Binding Affinities and Kinetic Constants for CRY2:PER2 and BMAL1:CLOCK Interaction

C (nM)	k_a ($M^{-1}s^{-1}$)	R_{max} (RU)	L_r (m/s)	F (µl/min)	L_m (m/s)	Calc %MTL
25.0	6.38×10^{-6}	32	$1.23x\ 10^{-6}$	50	$4.26x\ 10^{-3}$	0.03
10.0	4.66×10^{-6}	32	$8.98x\ 10^{-6}$	50	$4.26x\ 10^{-3}$	0.02
5.0	6.84×10^{-6}	32	$1.32x\ 10^{-6}$	50	$4.26x\ 10^{-3}$	0.03

Table 18. %MTL calculation for CRY2:PER2 and BMAL1:CLOCK Interaction

To analyze the success of the nonlinear regression curve fitting with pseudo-first order approximation, residual standard deviation of the fitted curves from the actual data curve was calculated which is within 10% confidence gap (Table 17). Therefore, fitted kinetic constants are good estimates of the true kinetic constants.

Interaction of PER2 with BMAL1:CLOCK complex

PER2 protein was injected over BMAL1:CLOCK complex immobilized surface at concentrations of 0.29, 1.47, and 14.7 nM (Figure 20). While analyzing SPR Data, all fitted parameters were fitted as a local parameter. In the SPR data, as concentration of analyte increases, the plateau response unit also increases. The response versus concentration data ensures that the SPR signal in response units is directly proportional to analyte concentration (Figure 21).The association constant of was within $1.75x10^{6}$ - $1.77x10^{7}$ $M^{-1}s^{-1}$, where dissociation constant was calculated as 0.07-0.08s^{-1} The percent of mass transfer limitation ranges between 0.02 -0.22, which indicates the absence of mass

Figure 20. Response Unit vs. Time Graph for Interaction between PER2 and BMAL1:CLOCK

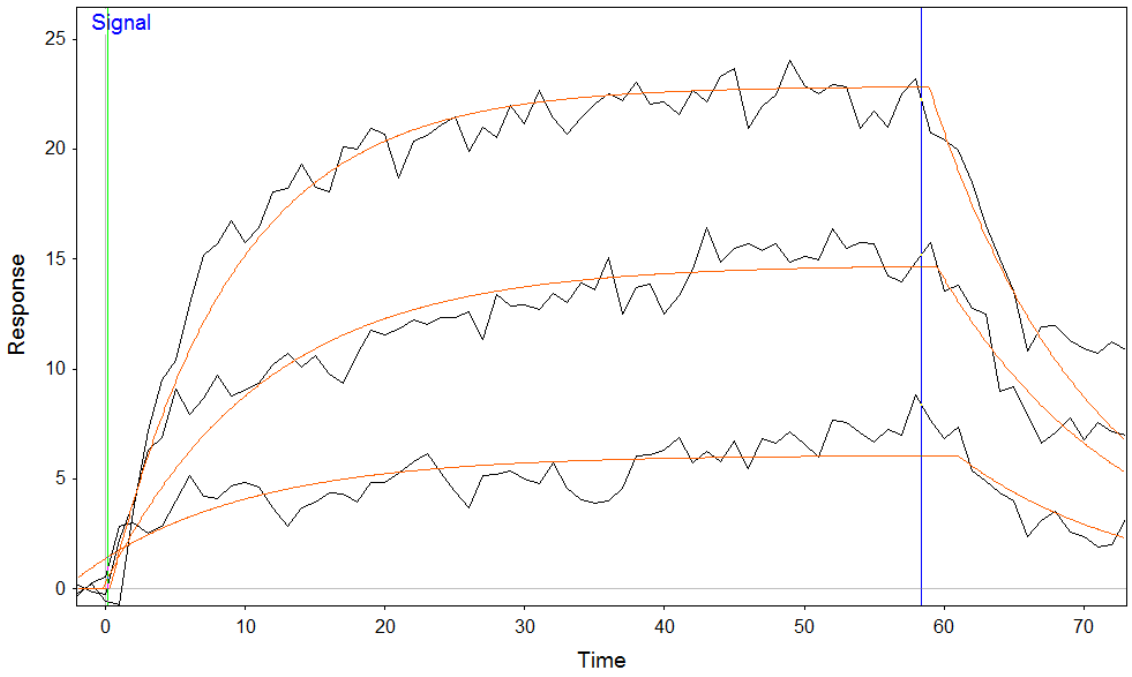

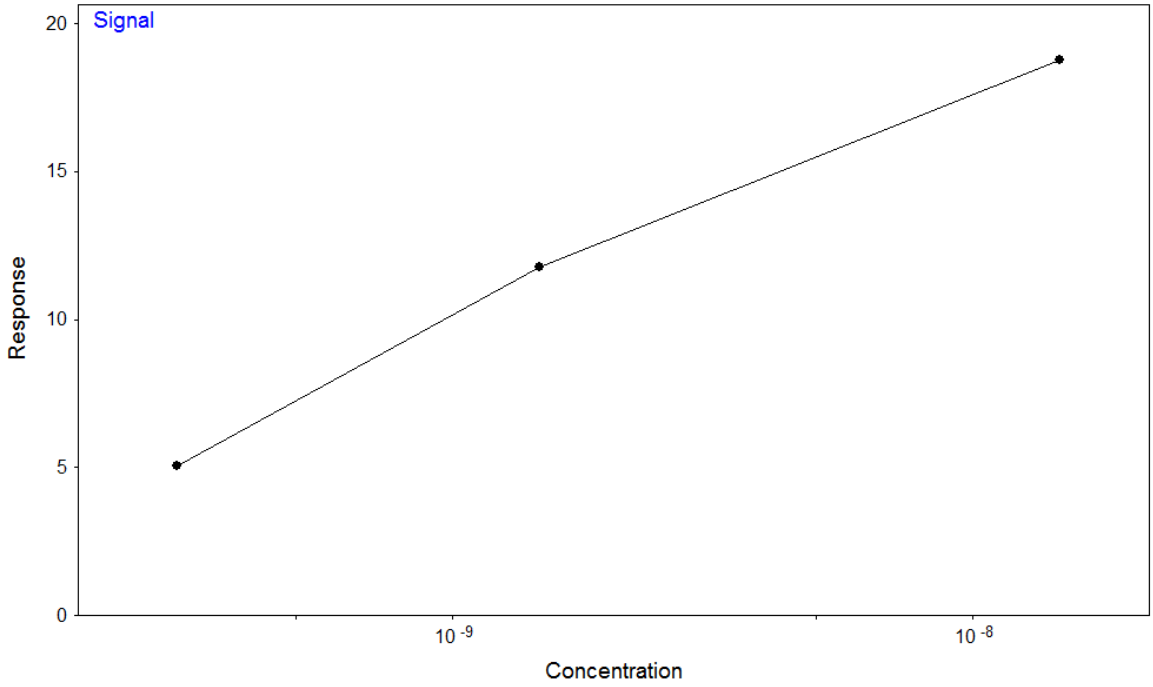

Figure 21. Response vs. Concentration Graph for PER2 and BMAL1:CLOCK Interaction

transfer effect on reaction kinetics (Table 20). PER2 has been recently reported to directly bind to BMAL1:CLOCK heterodimer to bring CRY protein to the reaction; [59] however, a quantitative data for the PER2 and BMAL1:CLOCK interaction has not been provided. Here, the binding constant calculated within the range of 4.54-49.6 nM suggests that a strong interaction exists between PER2 and BMAL1:CLOCK complex (Table 19).

To analyze the success of the nonlinear regression curve fitting with pseudo-first order approximation, residual standard deviation of the fitted curves from the actual data curve was calculated. Residual standard deviation values are small and in the range of 0.977 and 1.383 while the maximum SPR signal gained during experiment is 25 RU (Table 19). The deviation from the linearity is lower than 10%. Therefore, fitted kinetic constants are good estimates of the true kinetic constants.

C (nM)	k_a ($M^{-1}s^{-1}$)	k_d (s^{-1})	K_D (nM)	Res SD
14.7	1.75×10^6	0.0868	49.6	1.383
1.47	8.90×10^6	0.0756	8.50	1.190
0.29	1.77×10^7	0.0805	4.54	0.977

Table 19. Binding Affinities and Kinetic Constants for PER2 and BMAL1:CLOCK Interaction

C (nM)	k_a ($M^{-1}s^{-1}$)	R_{max} (RU)	L_r (m/s)	F (µl/min)	L_m (m/s)	Calc %MTL
14.7	1.75×10^6	100	1.05×10^{-6}	50	4.77×10^{-2}	0.02
1.47	8.90×10^6	100	5.36×10^{-6}	50	4.77×10^{-2}	0.11
0.294	1.77×10^7	100	1.07×10^{-5}	50	4.77×10^{-2}	0.22

Table 20. %MTL calculation for PER2 and BMAL1:CLOCK Interaction

Interaction of CRY2 with EBOX complex

Before quantifying the reaction kinetics and binding affinity of EBOX complex to CRY2, PER2 and PER2:CRY2 proteins, we wanted to ensure the posttranslational modification requirements and folding errors do not prevent binding *in vitro*. Therefore, to ensure that along with BMAL1 and CLOCK proteins PER2 and CRY2 proteins form complexes separately *in vitro*, pairwise interaction experiments were conducted. Additionally PER2, CRY2 and PER2:CRY2 complex was reacted with BMAL1:CLOCK off of DNA motif to ensure that they bind to BMAL1:CLOCK *in vitro*. Also the activities of the proteins were estimated via co-immunoprecipitation studies before proteins were provided by Kavakli Laboratory. After formation of BMAL1:CLOCK:EBOX ternary

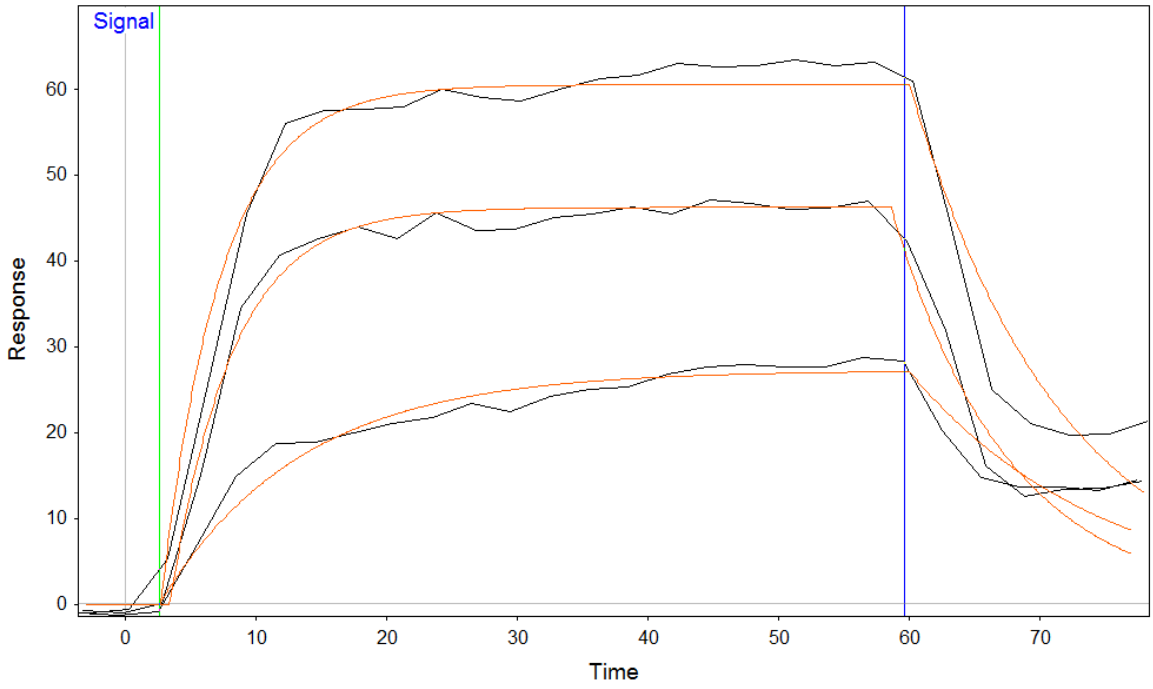

Figure 22. Response Unit vs. Time Graph for Interaction between CRY2 and EBOX Complex

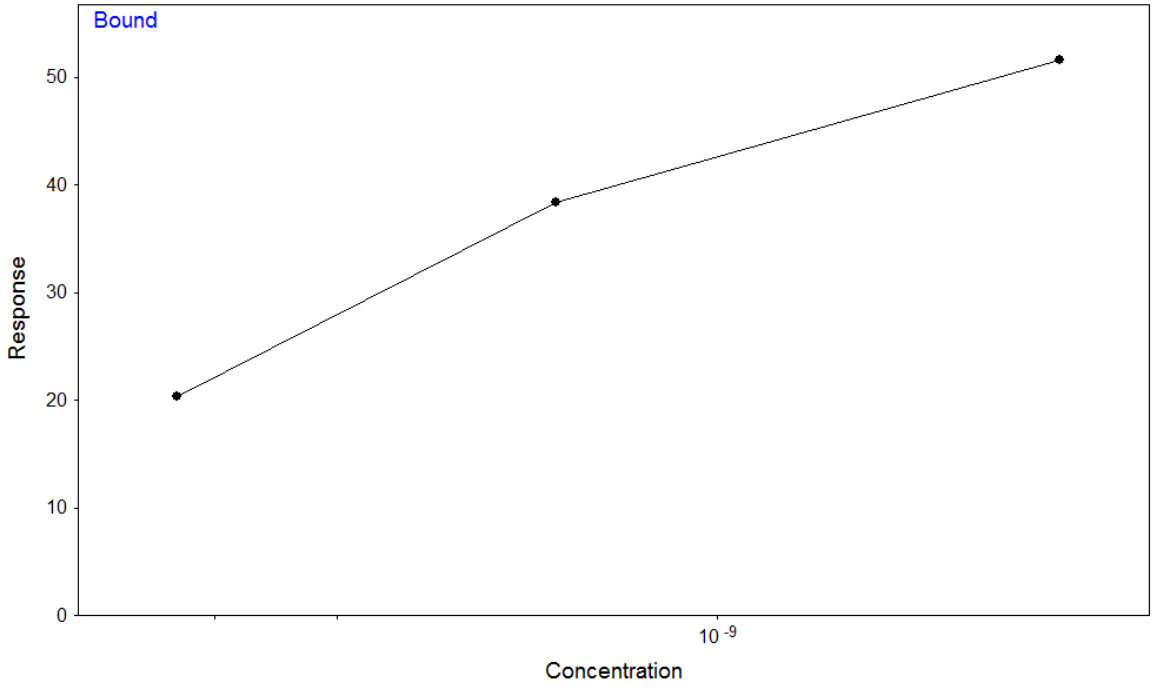

Figure 23. Response vs. Concentration Graph for CRY2 and EBOX Complex Interaction

complex in vitro at room temperature, this complex is successfully immobilized to sensor surface via amine coupling.

In this part of the study, we investigated the real-time interaction kinetics and the strength of the interaction between EBOX complex and PER2, CRY2 proteins or PER2:CRY2 complex separately. Through pairwise interaction analysis, we observed that BMAL1 and CLOCK as well as CRY2 and PER2 can form complexes. After formation of BMAL1:CLOCK:EBOX ternary complex *in vitro*, this complex is successfully immobilized to sensor surface via amine coupling.

To investigate interaction of CRY2 with BMAL1:CLOCK:EBOX ternary complex, ternary complex was immobilized onto the surface via amine coupling, subsequent CRY2 injections were performed. Figure 22 shows the sensograms for CRY2 and EBOX complex

interaction within a concentration range of 10-50 nM. In the SPR data, as concentration of analyte increases, the plateau response unit also increases. The response versus concentration data ensures that the SPR signal in response units is directly proportional to analyte concentration (Figure 23). While analyzing SPR Data, all fitted parameters were fitted as a local parameter. The obtained SPR data was analyzed with pseudo first order kinetics approximation since percent mass transfer limitation was insignificant. The percent mass transfer limitation was calculated between 0.61 and 1.16 for the used analyte concentrations (Table 22). The association rate constant of interaction between CRY2 with EBOX complex ranged between $6.77x10^{7}$ - $1.29x10^{8}$ $M^{-1}s^{-1}$, where dissociation rate constant varied between 0.06 - 0.11 s^{-1}. The binding constant of interaction between CRY2 and EBOX was calculated within 0.87-1.22 nM range, which suggested high affinity of CRY2 towards EBOX complex (Table 21). These results are also consistent with Ye et

C (nM)	k_a ($M^{-1}s^{-1}$)	k_d (s^{-1})	K_D (nM)	Res SD
1.87	$7.04x10^{7}$	0.0858	1.22	3.813
0.74	$1.29x10^{8}$	0.1124	0.87	3.018
0.37	$6.77x10^{7}$	0.0675	0.99	2.290

Table 21. Binding Affinities and Kinetic Constants for CRY2 and EBOX Complex Interaction

C (nM)	k_a ($M^{-1}s^{-1}$)	R_{max} (RU)	L_r (m/s)	F (µl/min)	L_m (m/s)	Calc %MTL
1.87	$7.04x10^{7}$	100	$3.70x10^{-5}$	50	$5.84x10^{-3}$	0.63
0.74	$1.29x10^{8}$	100	$6.82x10^{-5}$	50	$5.84x10^{-3}$	1.16
0.37	$6.77x10^{7}$	100	$3.56x10^{-5}$	50	$5.84x10^{-3}$	0.61

Table 22. %MTL Calculation for CRY2 and EBOX Complex Interaction

al.'s previous work, where the interaction of CRY2 with BMAL1:CLOCK:EBOX ternary complex was observed with the use of gel mobility shift assay.[26]

To analyze the success of the nonlinear regression curve fitting with pseudo-first order approximation, residual standard deviation of the fitted curves from the actual data curve was calculated. The residual standard deviation is between 2.290 and 3.813 while the maximum response unit obtained is 60 RU during experimentation (Table 21). Therefore, calculated standard deviations are in the convenience gap and this indicates that pseudo-first order approximation is a good estimation.

Interaction of CRY2: PER2 with EBOX complex

Next, BMAL1:CLOCK:EBOX complex was immobilized onto the surface and CRY2:PER2 was injected over the surface subsequently within the concentration range of 10.0-50.0 nM. (Figure 24) In the SPR data, as concentration of analyte increases, the plateau response unit also increases. The response versus concentration data ensures that the SPR signal in response units is directly proportional to analyte concentration (Figure 25). Figure 24 demonstrates the obtained sensograms, which were analyzed according to rapid mixing model, as the percent mass transfer limitation was found to be within 0.01 and 0.02 range (Table 24). During analysis, all fitted parameters were fitted as a local parameter. The association rate constant of this interaction ranged between $1.10x10^{6}$ - $1.96x10^{6}$ $M^{-1}s^{-1}$, where the dissociation constant varied between 0.04 - 0.07s^{-1} , with an

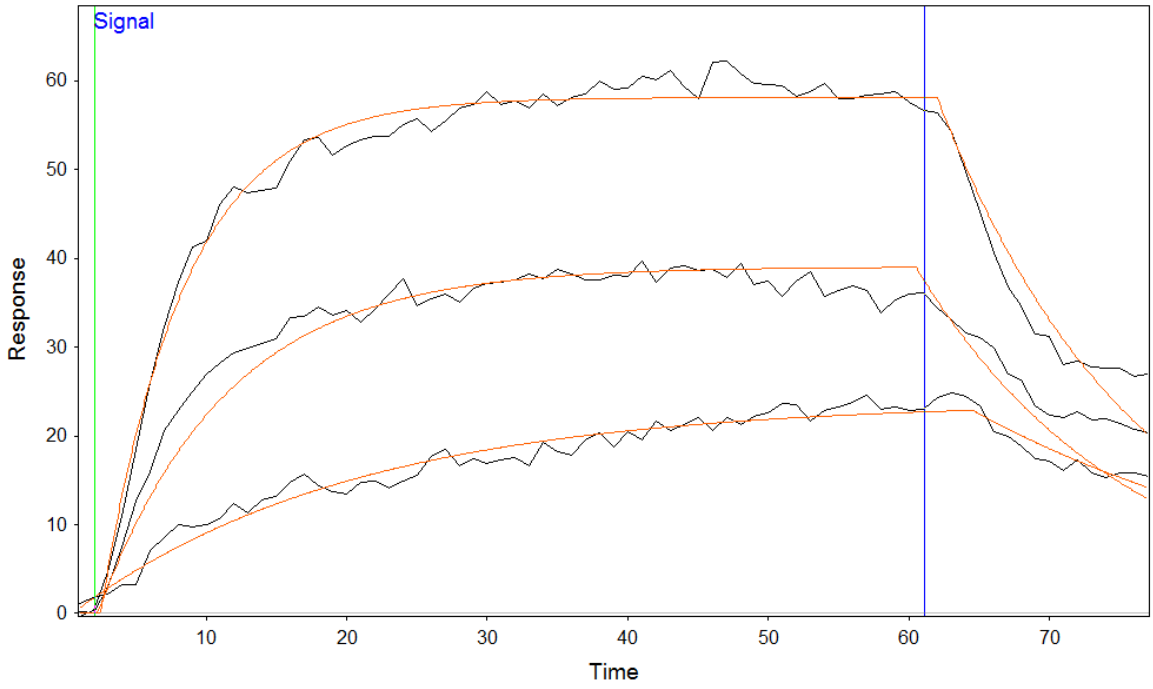

Figure 24. Response Unit vs. Time Graph for Interaction between CRY2:PER2 and EBOX Complex

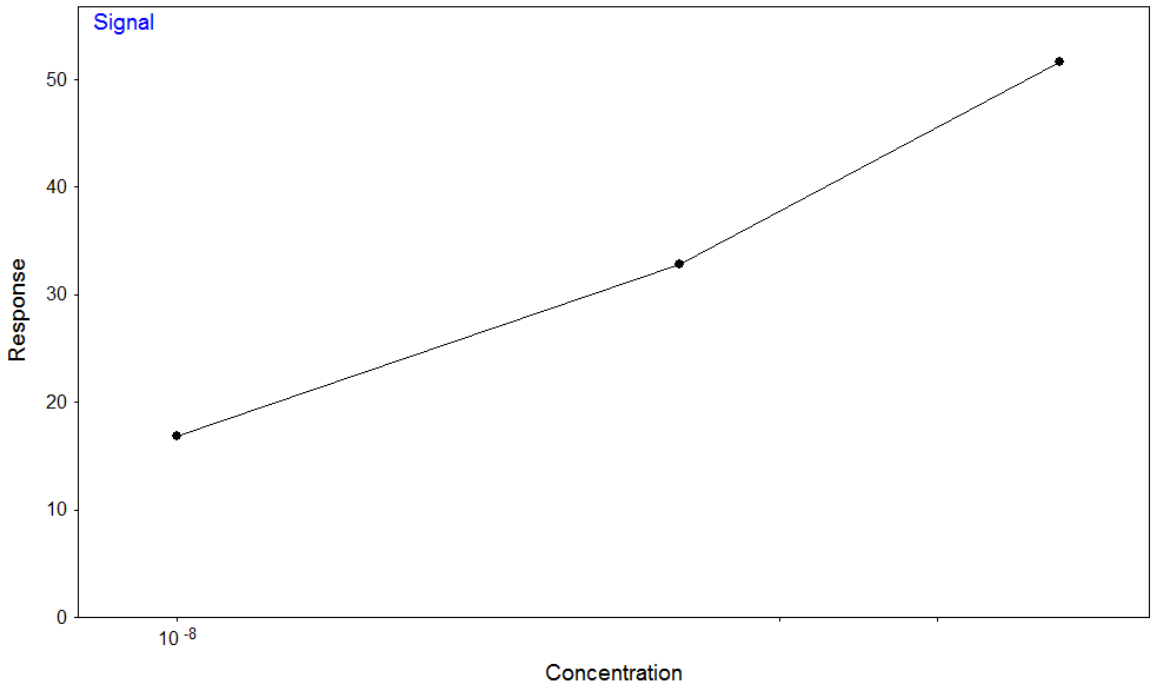

Figure 25. Response vs. Concentration Graph for CRY2:PER2 and EBOX Complex Interaction

overall binding constant range of 31.06-39.05 nM (Table 23).

To analyze the success of the nonlinear regression curve fitting with pseudo-first order approximation, residual standard deviation of the fitted curves from the actual data curve was calculated. The residual standard deviations for different analyte concentrations vary between 1.230 and 2.169 while the maximum observed signal during experimentation is 60RU (Table 23). This indicates that the residual standard deviation is in the convenience gap and pseudo-first order assumption is a good estimate. The calculated kinetic constants are good estimates of true kinetic constants.

C (nM)	k_a ($M^{-1}s^{-1}$)	k_d (s^{-1})	K_D (nM)	Res SD
50.0	1.96x106	0.0706	36.06	2.169
25.0	1.72x106	0.0670	39.05	2.757
10.0	1.19x106	0.0383	31.96	1.230

Table 23. Binding Affinities and Kinetic Constants for CRY2:PER2 and EBOX Complex Interaction

C (nM)	k_a ($M^{-1}s^{-1}$)	R_{max} (RU)	L_r (m/s)	F (µl/min)	L_m (m/s)	Calc %MTL
50.0	$1.96x10^{6}$	100	$1.03x10^{-6}$	50	$4.25x10^{-3}$	0.02
25.0	$1.72x10^{6}$	100	$9.04x10^{-7}$	50	$4.25x10^{-3}$	0.02
10.0	$1.19x10^{6}$	100	$6.31x10^{-7}$	50	$4.25x10^{-3}$	0.01

Table 24. %MTL calculation for CRY2:PER2 and EBOX Complex Interaction

Interaction of PER2 with EBOX complex

Finally, interactions between PER2 and EBOX complex are investigated with simple one-to-one simple approximation, since percent mass transfer limitation for the interaction was calculated as 0.01 (Table 26). The obtained sensogram (Figure 27) was analyzed via nonlinear regression curve fitting for every concentration of PER2 in the range of 14.7-

C (nM)	k_a ($M^{-1}s^{-1}$)	k_d (s^{-1})	K_D (nM)	Res SD
73.5	8.49×10^{5}	0.0903	106.33	2.722
29.4	9.05×10^{5}	0.1245	137.53	1.123
14.7	4.99×10^{5}	0.0859	171.76	0.973

Table 25. Binding Affinities and Kinetic Constants for PER2 and EBOX Complex Interaction

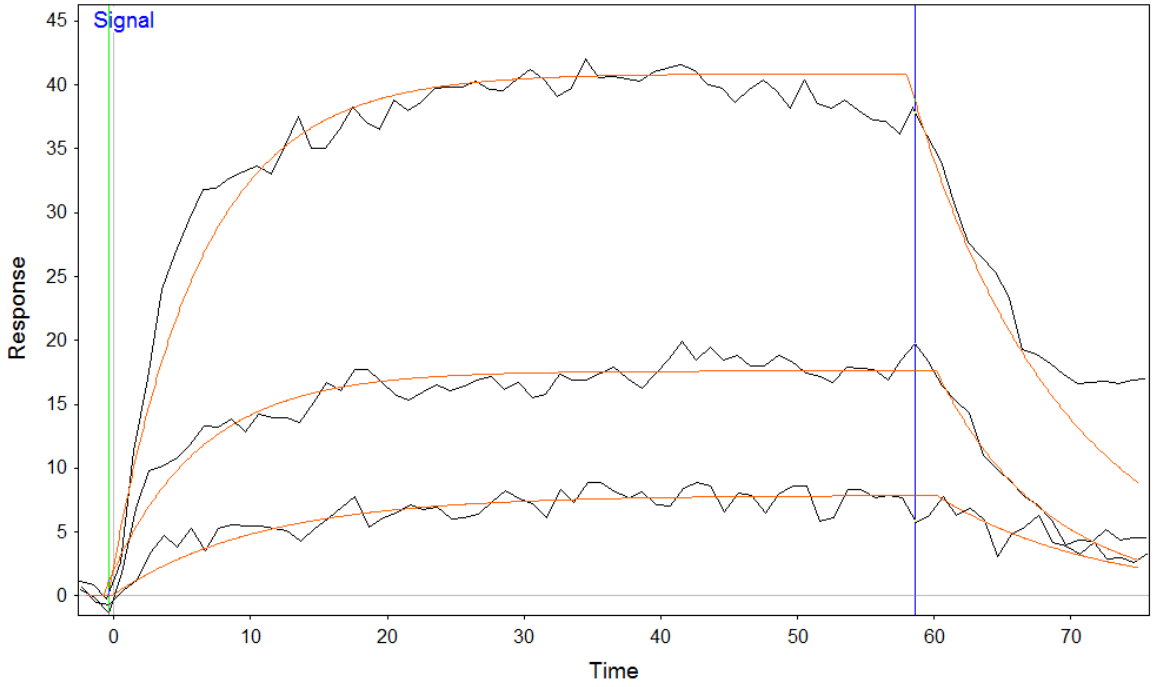

Figure 26. Response Unit vs. Time Graph for Interaction between PER2 and EBOX Interaction

C (nM)	k_a ($M^{-1}s^{-1}$)	R_{max} (RU)	L_r (m/s)	F (µl/min)	L_m (m/s)	Calc %MTL
73.5	8.49×10^5	100	4.47×10^{-7}	50	4.77×10^{-3}	0.01
29.4	9.05×10^5	100	4.76×10^{-7}	50	4.77×10^{-3}	0.01
14.7	4.99×10^5	100	2.63×10^{-7}	50	4.77×10^{-3}	0.01

Table 26. %MTL calculation for PER2 and EBOX Complex Interaction

73.5 nM. In the SPR data, as concentration of analyte increases, the plateau response unit also increases. The response versus concentration data ensures that the SPR signal in response units is directly proportional to analyte concentration (Figure 26). For analysis,

rapid mixing model has been selected since the percent mass transfer limitation was calculated as 0.01 which indicates that mass transfer limitation effect on reaction kinetics is negligible.. (Table 26) The association and dissociation rate constants were within the ranges of $4.00x10^5$ - $9.05x10^5$ $M^{-1}s^{-1}$, and 0.08 -0.12 s^{-1} , respectively. The binding constant within the range of 0.10-0.17 µM between PER2 and EBOX suggested that PER2 has a lower affinity, compared to the affinities of CRY2 or CRY2:PER2 complex towards EBOX complex (Table 25). In a previous study, Ye et al.'s suggested the absence of interaction of PER2 with BMAL1:CLOCK:EBOX ternary complex according to gel shift assay combined with ChIP assay in fibroblast cells.[26]

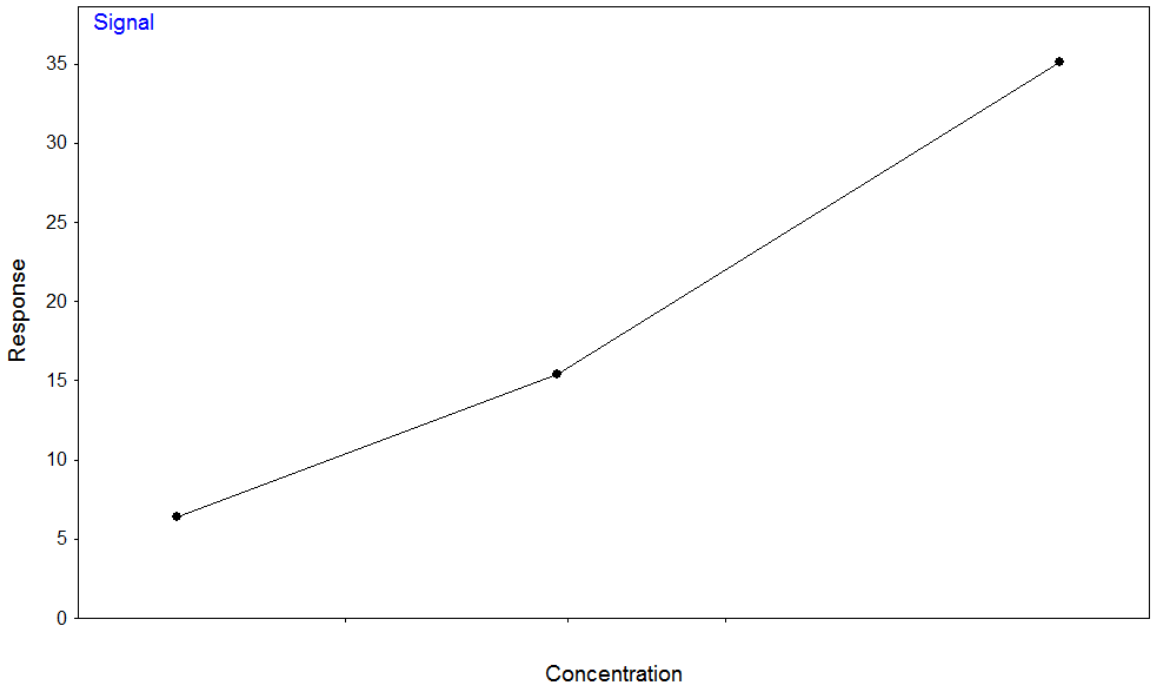

Figure 27. Response vs. Concentration Graph for PER2 and EBOX Complex Interaction

To analyze the success of the nonlinear regression curve fitting with pseudo-first order approximation, residual standard deviation of the fitted curves from the actual data curve

was calculated which is within 10% confidence gap. The residual standard deviation ranges between 0.973 and 2.722 where the maximum attained SPR signal is 40 RU in the experiment (Table 25). Therefore, fitted kinetic constants are good estimates of the true kinetic constants.

Overall Evaluation of Binding Affinities and Kinetic Constants of Interactions between Core Circadian Clock Proteins

The list of kinetic constants and binding affinities for interactions between core circadian clock components are tabulated in Table 27. For the pairwise interactions, the affinity order is BMAL1-CLOCK > CRY2-PER2 > BMAL1-PER2 > PER2-CLOCK > CRY2-BMAL1 > CRY2-CLOCK. It has been suggested that BMAL1 and CLOCK has the highest affinity toward each other among any other pairwise interaction between individual clock proteins via luciferase reporter gene assays.[58, 257] CRY2 has been found to have a higher affinity to BMAL1 than PER2. And PER2 has been found to have higher affinity toward CLOCK than CRY2. This ordering have been provided before via co-immunoprecipitation assays[25-26] ; however, an affinity order for the rest of the pairwise interactions between clock proteins has not been provided yet.

The interactions from the experiments studied with BMAL1:CLOCK, PER2, CRY2, and PER2: CRY2 complex demonstrated that CRY2 has the highest affinity toward BMAL1:CLOCK. The binding constants, K_D, values have all similar orders of magnitude, and are in the nanomolar range, which also suggest that PER2, CRY2 and CRY2:PER2 proteins have all strong affinities toward BMAL1:CLOCK complex. Interaction of PER2, CRY2 or PER2:CRY2 with BMAL1 and CLOCK off of DNA has been investigated in previous studies.[26] For example, CRY2 was studied via luciferase reporter gene assay to inhibit BMAL1:CLOCK complex mediated transcription by direct binding to this complex.[44] PER2 and CRY2 proteins were also reported to react with BMAL1 and CLOCK off of DNA motifs.[26] In those studies, PER2 was found to establish direct

interaction with BMAL1:CLOCK, and bridged CRY1 to suppress BMAL1:CLOCK mediated transcription. PER2:CRY2 was reported to react with BMAL1:CLOCK from its CLOCK to block activity of the transcription factor.[258] Those previous assays were run in a batch mode, where the results provided positive or negative information about the interactions between those protein-complex pairs. This high affinity constant indicates that BMAL1 and CLOCK also forms complexes in vivo like PER2 and CRY2 proteins. The strength of BMAL1:CLOCK complex is slightly higher than the strength of PER2:CRY2.

Interaction Pair	**k_a (M^{-1} s^{-1})**	**k_d (s^{-1})**	**K_D (nM)**
BMAL1-CRY2	$0.67x10^7$ - $1.07x10^7$	0.28 - 0.36	34.70-45.10 (±6.31)
BMAL1- PER2	$0.43x10^7$ - $1.42x10^7$	0.13 - 0.14	9.85-32.30 (±12.30)
CRY2-PER2	$1.46x10^7$ - $2.78x10^7$	0.11 - 0.25	7.54-9.00 (± 0.73)
CRY2-CLOCK	$0.26x10^7$ - $0.53x10^7$	0.21 - 0.31	47.40-78.50 (±15.80)
BMAL1-CLOCK	$3.33x10^7$ – $5.56x10^7$	0.23 - 0.20	3.60-6.90 (±1.86)
PER2-CLOCK	$1.09x10^7$ - $1.09x10^7$	0.21 - 0.26	19.3-24.2 (±2.59)
CRY2-BMAL1:CLOCK	$6.96x10^6$-$2.85x10^7$	0.07-0.09	2.51-10.4 (± 3.95)
CRY2:PER2-BMAL1:CLOCK	$4.66x10^6$-$6.83x10^6$	0.08-0.09	12.83-17.13 (± 2.22)
PER2-BMAL1:CLOCK	$1.75x10^6$-$8.90x10^6$	0.07-0.09	4.53-49.6 (±24.9)
CRY2-EBOX Complex	$6.77x10^7$-$1.29x10^8$	0.06-0.11	0.87-1.22 (± 0.18)
CRY2:PER2-EBOX Complex	$1.19x10^6$-$1.96x10^6$	0.04-0.07	31.96-39.05 (±3.56)
PER2-EBOX Complex	$4.99x10^5$-$9.05x10^5$	0.09-0.12	106.33-171.76 (±32.73)

Table 27. The List of Binding Affinities and Kinetic Constants of Interaction between Core Circadian Clock Proteins

According to the binding constants calculated here, CRY2 has the highest affinity towards EBOX complex among the clock proteins studied, while PER2:CRY2 follows CRY2 in the affinity order. PER2 has the smallest affinity towards EBOX complex. These results are consistent with other studies, which previously suggested CRY as the main repressor of the BMAL1:CLOCK binding to EBOX.[26] The highest affinity of CRY2 protein towards ternary EBOX complex may support CRY2 as the main regulator of BMAL1:CLOCK mediated transcription suppression. Also, in liver cells PER2 was detected to bind to cognate promoters in stabilizing loop of liver nuclei via ChIP assay.[60] PER2 have been reported to have a similar structure to BMAL1 region of EBOX ternary complex, which may stimulate interaction between them.[47] In addition to these observations, it was suggested in another study that PER:CRY could bind to BMAL1:CLOCK from its PER2.[59] However, the results for PER2:CRY and PER2 binding with EBOX complex conflicts with Ye et al, where the authors observed that PER2:CRY1 and PER2 could not bind to ternary EBOX complex in fibroblast cells according to gel mobility shift assays combined with ChIP assays. [26] ChIP assays are mapping techniques, and provide information about the existence of direct binding between ligand and ligate pairs instead of dynamic transcriptional information at the steady state.[261] Low affinity interactions among ligand and ligate pairs occurs within a small time period, which may continue from ten to fifteen minutes. [26] The lack of observation of interactions could be attributed to this short time period of the assay. The dissociation rate constant of interaction between PER2 and EBOX complex ranges between 0.08 -0.12 s^{-1}, which means that the dissociation half-life of PER2 and EBOX interaction varies between 5.77-8.66 s *in vitro* according to pseudo first order kinetics. Therefore, low affinity of PER2 towards ternary EBOX complex may not be detected in an assay setting carried out in a batch format. Our analyses with SPR demonstrated lower affinity of PER2:CRY2 complex than the affinity of CRY2 towards EBOX region. In the study of Ye et al., it was suggested that PER2

interfered with the interaction of CRY and ternary EBOX complex.[26] Hence, lower affinity of PER2:CRY2 complex towards ternary EBOX complex compared to that of CRY2 may be attributed to the presence of PER2 in this PER2:CRY2 and EBOX interaction.

CRY2 has higher affinity towards BMAL1:CLOCK:EBOX ternary complex than its affinity towards BMAL1:CLOCK, however, PER2 and PER2:CRY2 have lower affinity towards BMAL1:CLOCK:EBOX ternary complex than the affinity towards BMAL1:CLOCK complex. This may indicate that CRY2 is the main regulator of BMAL1:CLOCK:EBOX. [40, 44, 57, 117, 251] The presence of EBOX in these interactions might interfere with the participation of PER2 and PER2:CRY2 in the reaction (Table 1). This result may indicate that in a competitive cellular environment, CRY2 binding may dominate the binding of PER2 or PER2:CRY2 towards ternary EBOX complex due to its higher affinity in *in vitro* conditions.

In the previous biochemical assays, where clock protein interactions were investigated, various conflicting results were obtained. For example, Gekakis et al. [58] and Sangoram [262]suggested that PER was the main regulator of BMAL1:CLOCK:EBOX suppression., while in another study, CRY was the main repressor of this complex, and PER2 was found to interfere with the binding of CRY1 to the BMAL1:CLOCK:EBOX complex. [26 47] In a different study by Horst et al., CRY2 was found as the main regulator of BMAL1:CLOCK:EBOX suppression *in vivo*. The study involved animal model, where mice lacking both mCRY1 and mCRY2 genes lost its circadian rhythmicity in wheel-running behavior completely.[263] The *in vivo* assays are advantageous, as they provide all posttranslational modifications that the interaction requires. [176] However, detection of weak interactions through biochemical methods is challenging due to the presence of extra rinsing steps.[44] Also, these assays, such as yeast two hybrids, may cause false positive results, which labels these interactions as “potential interactions”. [138] Many of the biochemical methods involve solution depletion, which usually require a chromatographic

adsorption media that may denature proteins. Also since these methods require high number of washing steps, the equilibrium bulk concentration cannot be accurately defined.[135] Therefore, a critical look for postulated transcriptional-translational loop theory with SPR is advantageous since it provides label free analysis along with real time binding data.

The equilibrium constants of clock proteins toward each other hinder important pharmacological implications. If circadian physiology is completely revealed, the most suitable drug delivery regimens can be scheduled according to the daytime dependent activity and toxicity of drugs for chronopharmacology and chronotherapy fields.[64-65] For instance, by exploiting the circadian timing, chronotherapeutic schedules are formed to optimize drug treatments and to reduce side effects of medications. [3, 264-266]. A drug which manipulate biological clock may be a useful therapeutic to treat clock related diseases.[65] With the affinity knowledge among circadian components, some drugs may be designed to interfere with dimerization of biological clock proteins as a chemical competitor. As a result, a free oscillating individual daily rhythm under dynamic conditions can be created to help night shift workers or military man in duty. Also kinetic information such as association and dissociation constants would be critical to analyze the activity of proteins *in vitro*.[151-152]

Chapter 4: CONCLUSION

In this study, kinetic constants and binding affinities of pairwise interactions among clock proteins, as well as PER2, CRY2 and PER2:CRY2 proteins with BMAL1:CLOCK complex in the presence and absence of EBOX motif are presented using SPR. Either one of the clock proteins individually, BMAL1:CLOCK complex or BMAL1:CLOCK:EBOX ternary complex were immobilized on the sensor surface as ligands. Individual clock proteins or PER2:CRY2 complex was injected over immobilized surface to investigate the reaction between clock components. The SPR experiments performed as tandem settings of association and dissociation for sequential analyte concentrations. Interaction among circadian clock components resulted in typical SPR response curves, i.e. an increase in the injection mode and a decrease in the load mode. The binding constant of the interaction among circadian clock components were determined by the analysis of association and dissociation phases in the sensograms via nonlinear regression curve fitting analysis by pseudo-first order reaction kinetics approximation. Percent MTL values for the interaction pairs indicated the absence of mass transfer limitation on reaction kinetics. It is observed that CRY2, PER2 proteins as well as BMAL1 and CLOCK proteins form complexes *in vitro*. For pairwise interactions, CRY2 has been found to have a higher affinity to BMAL1 than PER2. And PER2 has been found to have a higher affinity toward CLOCK than CRY2. Among pairwise interactions, BMAL1 and CLOCK presented highest affinity toward each other while the lowest pairwise affinity was defined between CLOCK and CRY2. For complex interactions, PER2, CRY2 and PER2:CRY2 have similar affinities towards BMAL1:CLOCK complex, where the binding constant of these interactions are

within nanomolar range. When an EBOX motif was immobilized on SPR surface, CRY2 protein had the highest affinity towards EBOX complex, while PER2 and CRY2:PER2 complexes displayed lower affinities towards EBOX. Our results support separate biochemical assay findings in the literature and confirms CRY2 as the main regulator of repression of BMAL1:CLOCK activated clock gene expression. Lower interaction between PER2 and BMAL1:CLOCK:EBOX complex or CRY2:PER2 and BMAL1:CLOCK:EBOX complex binding were observed. Since interaction affinities between clock proteins are quantified, this study would be significant for the discovery and design of drugs for clock related diseases.

BIBLIOGRAPHY

1. Mohawk JA, Green CB, Takahashi JS. Central and peripheral circadian clocks in mammals. *Annu Rev Neurosci.* 2012;35:445-462.

2. Dibner C, Schibler U, Albrecht U. The mammalian circadian timing system: organization and coordination of central and peripheral clocks. *Annu Rev Physiol.* 2010;72:517-549.

3. Scheer FA, Van Montfrans GA, van Someren EJ, Mairuhu G, Buijs RM. Daily nighttime melatonin reduces blood pressure in male patients with essential hypertension. *Hypertension.* Feb 2004;43(2):192-197.

4. Hirota T, Fukada Y. Resetting mechanism of central and peripheral circadian clocks in mammals. *Zoolog Sci.* Apr 2004;21(4):359-368.

5. Albrecht U. Timing to perfection: the biology of central and peripheral circadian clocks. *Neuron.* Apr 26 2012;74(2):246-260.

6. Albrecht U, Eichele G. The mammalian circadian clock. *Curr Opin Genet Dev.* Jun 2003;13(3):271-277.

7. Okamura H, Doi M, Fustin JM, Yamaguchi Y, Matsuo M. Mammalian circadian clock system: Molecular mechanisms for pharmaceutical and medical sciences. *Adv Drug Deliv Rev.* Jul 31 2010;62(9-10):876-884.

8. Takahashi JS, Hong HK, Ko CH, McDearmon EL. The genetics of mammalian circadian order and disorder: implications for physiology and disease. *Nat Rev Genet.* Oct 2008;9(10):764-775.

9. Bass J, Turek FW. Sleepless in America: a pathway to obesity and the metabolic syndrome? *Arch Intern Med.* Jan 10 2005;165(1):15-16.

10. Turek FW, Joshu C, Kohsaka A, et al. Obesity and metabolic syndrome in circadian Clock mutant mice. *Science.* May 13 2005;308(5724):1043-1045.

11. Sahar S, Sassone-Corsi P. Metabolism and cancer: the circadian clock connection. *Nat Rev Cancer.* Dec 2009;9(12):886-896.

12. Filipski E, King VM, Li X, et al. Host circadian clock as a control point in tumor progression. *J Natl Cancer Inst.* May 1 2002;94(9):690-697.

13. Cao Q, Gery S, Dashti A, et al. A role for the clock gene per1 in prostate cancer. *Cancer Res.* Oct 1 2009;69(19):7619-7625.

14. You S, Wood PA, Xiong Y, Kobayashi M, Du-Quiton J, Hrushesky WJ. Daily coordination of cancer growth and circadian clock gene expression. *Breast Cancer Res Treat.* May 2005;91(1):47-60.

15. Reiter RJ, Tan DX, Erren TC, Fuentes-Broto L, Paredes SD. Light-mediated perturbations of circadian timing and cancer risk: a mechanistic analysis. *Integr Cancer Ther.* Dec 2009;8(4):354-360.
16. Anea CB, Zhang M, Stepp DW, et al. Vascular disease in mice with a dysfunctional circadian clock. *Circulation.* Mar 24 2009;119(11):1510-1517.
17. Maemura K, Takeda N, Nagai R. Circadian rhythms in the CNS and peripheral clock disorders: role of the biological clock in cardiovascular diseases. *J Pharmacol Sci.* Feb 2007;103(2):134-138.
18. Shi SQ, Ansari TS, McGuinness OP, Wasserman DH, Johnson CH. Circadian disruption leads to insulin resistance and obesity. *Curr Biol.* Mar 4 2013;23(5):372-381.
19. Knutson KL, Ryden AM, Mander BA, Van Cauter E. Role of sleep duration and quality in the risk and severity of type 2 diabetes mellitus. *Arch Intern Med.* Sep 18 2006;166(16):1768-1774.
20. Knutson KL, Cauter E. Associations between sleep loss and increased risk of obesity and diabetes. *Ann Ny Acad Sci.* 2008;1129:287-304.
21. Doi M, Takahashi Y, Komatsu R, et al. Salt-sensitive hypertension in circadian clock-deficient Cry-null mice involves dysregulated adrenal Hsd3b6. *Nat Med.* Jan 2010;16(1):67-74.
22. Rudic RD, Fulton DJ. Pressed for time: the circadian clock and hypertension. *J Appl Physiol.* Oct 2009;107(4):1328-1338.
23. Bunney BG, Bunney WE. Mechanisms of Rapid Antidepressant Effects of Sleep Deprivation Therapy: Clock Genes and Circadian Rhythms. *Biol Psychiatry.* Aug 17 2012.
24. Bunney BG, Bunney WE. Rapid-acting antidepressant strategies: mechanisms of action. *Int J Neuropsychopharmacol.* Jun 2012;15(5):695-713.
25. Langmesser S, Tallone T, Bordon A, Rusconi S, Albrecht U. Interaction of circadian clock proteins PER2 and CRY with BMAL1 and CLOCK. *BMC Mol Biol.* 2008;9:41.
26. Ye R, Selby CP, Ozturk N, Annayev Y, Sancar A. Biochemical analysis of the canonical model for the mammalian circadian clock. *J Biol Chem.* Jul 22 2011;286(29):25891-25902.
27. Yagita K, Yamaguchi S, Tamanini F, et al. Dimerization and nuclear entry of mPER proteins in mammalian cells. *Genes Dev.* Jun 1 2000;14(11):1353-1363.
28. Rosato E, Codd V, Mazzotta G, et al. Light-dependent interaction between Drosophila CRY and the clock protein PER mediated by the carboxy terminus of CRY. *Curr Biol.* Jun 26 2001;11(12):909-917.

29. Schuck P. Use of surface plasmon resonance to probe the equilibrium and dynamic aspects of interactions between biological macromolecules. *Annu Rev Bioph Biom.* 1997;26:541-566.

30. Myszka DG, He X, Dembo M, Morton TA, Goldstein B. Extending the range of rate constants available from BIACORE: interpreting mass transport-influenced binding data. *Biophys J.* Aug 1998;75(2):583-594.

31. Karlsson R, Falt A. Experimental design for kinetic analysis of protein-protein interactions with surface plasmon resonance biosensors. *J Immunol Methods.* Jan 15 1997;200(1-2):121-133.

32. Katsamba PS, Navratilova I, Calderon-Cacia M, et al. Kinetic analysis of a high-affinity antibody/antigen interaction performed by multiple Biacore users. *Anal Biochem.* May 15 2006;352(2):208-221.

33. Lung FD, Chen CH, Liou CC, Chen HY. Surface plasmon resonance detection of interactions between peptide fragments of N-telopeptide and its monoclonal antibodies. *J Pept Res.* Apr 2004;63(4):365-370.

34. Kizilel R, Demir E, Azizoglu S, Asimgi H, Kavakli IH, Kizilel S. Investigation of real-time photorepair activity on DNA via surface plasmon resonance. *PLoS One.* 2012;7(8):e44392.

35. Bo Liedberg CN, Ingemar Lunström. Surface plasmon resonance for gas detection and biosensing. *Sensors and Actuators.* 1983;4:299-304.

36. O'Shannessy DJ, Brigham-Burke M, Soneson KK, Hensley P, Brooks I. Determination of rate and equilibrium binding constants for macromolecular interactions using surface plasmon resonance: use of nonlinear least squares analysis methods. *Anal Biochem.* Aug 1 1993;212(2):457-468.

37. Kortt AA, Nice E, Gruen LC. Analysis of the binding of the Fab fragment of monoclonal antibody NC10 to influenza virus N9 neuraminidase from tern and whale using the BIAcore biosensor: effect of immobilization level and flow rate on kinetic analysis. *Anal Biochem.* Aug 15 1999;273(1):133-141.

38. Goldstein B, Coombs D, He X, Pineda AR, Wofsy C. The influence of transport on the kinetics of binding to surface receptors: application to cells and BIAcore. *J Mol Recognit.* Sep-Oct 1999;12(5):293-299.

39. De Crescenzo G, Grothe S, Lortie R, Debanne MT, O'Connor-McCourt M. Real-time kinetic studies on the interaction of transforming growth factor alpha with the epidermal growth factor receptor extracellular domain reveal a conformational change model. *Biochemistry.* Aug 8 2000;39(31):9466-9476.

40. Kume K, Zylka MJ, Sriram S, et al. mCRY1 and mCRY2 are essential components of the negative limb of the circadian clock feedback loop. *Cell.* Jul 23 1999;98(2):193-205.

41. Duong HA, Robles MS, Knutti D, Weitz CJ. A molecular mechanism for circadian clock negative feedback. *Science.* Jun 17 2011;332(6036):1436-1439.
42. Lee C, Etchegaray JP, Cagampang FR, Loudon AS, Reppert SM. Posttranslational mechanisms regulate the mammalian circadian clock. *Cell.* Dec 28 2001;107(7):855-867.
43. Brown SA, Ripperger J, Kadener S, et al. PERIOD1-associated proteins modulate the negative limb of the mammalian circadian oscillator. *Science.* Apr 29 2005;308(5722):693-696.
44. Griffin EA, Jr., Staknis D, Weitz CJ. Light-independent role of CRY1 and CRY2 in the mammalian circadian clock. *Science.* Oct 22 1999;286(5440):768-771.
45. Jia S, Peng J, Gao B, et al. Relative quantification of protein-protein interactions using a dual luciferase reporter pull-down assay system. *PLoS One.* 2011;6(10):e26414.
46. Nader N, Chrousos GP, Kino T. Circadian rhythm transcription factor CLOCK regulates the transcriptional activity of the glucocorticoid receptor by acetylating its hinge region lysine cluster: potential physiological implications. *FASEB J.* May 2009;23(5):1572-1583.
47. Huang N, Chelliah Y, Shan Y, et al. Crystal structure of the heterodimeric CLOCK:BMAL1 transcriptional activator complex. *Science.* Jul 13 2012;337(6091):189-194.
48. Phizicky EM, Fields S. Protein-protein interactions: methods for detection and analysis. *Microbiol Rev.* Mar 1995;59(1):94-123.
49. Kaushansky A, Allen JE, Gordus A, et al. Quantifying protein-protein interactions in high throughput using protein domain microarrays. *Nat Protoc.* Apr 2010;5(4):773-790.
50. Chavane N, Jacquemart R, Hoemann CD, Jolicoeur M, De Crescenzo G. At-line quantification of bioactive antibody in bioreactor by surface plasmon resonance using epitope detection. *Anal Biochem.* Jul 15 2008;378(2):158-165.
51. Hieb AR, D'Arcy S, Kramer MA, White AE, Luger K. Fluorescence strategies for high-throughput quantification of protein interactions. *Nucleic Acids Res.* Mar 2012;40(5):e33.
52. Jameson DM, Seifried SE. Quantification of protein-protein interactions using fluorescence polarization. *Methods.* Oct 1999;19(2):222-233.
53. Yan Z, Guo L, Hu L, Wang J. Specificity and affinity quantification of protein-protein interactions. *Bioinformatics.* Mar 7 2013.
54. Piliarik M, Homola J. Surface plasmon resonance (SPR) sensors: approaching their limits? *Opt Express.* Sep 14 2009;17(19):16505-16517.
55. Scarano S, Mascini M, Turner AP, Minunni M. Surface plasmon resonance imaging for affinity-based biosensors. *Biosens Bioelectron.* Jan 15 2010;25(5):957-966.

56. Azizoglu S, Kizilel R, Marusic M, Kavakli IH, Erman B, Kizilel S. Computational and experimental investigation of DNA repair protein photolyase interactions with low molecular weight drugs. *J Mol Recognit.* Jul 2013;26(7):297-307.
57. Shearman LP, Sriram S, Weaver DR, et al. Interacting molecular loops in the mammalian circadian clock. *Science.* May 12 2000;288(5468):1013-1019.
58. Gekakis N, Staknis D, Nguyen HB, et al. Role of the CLOCK protein in the mammalian circadian mechanism. *Science.* Jun 5 1998;280(5369):1564-1569.
59. Chen R, Schirmer A, Lee Y, et al. Rhythmic PER abundance defines a critical nodal point for negative feedback within the circadian clock mechanism. *Mol Cell.* Nov 13 2009;36(3):417-430.
60. Schmutz I, Ripperger JA, Baeriswyl-Aebischer S, Albrecht U. The mammalian clock component PERIOD2 coordinates circadian output by interaction with nuclear receptors. *Genes Dev.* Feb 15 2010;24(4):345-357.
61. Lavie P, NetLibrary Inc. The enchanted world of sleep. New Haven: Yale University Press; 1996: http://www.netLibrary.com/urlapi.asp?action=summary&v=1&bookid=53063.
62. Hartwell LH, Hopfield JJ, Leibler S, Murray AW. From molecular to modular cell biology. *Nature.* Dec 2 1999;402(6761 Suppl):C47-52.
63. Brown FA, Jr. The "clocks" timing biological rhythms. *Am Sci.* Nov-Dec 1972;60(6):756-766.
64. Schibler U. The daily rhythms of genes, cells and organs. Biological clocks and circadian timing in cells. *EMBO Rep.* Jul 2005;6 Spec No:S9-13.
65. Johnson CH, Hastings JW. The Elusive Mechanism of the Circadian Clock. *Am Sci.* Jan-Feb 1986;74(1):29-36.
66. Mizoguchi A, Ishizaki H. Prothoracic glands of the saturniid moth Samia cynthia ricini possess a circadian clock controlling gut purge timing. *Proc Natl Acad Sci U S A.* Apr 1982;79(8):2726-2730.
67. Takahashi JS, DeCoursey PJ, Bauman L, Menaker M. Spectral sensitivity of a novel photoreceptive system mediating entrainment of mammalian circadian rhythms. *Nature.* Mar 8-14 1984;308(5955):186-188.
68. Jacklet JW. Neural organization and cellular mechanisms of circadian pacemakers. *Int Rev Cytol.* 1984;89:251-294.
69. Buijs RM, van Eden CG, Goncharuk VD, Kalsbeek A. The biological clock tunes the organs of the body: timing by hormones and the autonomic nervous system. *J Endocrinol.* Apr 2003;177(1):17-26.
70. Foster RG, Hankins MW. Circadian vision. *Curr Biol.* Sep 4 2007;17(17):R746-751.
71. Provencio I, Rodriguez IR, Jiang G, Hayes WP, Moreira EF, Rollag MD. A novel human opsin in the inner retina. *J Neurosci.* Jan 15 2000;20(2):600-605.

72. Brainard GC, Hanifin JP, Greeson JM, et al. Action spectrum for melatonin regulation in humans: evidence for a novel circadian photoreceptor. *J Neurosci.* Aug 15 2001;21(16):6405-6412.
73. Moore RY. Entrainment pathways and the functional organization of the circadian system. *Prog Brain Res.* 1996;111:103-119.
74. Katzenberg D, Young T, Finn L, et al. A CLOCK polymorphism associated with human diurnal preference. *Sleep.* Sep 15 1998;21(6):569-576.
75. Toh KL, Jones CR, He Y, et al. An hPer2 phosphorylation site mutation in familial advanced sleep phase syndrome. *Science.* Feb 9 2001;291(5506):1040-1043.
76. Ebisawa T, Uchiyama M, Kajimura N, et al. Association of structural polymorphisms in the human period3 gene with delayed sleep phase syndrome. *EMBO Rep.* Apr 2001;2(4):342-346.
77. Fu L, Lee CC. The circadian clock: pacemaker and tumour suppressor. *Nat Rev Cancer.* May 2003;3(5):350-361.
78. Stevens RG. Circadian disruption and breast cancer: from melatonin to clock genes. *Epidemiology.* Mar 2005;16(2):254-258.
79. Kappers JA. Survey of the Innervation of the Epiphysis Cerebri and the Accessory Pineal Organs of Vertebrates. *Prog Brain Res.* 1965;10:87-153.
80. Kappers JA. The mammalian pineal organ. *J Neurovisc Relat.* 1969;31:Suppl 9:140+.
81. Quay WB. Histological Structure and Cytology of the Pineal Organ in Birds and Mammals. *Prog Brain Res.* 1965;10:49-86.
82. Reiter RJ. The melatonin rhythm: both a clock and a calendar. *Experientia.* Aug 15 1993;49(8):654-664.
83. Reiter RJ. Pineal control of a seasonal reproductive rhythm in male golden hamsters exposed to natural daylight and temperature. *Endocrinology.* Feb 1973;92(2):423-430.
84. Maestroni GJ, Conti A, Pierpaoli W. Role of the pineal gland in immunity. Circadian synthesis and release of melatonin modulates the antibody response and antagonizes the immunosuppressive effect of corticosterone. *J Neuroimmunol.* Nov 1986;13(1):19-30.
85. Angeli A, Gatti G, Sartori ML, Delponte D, Carignola R. Effect of Exogenous Melatonin on Human Natural-Killer (Nk) Cell-Activity - an Approach to the Immunomodulatry Role of the Pineal-Gland. *Neuroendocrinol Lett.* Oct 1987;9(5):286-286.
86. Viswanathan AN, Schernhammer ES. Circulating melatonin and the risk of breast and endometrial cancer in women. *Cancer Lett.* Aug 18 2009;281(1):1-7.
87. Arjona A, Sarkar DK. Circadian oscillations of clock genes, cytolytic factors, and cytokines in rat NK cells. *J Immunol.* Jun 15 2005;174(12):7618-7624.

88. Esquifino AI, Selgas L, Arce A, Maggiore VD, Cardinali DP. Twenty-four-hour rhythms in immune responses in rat submaxillary lymph nodes and spleen: effect of cyclosporine. *Brain Behav Immun.* Jun 1996;10(2):92-102.

89. Vgontzas AN, Chrousos GP. Sleep, the hypothalamic-pituitary-adrenal axis, and cytokines: multiple interactions and disturbances in sleep disorders. *Endocrinol Metab Clin North Am.* Mar 2002;31(1):15-36.

90. Gamaleia NF, Skivka LM, Fedorchuk AG, Shishko ED. Circadian rhythms of cytotoxic activity in peripheral blood mononuclear cells of patients with malignant melanoma. *Exp Oncol.* Mar 2006;28(1):54-60.

91. Kramer A, Yang FC, Snodgrass P, et al. Regulation of daily locomotor activity and sleep by hypothalamic EGF receptor signaling. *Science.* Dec 21 2001;294(5551):2511-2515.

92. Cheng MY, Bullock CM, Li C, et al. Prokineticin 2 transmits the behavioural circadian rhythm of the suprachiasmatic nucleus. *Nature.* May 23 2002;417(6887):405-410.

93. Jin X, Shearman LP, Weaver DR, Zylka MJ, de Vries GJ, Reppert SM. A molecular mechanism regulating rhythmic output from the suprachiasmatic circadian clock. *Cell.* Jan 8 1999;96(1):57-68.

94. Filipski E, Levi F. Circadian disruption in experimental cancer processes. *Integr Cancer Ther.* Dec 2009;8(4):298-302.

95. Erren TC, Reiter RJ. Defining chronodisruption. *J Pineal Res.* Apr 2009;46(3):245-247.

96. Arendt J. Jet-lag and shift work: (2). Therapeutic use of melatonin. *J R Soc Med.* Aug 1999;92(8):402-405.

97. Schernhammer ES, Laden F, Speizer FE, et al. Rotating night shifts and risk of breast cancer in women participating in the nurses' health study. *J Natl Cancer Inst.* Oct 17 2001;93(20):1563-1568.

98. Stevens RG, Davis S, Thomas DB, Anderson LE, Wilson BW. Electric power, pineal function, and the risk of breast cancer. *FASEB J.* Feb 1 1992;6(3):853-860.

99. Stevens RG. Light-at-night, circadian disruption and breast cancer: assessment of existing evidence. *Int J Epidemiol.* Aug 2009;38(4):963-970.

100. Zhu Y, Zheng TZ, Stevens RG, Zhang YW, Boye P. Does "clock" matter in prostate cancer? *Cancer Epidem Biomar.* Jan 2006;15(1):3-5.

101. Schernhammer ES, Razavi P, Li TY, Qureshi AA, Han J. Rotating night shifts and risk of skin cancer in the nurses' health study. *J Natl Cancer Inst.* Apr 6 2011;103(7):602-606.

102. Schernhammer ES, Laden F, Speizer FE, et al. Night-shift work and risk of colorectal cancer in the nurses' health study. *J Natl Cancer Inst.* Jun 4 2003;95(11):825-828.

103. Bjarnason GA, Jordan RC, Sothern RB. Circadian variation in the expression of cell-cycle proteins in human oral epithelium. *Am J Pathol.* Feb 1999;154(2):613-622.
104. Morin PJ. beta-catenin signaling and cancer. *Bioessays.* Dec 1999;21(12):1021-1030.
105. Lieu SJ, Curhan GC, Schernhammer ES, Forman JP. Rotating night shift work and disparate hypertension risk in African-Americans. *J Hypertens.* Jan 2012;30(1):61-66.
106. Kawachi I, Colditz GA, Stampfer MJ, et al. Prospective study of shift work and risk of coronary heart disease in women. *Circulation.* Dec 1 1995;92(11):3178-3182.
107. Knutsson A, Akerstedt T, Jonsson BG, Orth-Gomer K. Increased risk of ischaemic heart disease in shift workers. *Lancet.* Jul 12 1986;2(8498):89-92.
108. Brown DL, Feskanich D, Sanchez BN, Rexrode KM, Schernhammer ES, Lisabeth LD. Rotating night shift work and the risk of ischemic stroke. *Am J Epidemiol.* Jun 1 2009;169(11):1370-1377.
109. Marino JL, Holt VL, Chen C, Davis S. Shift work, hCLOCK T3111C polymorphism, and endometriosis risk. *Epidemiology.* May 2008;19(3):477-484.
110. Shoji S, Shoji Y. [Insomnia in diabetes]. *Nihon Rinsho.* Aug 2009;67(8):1525-1531.
111. Pan A, Schernhammer ES, Sun Q, Hu FB. Rotating night shift work and risk of type 2 diabetes: two prospective cohort studies in women. *PLoS Med.* Dec 2011;8(12):e1001141.
112. Gale JE, Cox HI, Qian J, Block GD, Colwell CS, Matveyenko AV. Disruption of circadian rhythms accelerates development of diabetes through pancreatic beta-cell loss and dysfunction. *J Biol Rhythms.* Oct 2011;26(5):423-433.
113. Srinivasan V, Smits M, Spence W, et al. Melatonin in mood disorders. *World J Biol Psychiatry.* 2006;7(3):138-151.
114. Lanfumey L, Mongeau R, Hamon M. Biological rhythms and melatonin in mood disorders and their treatments. *Pharmacol Ther.* May 2013;138(2):176-184.
115. Srinivasan V, De Berardis D, Shillcutt SD, Brzezinski A. Role of melatonin in mood disorders and the antidepressant effects of agomelatine. *Expert Opin Investig Drugs.* Oct 2012;21(10):1503-1522.
116. Leproult R, Van Cauter E. Role of sleep and sleep loss in hormonal release and metabolism. *Endocr Dev.* 2010;17:11-21.
117. Ripperger JA, Albrecht U. The circadian clock component PERIOD2: from molecular to cerebral functions. *Prog Brain Res.* 2012;199:233-245.
118. Lowrey PL, Takahashi JS. Mammalian circadian biology: Elucidating genome-wide levels of temporal organization. *Annu Rev Genom Hum G.* 2004;5:407-441.
119. Young MW, Kay SA. Time zones: a comparative genetics of circadian clocks. *Nat Rev Genet.* Sep 2001;2(9):702-715.

120. Storch KF, Lipan O, Leykin I, et al. Extensive and divergent circadian gene expression in liver and heart. *Nature.* May 2 2002;417(6884):78-83.
121. Miller BH, McDearmon EL, Panda S, et al. Circadian and CLOCK-controlled regulation of the mouse transcriptome and cell proliferation. *Proc Natl Acad Sci U S A.* Feb 27 2007;104(9):3342-3347.
122. Ohno T, Onishi Y, Ishida N. A novel E4BP4 element drives circadian expression of mPeriod2. *Nucleic Acids Res.* 2007;35(2):648-655.
123. Maywood ES, Chesham JE, Meng QJ, Nolan PM, Loudon AS, Hastings MH. Tuning the period of the mammalian circadian clock: additive and independent effects of CK1epsilonTau and Fbxl3Afh mutations on mouse circadian behavior and molecular pacemaking. *J Neurosci.* Jan 26 2011;31(4):1539-1544.
124. Buhr ED, Takahashi JS. Molecular components of the Mammalian circadian clock. *Handb Exp Pharmacol.* 2013(217):3-27.
125. Reppert SM, Weaver DR. Coordination of circadian timing in mammals. *Nature.* Aug 29 2002;418(6901):935-941.
126. Edery I, Rutila JE, Rosbash M. Phase shifting of the circadian clock by induction of the Drosophila period protein. *Science.* Jan 14 1994;263(5144):237-240.
127. Yan L, Silver R. Resetting the brain clock: time course and localization of mPER1 and mPER2 protein expression in suprachiasmatic nuclei during phase shifts. *Eur J Neurosci.* Feb 2004;19(4):1105-1109.
128. Travnickova-Bendova Z, Cermakian N, Reppert SM, Sassone-Corsi P. Bimodal regulation of mPeriod promoters by CREB-dependent signaling and CLOCK/BMAL1 activity. *P Natl Acad Sci USA.* May 28 2002;99(11):7728-7733.
129. Preitner N, Damiola F, Lopez-Molina L, et al. The orphan nuclear receptor REV-ERBalpha controls circadian transcription within the positive limb of the mammalian circadian oscillator. *Cell.* Jul 26 2002;110(2):251-260.
130. Guillaumond F, Dardente H, Giguere V, Cermakian N. Differential control of Bmal1 circadian transcription by REV-ERB and ROR nuclear receptors. *J Biol Rhythms.* Oct 2005;20(5):391-403.
131. Cho H, Zhao X, Hatori M, et al. Regulation of circadian behaviour and metabolism by REV-ERB-alpha and REV-ERB-beta. *Nature.* May 3 2012;485(7396):123-127.
132. Liu AC, Tran HG, Zhang EE, Priest AA, Welsh DK, Kay SA. Redundant function of REV-ERBalpha and beta and non-essential role for Bmal1 cycling in transcriptional regulation of intracellular circadian rhythms. *PLoS Genet.* Feb 2008;4(2):e1000023.
133. Berggard T, Linse S, James P. Methods for the detection and analysis of protein-protein interactions. *Proteomics.* Aug 2007;7(16):2833-2842.
134. Golemis E. *Protein-protein interactions : a molecular cloning manual*. Cold Spring Harbor, NY: Cold Spring Harbor Laboratory Press; 2002.

135. Vladimir Hlady JB, Herbert P. Jennissen. Methods for Studying Protein Adsorption. *Methods in Enzymology.* 1999;309:402-429.
136. Calonder C, Tie Y, Van Tassel PR. History dependence of protein adsorption kinetics. *Proc Natl Acad Sci U S A.* Sep 11 2001;98(19):10664-10669.
137. Schreiber G. Kinetic studies of protein-protein interactions. *Curr Opin Struct Biol.* Feb 2002;12(1):41-47.
138. Lalonde S, Ehrhardt DW, Loque D, Chen J, Rhee SY, Frommer WB. Molecular and cellular approaches for the detection of protein-protein interactions: latest techniques and current limitations. *Plant J.* Feb 2008;53(4):610-635.
139. Fang F, Szleifer I. Kinetics and thermodynamics of protein adsorption: a generalized molecular theoretical approach. *Biophys J.* Jun 2001;80(6):2568-2589.
140. Milan Mrksich GMW. Using self-assembled monolayers to understand the interactions of man-made surfaces with proteins and cells. *Annu Rev Bioph Biom.* 1996;25:55-78.
141. Myszka DG. Kinetic analysis of macromolecular interactions using surface plasmon resonance biosensors. *Curr Opin Biotechnol.* Feb 1 1997;8(1):50-57.
142. Mirsky VM. Quantitative Characterization of Affinity Properties of Immobilized Receptors. In: V. M. Mirsky AKY, ed. *Artificial Receptors for Chemical Sensors*: WILEY-VCH Verlag GmbH & Co. KGaA; 2011.
143. Panayotou G, Gish G, End P, et al. Interactions between Sh2 Domains and Tyrosine-Phosphorylated Platelet-Derived Growth-Factor Beta-Receptor Sequences - Analysis of Kinetic-Parameters by a Novel Biosensors-Based Approach. *Mol Cell Biol.* Jun 1993;13(6):3567-3576.
144. Schuster SC, Swanson RV, Alex LA, Bourret RB, Simon MI. Assembly and Function of a Quaternary Signal-Transduction Complex Monitored by Surface-Plasmon Resonance. *Nature.* Sep 23 1993;365(6444):343-347.
145. Kim YT, Tabor S, Churchich JE, Richardson CC. Interactions of Gene 2.5 Protein and DNA-Polymerase of Bacteriophage-T7. *J Biol Chem.* Jul 25 1992;267(21):15032-15040.
146. Vincent JP, Lazdunski M. Trypsin-pancreatic trypsin inhibitor association. Dynamics of the interaction and role of disulfide bridges. *Biochemistry.* Aug 1 1972;11(16):2967-2977.
147. Mason SW, Li J, Greenblatt J. Direct interaction between two Escherichia coli transcription antitermination factors, NusB and ribosomal protein S10. *J Mol Biol.* Jan 5 1992;223(1):55-66.
148. Ottobruc A, Antonny B, Vuong TM, Chardin P, Chabre M. Interaction between the Retinal Cyclic-Gmp Phosphodiesterase Inhibitor and Transducin - Kinetics and Affinity Studies. *Biochemistry.* Aug 24 1993;32(33):8636-8645.

149. Warne PH, Viciana PR, Downward J. Direct Interaction of Ras and the Amino-Terminal Region of Raf-1 in-Vitro. *Nature.* Jul 22 1993;364(6435):352-355.
150. Duan X, Li Y, Rajan NK, Routenberg DA, Modis Y, Reed MA. Quantification of the affinities and kinetics of protein interactions using silicon nanowire biosensors. *Nat Nanotechnol.* Jun 2012;7(6):401-407.
151. Wang Y, Shen BJ, Sebald W. A mixed-charge pair in human interleukin 4 dominates high-affinity interaction with the receptor alpha chain. *Proc Natl Acad Sci U S A.* Mar 4 1997;94(5):1657-1662.
152. Pearce KH, Jr., Cunningham BC, Fuh G, Teeri T, Wells JA. Growth hormone binding affinity for its receptor surpasses the requirements for cellular activity. *Biochemistry.* Jan 5 1999;38(1):81-89.
153. Wilkinson KD. Quantitative analysis of protein-protein interactions. *Methods Mol Biol.* 2004;261:15-32.
154. Merwe APvd. *Surface Plasmon Resonance*: Oxford University Press; 2001.
155. Lakey JH, Raggett EM. Measuring protein-protein interactions. *Curr Opin Struct Biol.* Feb 1998;8(1):119-123.
156. Cornish-Bowden A. Detection of errors of interpretation in experiments in enzyme kinetics. *Methods.* Jun 2001;24(2):181-190.
157. Chen J, Sawyer N, Regan L. Protein-protein interactions: general trends in the relationship between binding affinity and interfacial buried surface area. *Protein Sci.* Apr 2013;22(4):510-515.
158. Miernyk JA, Thelen JJ. Biochemical approaches for discovering protein-protein interactions. *Plant J.* Feb 2008;53(4):597-609.
159. Johnsson N, Varshavsky A. Split ubiquitin as a sensor of protein interactions in vivo. *Proc Natl Acad Sci U S A.* Oct 25 1994;91(22):10340-10344.
160. Monti M, Orru S, Pagnozzi D, Pucci P. Interaction proteomics. *Biosci Rep.* Feb-Apr 2005;25(1-2):45-56.
161. Phee BK, Shin DH, Cho JH, et al. Identification of phytochrome-interacting protein candidates in Arabidopsis thaliana by co-immunoprecipitation coupled with MALDI-TOF MS. *Proteomics.* Jun 2006;6(12):3671-3680.
162. Uetz P, Giot L, Cagney G, et al. A comprehensive analysis of protein-protein interactions in Saccharomyces cerevisiae. *Nature.* Feb 10 2000;403(6770):623-627.
163. Stelzl U, Worm U, Lalowski M, et al. A human protein-protein interaction network: a resource for annotating the proteome. *Cell.* Sep 23 2005;122(6):957-968.
164. Rual JF, Venkatesan K, Hao T, et al. Towards a proteome-scale map of the human protein-protein interaction network. *Nature.* Oct 20 2005;437(7062):1173-1178.
165. Parrish JR, Gulyas KD, Finley RL, Jr. Yeast two-hybrid contributions to interactome mapping. *Curr Opin Biotechnol.* Aug 2006;17(4):387-393.

166. Cusick ME, Klitgord N, Vidal M, Hill DE. Interactome: gateway into systems biology. *Hum Mol Genet.* Oct 15 2005;14 Spec No. 2:R171-181.
167. Gavin AC, Bosche M, Krause R, et al. Functional organization of the yeast proteome by systematic analysis of protein complexes. *Nature.* Jan 10 2002;415(6868):141-147.
168. Krogan NJ, Cagney G, Yu H, et al. Global landscape of protein complexes in the yeast Saccharomyces cerevisiae. *Nature.* Mar 30 2006;440(7084):637-643.
169. Guimaraes KS, Jothi R, Zotenko E, Przytycka TM. Predicting domain-domain interactions using a parsimony approach. *Genome Biol.* 2006;7(11):R104.
170. Pitre S, Dehne F, Chan A, et al. PIPE: a protein-protein interaction prediction engine based on the re-occurring short polypeptide sequences between known interacting protein pairs. *BMC Bioinformatics.* 2006;7:365.
171. Stagljar I, Korostensky C, Johnsson N, te Heesen S. A genetic system based on split-ubiquitin for the analysis of interactions between membrane proteins in vivo. *Proc Natl Acad Sci U S A.* Apr 28 1998;95(9):5187-5192.
172. Ingham RJ, Colwill K, Howard C, et al. WW domains provide a platform for the assembly of multiprotein networks. *Mol Cell Biol.* Aug 2005;25(16):7092-7106.
173. Belanger KD. Using affinity chromatography to investigate novel protein-protein interactions in an undergraduate cell and molecular biology lab course. *CBE Life Sci Educ.* Fall 2009;8(3):214-225.
174. Rohila JS, Chen M, Chen S, et al. Protein-protein interactions of tandem affinity purification-tagged protein kinases in rice. *Plant J.* Apr 2006;46(1):1-13.
175. Babu M, Krogan NJ, Awrey DE, Emili A, Greenblatt JF. Systematic characterization of the protein interaction network and protein complexes in Saccharomyces cerevisiae using tandem affinity purification and mass spectrometry. *Methods Mol Biol.* 2009;548:187-207.
176. Kouichi Kuroda MK, Joji Mima, Mitsuyoshi Ueda. Systems for the detection and analysis of protein-protein interactions. *Applied Microbiology and Biotechnology.* 2006;71:127-136.
177. Hall RA. Studying protein-protein interactions via blot overlay or Far Western blot. *Methods Mol Biol.* 2004;261:167-174.
178. Gentz R, Chen CH, Rosen CA. Bioassay for trans-activation using purified human immunodeficiency virus tat-encoded protein: trans-activation requires mRNA synthesis. *Proc Natl Acad Sci U S A.* Feb 1989;86(3):821-824.
179. Bedouelle H, Duplay P. Production in Escherichia coli and one-step purification of bifunctional hybrid proteins which bind maltose. Export of the Klenow polymerase into the periplasmic space. *Eur J Biochem.* Feb 1 1988;171(3):541-549.
180. Einarson MB, Pugacheva EN, Orlinick JR. Far Western: Labeling GST Fusion Proteins. *CSH Protoc.* 2007;2007:pdb prot4758.

181. Li Y, Hua F, Carraway KL, Carraway CA. The p185(neu)-containing glycoprotein complex of a microfilament-associated signal transduction particle. Purification, reconstitution, and molecular associations with p58(gag) and actin. *J Biol Chem.* Sep 3 1999;274(36):25651-25658.

182. Pennypacker KR, Kyritsis A, Chader GJ, Billingsley ML. Calmodulin-binding proteins in human Y-79 retinoblastoma and HTB-14 glioma cell lines. *J Neurochem.* May 1988;50(5):1648-1654.

183. Hausken ZE, Coghlan VM, Scott JD. Overlay, ligand blotting, and band-shift techniques to study kinase anchoring. *Methods Mol Biol.* 1998;88:47-64.

184. Carr DW, Hausken ZE, Fraser ID, Stofko-Hahn RE, Scott JD. Association of the type II cAMP-dependent protein kinase with a human thyroid RII-anchoring protein. Cloning and characterization of the RII-binding domain. *J Biol Chem.* Jul 5 1992;267(19):13376-13382.

185. Soderblom EJ, Goshe MB. Collision-induced dissociative chemical cross-linking reagents and methodology: Applications to protein structural characterization using tandem mass spectrometry analysis. *Anal Chem.* Dec 1 2006;78(23):8059-8068.

186. David LΓeres SS, Angus I. Lamond. Detecting protein-protein interactions in vivo with FRET using multiphoton fluorescence lifetime imaging microscopy (FLIM). *Current Protocols in Cytometry*: Jhon Wiley & Sons, ınc; 2007.

187. Duncan RR. Fluorescence lifetime imaging microscopy (FLIM) to quantify protein-protein interactions inside cells. *Biochemical Society Transactions.* 2006;35:679-682.

188. Xu X, Soutto M, Xie Q, et al. Imaging protein interactions with bioluminescence resonance energy transfer (BRET) in plant and mammalian cells and tissues. *Proc Natl Acad Sci U S A.* Jun 12 2007;104(24):10264-10269.

189. Xu Y, Piston DW, Johnson CH. A bioluminescence resonance energy transfer (BRET) system: application to interacting circadian clock proteins. *Proc Natl Acad Sci U S A.* Jan 5 1999;96(1):151-156.

190. Lakowicz JR. *Principles of Fluorescence Spectroscopy*. 3rd ed: Springer; 2007.

191. M.A Hink JWB, A. Visser. Fluorescence correlation spectroscopy of GFP fusion proteins in living plant cells. *Method in Enzymology.* 2003;361:93-112.

192. Doyle ML. Characterization of binding interactions by isothermal titration calorimetry. *Curr Opin Biotechnol.* Feb 1 1997;8(1):31-35.

193. Homola J. Present and future of surface plasmon resonance biosensors. *Analytical and Bioanalytical Chemistry.* 2003;377:528-539.

194. Rebecca L. Rich DGM. Why you should be using more SPR biosensor technology. *Drug Discovery Today: Technologies.* 2004;1(3):301-308.

195. Wood RW. XLII. On a remarkable case of un even distribution of light in a diffraction grating spectrum. *Philosophical Magazine Series 6.* 1902;4(21):396-402.

196. Rayleigh L. On the dynamical theory of gratings. *Proceedings of the Royal Society A: Mathematical, Physical & Engineering Sciences.* 1907;LXXIX:399-415.
197. Fano U. The theory of anomalous diffraction gratings and of quasi-stationary waves on metallic surfaces (Sommerfeld's waves). 1941;31(The Journal of the Optical Society of America):213-222.
198. E. Kretschmann HR. Radiative decay of nonradiative surface plasmons excited by light. *Z. Naturforsch. A.* 1968;23:2135-2136.
199. Otto A. Excitation of surface plasma waves in silver by the method of frustrated total reflection. *Zeitschrift für Physik.* 1968;216:398-410.
200. I. Pockrand JDS, J.G Gordon. Surface plasmon spectroscopy of organic monolayer assemblies. *Surface Science.* 1978;101:499-506.
201. R. P. H. Kooyman hK, J. van Gent, J. Greve. Surface plasmon resonance immunosensors: sensitivity considerations. *Analytica Chimica Acta.* 1988;213:35-45.
202. Homola J. Surface plasmon resonance sensors for detection of chemical and biological species. *Chem Rev.* Feb 2008;108(2):462-493.
203. Chinowsky TM, Soelberg SD, Baker P, et al. Portable 24-analyte surface plasmon resonance instruments for rapid, versatile biodetection. *Biosens Bioelectron.* Apr 15 2007;22(9-10):2268-2275.
204. Tanious FA, Nguyen B, Wilson WD. Biosensor-surface plasmon resonance methods for quantitative analysis of biomolecular interactions. *Methods Cell Biol.* 2008;84:53-77.
205. Peter Schuck LB, Peter Andersen. Measuring Protein Interactions by Optical Biosensors. *Current Protocols in Cell Biology*: John Wiley & Sons, Inc.; 2004:Unit 17.16.11-17.16.22.
206. Katsamba PS, Park S, Laird-Offringa IA. Kinetic studies of RNA-protein interactions using surface plasmon resonance. *Methods.* Feb 2002;26(2):95-104.
207. Myszka DG. Improving biosensor analysis. *J Mol Recognit.* Sep-Oct 1999;12(5):279-284.
208. Fischer MJ. Amine coupling through EDC/NHS: a practical approach. *Methods Mol Biol.* 2010;627:55-73.
209. J. A. Dionne LAS, H. A. Atwater. Planar metal plasmon waveguides: frequency-dependent dispersion, propagation, localization, and loss beyond the free electron model. *Physical Review B.* 2005;72.
210. M.A. Ordal LLL, R.J Bell, S.E Bell, R.R Bell, R.W Alexander, J. Ward, C.A Ward. Optical properties of metals Al, Co, Cu, Au, Fe, Pb, Ni, Pd, Pt, Ag, Ti and W in the infrared and far infrared. *Applied optics.* 1983;11:1099-1119.
211. O. Parriaux GV. Plasmon wave versus dielectric waveguiding for surface wave sensing. *Sensors and Actuators A.* 1990;23:1137-1141.

212. Yu Z, Fan S. Extraordinarily high spectral sensitivity in refractive index sensors using multiple optical modes. *Opt Express.* May 23 2011;19(11):10029-10040.
213. G. Margheri AM, F. Quercioli. A new high-resolution displacement sensor based on surface plasmon resonance. *Proceedings of the Society of photo-Optical Instrumentation.* 1996;2783:211-220.
214. J.K Schaller RC, C.G Stojanoff. Plasmon spectroscopy for high resolution angular measurements. *Proceedings of the Society of photo-Optical Instrumentation.* 1997;3098:476-486.
215. M.N. Weiss RS, H. Groger. Experimental investigation of a surface plasmon-based integrated-optic humidity sensor. *Electronics Letters.* 1996;32:842-843.
216. B. Chadwick MG. An optical temperature sensor using sensor plasmons. *Japanese Journal of Applied Physics.* 1993;32:2716-2717.
217. Chapple DS, Mason DJ, Joannou CL, Odell EW, Gant V, Evans RW. Structure-function relationship of antibacterial synthetic peptides homologous to a helical surface region on human lactoferrin against Escherichia coli serotype O111. *Infect Immun.* Jun 1998;66(6):2434-2440.
218. Kim E, DeMarco SJ, Marfatia SM, Chishti AH, Sheng M, Strehler EE. Plasma membrane Ca2+ ATPase isoform 4b binds to membrane-associated guanylate kinase (MAGUK) proteins via their PDZ (PSD-95/Dlg/ZO-1) domains. *J Biol Chem.* Jan 16 1998;273(3):1591-1595.
219. S. Miwa TA. Selective gas detection by means of surface plasmon resonance sensors. *Thin Solid Films.* 1996;281-282:466-468.
220. J. W. Waswa CD, J. Irudayaraj. Rapid Detection of Salmonella Enteritidis and Escherichia Coli Using Surface Plasmon Resonance Biosensor. *Journal of Food Process Engineering.* 2006;29:373-385.
221. Tang DP, Yuan R, Chai YQ. Novel immunoassay for carcinoembryonic antigen based on protein A-conjugated immunosensor chip by surface plasmon resonance and cyclic voltammetry. *Bioprocess Biosyst Eng.* Apr 2006;28(5):315-321.
222. Muller-Loennies S, Gronow S, Brade L, MacKenzie R, Kosma P, Brade H. A monoclonal antibody against a carbohydrate epitope in lipopolysaccharide differentiates Chlamydophila psittaci from Chlamydophila pecorum, Chlamydophila pneumoniae, and Chlamydia trachomatis. *Glycobiology.* Mar 2006;16(3):184-196.
223. Hana Vaisocherova JH. SPR Biosensors for Medical Diagnostics. *Surface Plasmon Resonance Based Sensors: Springer Series on Chemical Sensors and Biosensors.* 2006;4:229-247.
224. Geukens N, Rao CVS, Mellado RP, et al. Surface plasmon resonance-based interaction studies reveal competition of Streptomyces lividans type I signal peptidases for binding preproteins. *Microbiology.* May 2006;152(Pt 5):1441-1450.

225. Teramura Y, Iwata H. Label-free immunosensing for alpha-fetoprotein in human plasma using surface plasmon resonance. *Anal Biochem.* Jun 15 2007;365(2):201-207.
226. Rich RL, Myszka DG. Grading the commercial optical biosensor literature-Class of 2008: 'The Mighty Binders'. *J Mol Recognit.* Jan-Feb 2010;23(1):1-64.
227. Edwards PR, Gill A, Pollard-Knight DV, et al. Kinetics of protein-protein interactions at the surface of an optical biosensor. *Anal Biochem.* Oct 10 1995;231(1):210-217.
228. Vogler EA. Protein adsorption in three dimensions. *Biomaterials.* Feb 2012;33(5):1201-1237.
229. Myszka DG, Morton TA, Doyle ML, Chaiken IM. Kinetic analysis of a protein antigen-antibody interaction limited by mass transport on an optical biosensor. *Biophys Chem.* Feb 28 1997;64(1-3):127-137.
230. Goldstein B, Coombs D, He XY, Pineda AR, Wofsy C. The influence of transport on the kinetics of binding to surface receptors: application to cells and BIAcore. *Journal of Molecular Recognition.* Sep-Oct 1999;12(5):293-299.
231. Christensen LL. Theoretical analysis of protein concentration determination using biosensor technology under conditions of partial mass transport limitation. *Anal Biochem.* Jul 1 1997;249(2):153-164.
232. Glaser RW. Antigen-antibody binding and mass transport by convection and diffusion to a surface: a two-dimensional computer model of binding and dissociation kinetics. *Anal Biochem.* Aug 15 1993;213(1):152-161.
233. Schuck P. Kinetics of ligand binding to receptor immobilized in a polymer matrix, as detected with an evanescent wave biosensor. I. A computer simulation of the influence of mass transport. *Biophys J.* Mar 1996;70(3):1230-1249.
234. Gurard-Levin ZA, Mrksich M. Combining Self-Assembled Monolayers and Mass Spectrometry for Applications in Biochips. *Annu Rev Anal Chem.* 2008;1:767-800.
235. J. V. Koubova EB, L. Karasova, J. Skvor, J. Homola, Dostalek, P. Tobiska, J. Rosicky. Detection of foodborne pathogens using surface plasmon resonance biosensors. *Sensors and Actuators B.* 2001;74:100-105.
236. Daniel J. O'Shannessy MB-B, Kim Peck. Immobilization Chemistries Suitable for Use in the BIAcore Surface Plasmon Resonance Detector. *Analytical Biochemistry.* 1992;205:132-136.
237. Stefan Löfas AM. The Art of Immobilization for SPR Sensors. *Surface Plasmon Resonance Based Sensors: Springer Series on Chemical Sensors and Biosensors.* 2006;4:117-151.
238. Milan Mrksich GBS, George M. Whitesides. Plasmon resonance permits in situ measurement of protein adsorption on self-assembled monolayers of alkanethiolates on gold. *Langmuir.* 1995;11:4383-4385.

239. Knoll W, Liley M, Piscevic D, Spinke J, Tarlov MJ. Supramolecular architectures for the functionalization of solid surfaces. *Adv Biophys.* 1997;34:231-251.
240. Jung LS. Binding and dissociation kinetics of wil-type and mutant streptavidins on mixed bitoin-containing alkylthiolate monolayers. *Langmuir.* 2000;16(24):9421-9432.
241. Rich RL, Myszka DG. Advances in surface plasmon resonance biosensor analysis. *Curr Opin Biotechnol.* Feb 2000;11(1):54-61.
242. Nieba L, NiebaAxmann SE, Persson A, et al. BIACORE analysis of histidine-tagged proteins using a chelating NTA sensor chip. *Analytical Biochemistry.* Oct 15 1997;252(2):217-228.
243. Armstrong RN. Glutathione S-Transferases - Reaction-Mechanism, Structure, and Function. *Chem Res Toxicol.* Mar-Apr 1991;4(2):131-140.
244. Boozer C, Ladd J, Chen S, Jiang S. DNA-directed protein immobilization for simultaneous detection of multiple analytes by surface plasmon resonance biosensor. *Anal Chem.* Mar 1 2006;78(5):1515-1519.
245. Munoz EM, Yu H, Hallock J, Edens RE, Linhardt RJ. Poly(ethylene glycol)-based biosensor chip to study heparin-protein interactions. *Anal Biochem.* Aug 1 2005;343(1):176-178.
246. Bal T, Kepsutlu B, Kizilel S. Characterization of protein release from poly(ethylene glycol) hydrogels with crosslink density gradients. *J Biomed Mater Res A.* Mar 18 2013.
247. Bergfors TM. *Protein Crystallization*: International University Line; 2009.
248. Michael KE, Vernekar VN, Keselowsky BG, Meredith JC, Latour RA, Garcia AJ. Adsorption-induced conformational changes in fibronectin due to interactions with well-defined surface chemistries. *Langmuir.* Sep 16 2003;19(19):8033-8040.
249. Sato TK, Yamada RG, Ukai H, et al. Feedback repression is required for mammalian circadian clock function. *Nat Genet.* Mar 2006;38(3):312-319.
250. Hirayama J, Sahar S, Grimaldi B, et al. CLOCK-mediated acetylation of BMAL1 controls circadian function. *Nature.* Dec 13 2007;450(7172):1086-1090.
251. Miyazaki K, Wakabayashi M, Chikahisa S, Sei H, Ishida N. PER2 controls circadian periods through nuclear localization in the suprachiasmatic nucleus. *Genes Cells.* Nov 2007;12(11):1225-1234.
252. Munoz E, Brewer M, Baler R. Modulation of BMAL/CLOCK/E-Box complex activity by a CT-rich cis-acting element. *Mol Cell Endocrinol.* Jun 27 2006;252(1-2):74-81.
253. Rudic RD, McNamara P, Curtis AM, et al. BMAL1 and CLOCK, two essential components of the circadian clock, are involved in glucose homeostasis. *Plos Biol.* Nov 2004;2(11):1893-1899.

254. Bozek K, Relogio A, Kielbasa SM, et al. Regulation of Clock-Controlled Genes in Mammals. *Plos One.* Mar 16 2009;4(3).
255. Miller G. Neurobiology. Despite mutated gene, mouse circadian clock keeps on ticking. *Science.* May 5 2006;312(5774):673.
256. Amaral IP, Johnston IA. Circadian expression of clock and putative clock-controlled genes in skeletal muscle of the zebrafish. *Am J Physiol Regul Integr Comp Physiol.* Jan 1 2012;302(1):R193-206.
257. Hogenesch JB, Gu YZ, Jain S, Bradfield CA. The basic-helix-loop-helix-PAS orphan MOP3 forms transcriptionally active complexes with circadian and hypoxia factors. *Proc Natl Acad Sci U S A.* May 12 1998;95(10):5474-5479.
258. Choogon Lee J-PE, Felino R.A. Cagampang, Andrew S.I. Loudon, Steven M. Reppert. Posttranslatinal Mechanisms Regulate the Mammalian Circadian Clock. *Cell Press.* 2001;107:855-867.
259. Lee Y, Lee J, Kwon I, et al. Coactivation of the CLOCK-BMAL1 complex by CBP mediates resetting of the circadian clock. *J Cell Sci.* Oct 15 2010;123(20):3547-3557.
260. Kondratov RV, Chernov MV, Kondratova AA, Gorbacheva VY, Gudkov AV, Antoch MP. BMAL1-dependent circadian oscillation of nuclear CLOCK: posttranslational events induced by dimerization of transcriptional activators of the mammalian clock system. *Genes Dev.* Aug 1 2003;17(15):1921-1932.
261. Petricka JJ, Benfey PN. Reconstructing regulatory network transitions. *Trends Cell Biol.* Aug 2011;21(8):442-451.
262. Sangoram AM, Saez L, Antoch MP, et al. Mammalian circadian autoregulatory loop: a timeless ortholog and mPer1 interact and negatively regulate CLOCK-BMAL1-induced transcription. *Neuron.* Nov 1998;21(5):1101-1113.
263. van der Horst GT, Muijtjens M, Kobayashi K, et al. Mammalian Cry1 and Cry2 are essential for maintenance of circadian rhythms. *Nature.* Apr 15 1999;398(6728):627-630.
264. Levi F. Chronotherapeutics: the relevance of timing in cancer therapy. *Cancer Causes Control.* May 2006;17(4):611-621.
265. Labrecque G, Belanger PM. Biological rhythms in the absorption, distribution, metabolism and excretion of drugs. *Pharmacol Ther.* Oct 1991;52(1):95-107.
266. Ohdo S. Chronopharmacology focused on biological clock. *Drug Metab Pharmacokinet.* Feb 25 2007;22(1):3-14.

VITA

Burcu Kepsutlu was born in Balikesir, Turkey on July 19, 1988. She graduated from T.C Ziraat Bankasi Science High School, Balikesir in June 2006. She received her Bachelor of Science Degree in Chemical and Biological Engineering from Koc University, Istanbul in June 2011.

From 2011 to 2013, she was a research and teaching assistant in the Chemical and Biological Engineering Department of Koc University. Her research includes quantification of interaction between circadian clock proteins via Surface Plasmon Resonance technique.